DISSERTATION

RETINAL MEDIATORS OF UNIFORM COLOR APPEARANCE

Submitted by

Nathaniel D. Douda

Department of Psychology

In partial fulfillment of the requirements

For the Degree of Doctor of Philosophy

Colorado State University

Fort Collins, Colorado

Summer 2019

Doctoral Committee:

Advisor: Vicki Volbrecht

Janice Nerger
Bryan Dik
Bruce Draper

ABSTRACT

RETINAL MEDIATORS OF UNIFORM COLOR APPEARANCE

The landscape of retinal cell distribution changes drastically from the central retina (0˚ retinal eccentricity) out to the peripheral retina, with changes occurring both in the photoreceptor mosaic (i.e., ratios, densitiy, size, and distribution of both rod and cone photoreceptors) and physical structures within the eye (i.e. optic disc/blind-spot and macular pigment). With all of these changes to the retinal mosaic, it is no surprise that observers report differences in hue appearance between the same physical stimuli presented to different locations on the retina; however, when large stimuli simultaneously cover those same regions of the fovea and peripheral retina, observers report similar color appearance. The present study investigated how information from the fovea and peripheral retina are combined to produce a uniform perceptual experience.

In the first experiment, observers were presented full-field (1°, 23°, 35°) or annular (17° inner diameter/23° outer diameter, 5° inner diameter/35° outer diameter) monochromatic stimuli, ranging from 420 to 660 nm in 20 nm steps for 500 ms at 1.3 log tds. After 30 minutes of dark adaptation, four observers described their hue perceptions using the “4 + 1” hue-naming procedure, in which observers described the stimulus by assigning percentages to one or two of the four elemental hue terms (blue, green, yellow, and red) with the condition that the percentage(s) totaled 100%. Additionally, observers also described how saturated the stimulus appeared on a scale from 0 to 100%. The hue-naming data were similar between the annular and

full-field stimuli, suggesting that the peripheral retina holds more weight in determining the hue of large fields.

A second experiment was conducted to investigate whether one specific region of the peripheral retina had more influence over the hue of the annulus and large fields. Stimuli of 3° were centered at 10˚ eccentricity in the temporal, nasal, inferior, and superior retinas, and hue values from those locations (as well as the mean of all four locations) were compared to hue naming data from the 23˚ annulus. Results showed, in general, that observers varied in which retinal region the 3˚ field was most similar to in hue appearance of the 23˚ annulus, but that the mean of all four retinal locations was a good approximation of the 23˚ annulus.

A final experiment was conducted to investigate the impact of minimizing rod input (bleach conditions) relative to conditions with maximized rod input (dark-adaptation conditions). While the bleaching field influenced hue perception, the overall trend showed that the hue appearance of the annular stimuli most closely aligned with the hue appearance of the full-field stimuli. The findings of the present study are discussed with respect to factors such as rod photoreceptors, chromatic system suppression of rods, spatial integration, cone photoreceptor wiring and ganglion cell inputs, gain mechanisms, macular pigment, and cortical perceptual filling-in/out.

ACKNOWLEDGEMENTS

I would like to express my gratitude to the many people who helped support me throughout the completion of my doctorate.

I would like to extend my sincere thanks to my advisor, Dr. Vicki Volbrecht, for her continued support throughout my graduate school journey. Her unreleting attention to detail challenged me and resonates with my aspiration of pursuing excellence for whatever task lies ahead. Her strong support of my role as an instructor continues to provide opportunities I would not have had otherwise.

I am very appreciative of the support and contributions of my committee members, Dr. Bryan Dik, Dr. Bruce Draper, and Dr. Janice Nerger. Their collective wisdom and expertise was invaluable to the completion of my thesis, comprehensive examination, and dissertation.

The hundreds of hours of data collection that went into this research would not have been possible without the unwavering hard work of my colleague (Dr. Jamie Opper) and research assistants (Alexandra Lake, Andrew Wilson, and Katie Youngpeter), who helped to collect data and serve as observers in my experiments – both tasks requiring countless hours in the dark, which would have been much less tolerable without their witty and thoughtful conversations.

Lastly, I would like to express my deepest appreciation to my family. I am deeply indebted to my wonderful partner, Dr. Maeve O'Donnell, for her constant support and gentle encouragement to continue when I doubted myself. I am also thankful to my immediate family for their words of encouragement during the completion of my dissertation and for all of their love for my entire upbringing: my mother, Marilee Darling; my sister, Jackie Madison; and my brother, Gabe Douda. I am extremely grateful for my dog, Oliver, who has been my constant

companion – our steadfast dedication to daily walks gave me much-needed opportunities to take breaks and get some exercise during long days of work.

TABLE OF CONTENTS

LIST OF TABLES

LIST OF FIGURES

CHAPTER 1: INTRODUCTION

History – Color Vision

It would be difficult to pinpoint the exact moment, and for which specific species, that color vision first developed; however, it is clear that color vision has been an important aspect of life (i.e., survival) for a plethora of creatures for over 500 million years (Land and Nilsson, 2002). While an anthropocentric view, the vast majority of species who possessed color vision up until the relative present were unable to contemplate the faculties afforded by their own color vision. At the very least, humans are the only species to write about their experiences with color perception. In recorded history, ancient Greek philosophers (Early 400s BCE to early 300s BCE) were among the first to discuss the physicality of human color perception (Beare, 1906). Progress in understanding how we perceive light lay mostly dormant until Isaac Newton's (1730) revolutionary experiments using a prism to bend white light into seven spectral components [i.e. violet, indigo, blue, green, yellow, orange, and red]. Thomas Young (1802) expanded on Newton's ideas, and as a part of his wave theory of light, speculated that three primary colors could be combined in different ratios to produce all visible hues; however, it was not until Hermann von Helmholtz (1867/1962) and James Maxwell (1860) that psychophysical evidence supported this conclusion. Based on their psychophysical findings that varying proportions of blue, green, and red could be mixed to match any other hue, Helmholtz and Maxwell speculated there were three sensory mechanisms mediating color perception (known as the trichromatic theory of color vision).

The trichromatic theory quickly encountered some issues in explaining the entire gamut of color phenomena, as the theory mainly focused on the impact of physical stimuli on the sensory mechanisms. Ewald Hering's (1878/1964) work on afterimages argued that color perception was more complex than the trichromatic theory suggested. After staring at what he

termed the four elemental hues (blue, green, yellow, and red), afterimages were perceived that reflected the opposites of those hues (e.g., a yellow stimulus produced a blue afterimage and a red stimulus produced a green afterimage, and vice versa). Due to these perceptual pairings, Hering proposed that color perception was the result of three opponent mechanisms: blue/yellow (B/Y), red/green (R/G), and white/black (Wh/Bk). An additional component of Hering's opponent-process theory was that the chromatic opponent pairs were considered mutually exclusive, meaning hues that were opponent could not be perceived simultaneously, temporally or spatially, in a single stimulus (e.g., a reddish-greenish hue).

Hering's findings motivated Hurvich and Jameson's (1957) investigation of color perception using the hue cancellation procedure; a technique where observers increase the amount of one opponent hue in a stimulus until the appearance of the other opponent hue in a second stimulus has been entirely cancelled. For example, observers may be shown an orange stimulus and asked to add blue light until the yellow component is no longer present, and the stimulus appears only red. These measurements allowed Hurvich and Jameson (1957) to measure the strength of the chromatic response of each hue across the visible spectrum. Results from Hurvich and Jameson's experiments, along with the findings from their predecessors (Helmholtz, 1867; Hering, 1878), were used to formulate the two-stage model of color vision. The first stage of their model built upon Young and Helmholtz's assumption that there were three sensory detectors of light. These sensory mechanisms, which were not physiologically identified until much later (e.g., Bowmaker et al., 1980; Dartnall et al., 1983; Brown and Wald, 1964), are now referred to as the short-wavelength sensitive (S), middle-wavelength sensitive (M), and long-wavelength sensitive (L) cone photoreceptors; with each corresponding to a region of the electromagnetic spectrum of which human eyes are specifically tuned (i.e., 400 to 700 nm). The

second stage of their model improves upon Hering's opponent-process theory, by illustrating how output from the three sensory mechanisms are added and subtracted from one another, thus providing a linear model for the opponent mechanisms: the Y/B process = (M + L) – S, the R/G process = (S + L) – M, and the Wh/Bk process = S + M + L. It is important to note that Hurvich and Jameson's (1957) data were based purely on psychophysical data, as physiological support for these mechanisms was in its infancy. DeValois and DeValois (1993), who had the advantage of understanding the neurological underpinnings of color perception, expanded on Hurvich and Jameson's (1957) model and suggested a third cortical stage of color processing. The cortical stage of processing helped to explain the discrepancy between physiological recordings (i.e., DeValois, Abramov, and Jacobs, 1966; Kaplan, Lee, and Shapley, 1990) and psychophysical data (i.e., Hurvich and Jameson, 1957) at short wavelengths by suggesting the system responsible for the perception of blue becomes amplified at the cortical level.

Photoreceptors – Retinal Mosaic

The human retina is comprised of two types of light sensitive photoreceptors: rods and cones. Rod photoreceptors, named for their slender, rod-shaped appearance in the peripheral retina, are of primary use in low-light conditions (e.g., night vision), as they are much more sensitive than cone photoreceptors at detecting light; cone photoreceptors, however, provide better visual acuity and color perception under higher luminance conditions (e.g., day vision). Østerberg (1935) was among the first to measure the density and distribution of the two classes of photoreceptors across the retina. His findings provided new clues about the distribution differences between the two main types of photoreceptors (rods and cones), such as the lack of

rod photoreceptors and peak of cone photoreceptors in the fovea and the asymmetries between the nasal and temporal retinas (see Figure 1.1).

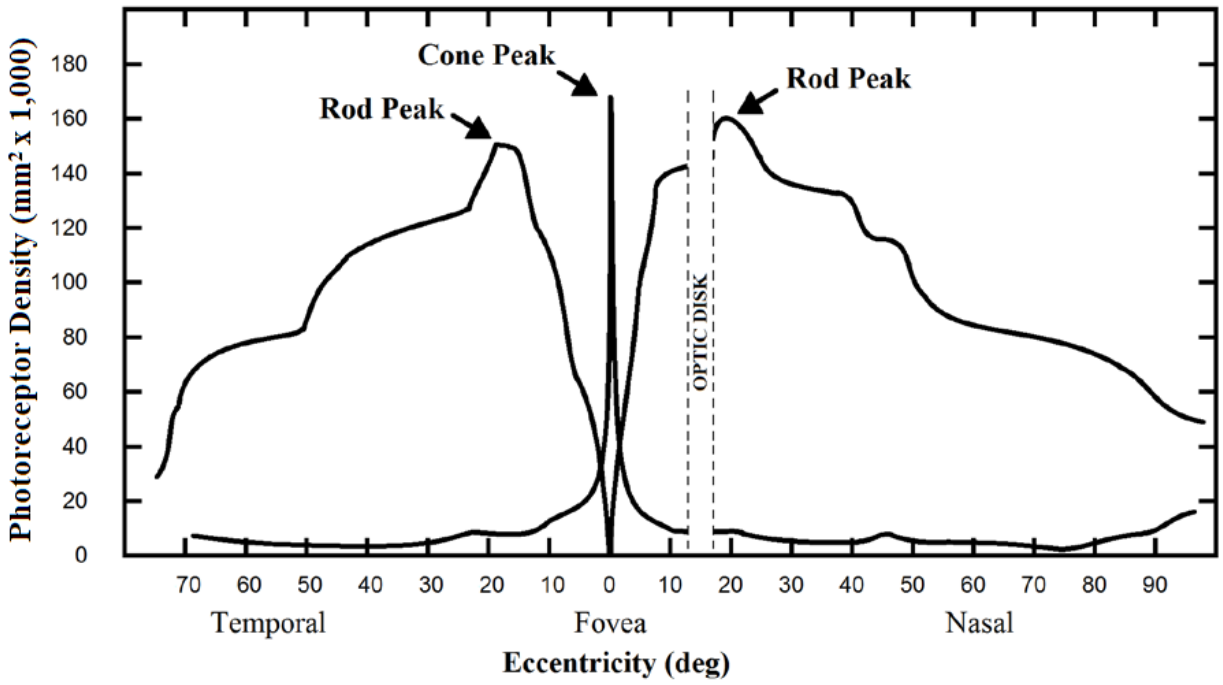

Figure 1.1. Adapted from Østerberg's (1935) measurements of photoreceptor density and distribution as a function of retinal eccentricity.

The academic field of color vision had yet to differentiate between the different cone types until Brown and Wald (1964) measured three distinct absorption spectra. Stemming from the work of Brown and Wald (1964), Bowmaker and Dartnall (1980) used more precise microspectrophotometric measurements to understand the wavelengths at which each cone type responded optimally. They determined that S cones had a peak absorbance at 420 nm, M cones a peak absorbance at 534 nm, and L cones a peak absorbance at 563 nm. In addition, it was not until the late 1980s that S cones were shown to be morphologically different than M and L cones (Ahnelt, Kolb, and Pflug, 1987).

The very center of our visual field, the fovea, comprises only a tiny portion of the retinal real estate and contains only cone photoreceptors (see Figure 1.1). Within the fovea, cone photoreceptor density and distribution is relatively uniform between the four retinal quadrants (i.e., nasal, inferior, superior, and inferior retinas); however, cone density and distribution is not uniform or symmetrical throughout most of the peripheral retina (Curcio, Sloan, Kalina, and Henderson, 1990). Part of this asymmetrical distribution is due to the presence of the optic disk, a photoreceptor-free region which is positioned in the nasal retina and is responsible for carrying photoreceptor signals out of the eye to the brain by means of the ganglion cells (see Figure 1.1, Curcio and Allen, 1990). While photoreceptors are not present in the area of the optic disk, the surrounding tissue compensates, in essence, by having a ring of densely packed cones around the disk (Curcio et al., 1990). From the fovea until approximately 3°, cone densities are similar between the nasal and temporal retinas; however, beyond 3°, the nasal retina has greater cone density than the temporal retina: approximately 25% higher around the region of the optic disk, 40-45% higher beyond the optic disk, and up to 219% higher density than the temporal retina in the far periphery (Curcio et al., 1990). Across the horizontal meridian, Curcio et al. (1990) estimated the average nasal retina contained 39% more cones than the average termporal retina. The differences between retinal regions on the vertical meridian are much less pronounced, with the inferior retina having approximately 2% more cones overall than the superior retina (Curcio et al., 1990).

S cones make up approximately 7-10% of the total number of cones in the average retina and are often not found in the very center of the fovea (i.e., 0° retinal eccentricity) (Ahnelt et al., 1987; Curcio et al., 1991). The highest concentration of S cones is found in a ring outside of the fovea (i.e. approximately 0.5 to 1.5° retinal eccentricity), and S cone density

declines until approximately 8° retinal eccentricity (Ahnelt et al., 1987; Curcio et al., 1991). From 10-20° retinal eccentricity, S cone densities are relatively stable (Ahnelt et al., 1987).

The highest concentration of middle-wavelength sensitive (M) and long-wavelength sensitive (L) cones is in the center of the fovea, and like the S-cones, they decrease in density with increasing retinal eccentricity until about 8° retinal eccentricity (Ahnelt et al., 1987; Curcio et al., 1990). From the fovea until 4° retinal eccentricity, the ratio of L:M cones remains relatively constant, and it has been found psychophysically that for most individuals there are roughly twice as many L cones as there are M cones (e.g., Nerger and Cicerone, 1992). The ratio of L to M cones increases as a function of increasing retinal eccentricity (Albrecht, Jagle, Hood, and Sharpe, 2002). On an individual basis, it has been found that there is a high degree of variability in the ratios of these two photoreceptors. For example, Roorda and Williams (1999), using retinal imaging, have shown a large range of variability in the L:M ratios (1.15:1 – 3.79:1) across observers.

As indicated above, rods are generally not found in the central fovea; however, they are found in large concentrations in the peripheral retina. Rod density increases sharply outside of the fovea until reaching a maximal density between 10 to 20° (see Figure 1.1), with peak densities occurring in a ring around the fovea that is generally the same distance away from the fovea as the optic disk; however, the ring is elongated on the horizontal axis so that peak densities are just beyond the blind spot in the nasal retina (Curcio et al., 1990). In general, rod density is greater where the rod ring crosses the vertical meridian than where it crosses the horizontal meridian. The superior retina generally contains the highest density of rod photoreceptors, while the nasal retinal generally contains the lowest density. This difference is also reflected with rod:cone ratios, as this ratio increases with retinal eccentricity and is higher

in the vertical meridian than it is in the horizontal meridian (i.e., the ratio of rods to cones is higher in the superior and inferior retinas than it is in the nasal and temporal retinas).

On average across the retina, there are nearly 20 rod photoreceptors to every cone photoreceptor, and 5 cones to each ganglion cell (Curcio and Allen, 1990). In the fovea, the evidence suggests that there is no neural convergence from the photoreceptors to the ganglion cells (if anything, there exists a neural divergence with cone:ganglion cell ratios between 1:2 and 1:3). Ganglion cell density is at its peak near the fovea and declines with eccentricity (Curcio and Allen, 1990). Since the rods reach their peak density in the periphery, and ganglion cell density is reduced compared to that of the fovea, neural convergence of rods is greater and may be part of the reason for the greater sensitivity of the rods over the cones.

Foveal and Peripheral Hue Perception

Light striking the rod and cone photoreceptors is the first step in processing the visual input into something chromatically meaningful. Depending on where stimuli are in the environment and the position of the eye at the time of viewing, stimuli land on different portions of the retina. As mentioned previously, the photoreceptor mosaic differs with changes in retinal eccentricity, retinal location (i.e., horizontal vs vertical meridian), and anatomical features (i.e., fovea, optic disk, rod ring) (Ahnelt et al., 1987; Albrecht et al., 2002; Curcio et al., 1990; Nerger and Cicerone, 1992). Due to the varied retinal mosaic, color perception of monochromatic stimuli has been shown to differ depending on which region of the retina is stimulated (Abramov, Gordon, and Chan, 1991; Boynton, Shafer, and Neun, 1964; Opper, Douda, Volbrecht, and Nerger, 2014; Stabell and Stabell, 1976). For example, Boynton et al. (1964) placed the same sized stimuli (3˚ fields at 23 wavelengths) in the fovea and 20˚and 40° in the periphery and found differences in the reported hue percentages of each stimulus depending on

retinal location. One of their major findings was the desaturated appearance (i.e., an achromatic component added to the chromatic component) of the chromatic stimuli as they were placed farther out in the peripheral retina, a finding which has since been replicated by other researchers (e.g., Abramov et al., 1991; Opper et al., 2014; Stabell and Stabell, 1976).

Abramov et al. (1991) have shown that stimuli in the peripheral retina are generally less saturated than the same stimuli presented to the fovea; however, when peripherally placed stimuli are made larger, they tend to become more fovea-like in color appearance and saturation. Although increasing stimulus size does play a role in making peripheral stimuli approach the appearance of foveal stimuli, there are cases in which the stimuli presented to the peripheral retina may appear more saturated than those same stimuli presented to the fovea (Moreland and Cruz, 1959; Opper et al., 2014; Stabell and Stabell, 1976). For example, Opper et al. (2014) have shown that certain wavelengths (specifically those perceived as green-yellow) presented to the peripheral retina can exceed the saturation experience of foveally placed stimuli.

As stimulus size increases in the peripheral retina, color perception at some point stabilizes and further changes in stimulus size no longer produce any changes in hue perception (Abramov et al., 1991). The point at which hue perception asymptotes or stabilizes is referred to as “filling a perceptive field” (Abramov et al., 1991), and can be thought of as the perceptual analog of a receptive field (Abramov et al., 1991; Troup, Pitts, Volbrecht, and Nerger, 2005); a receptive field being the region of the environment to which a sensory cell responds. The stimulus size at which this occurs varies from one retinal location to another, but in general, perceptive field sizes become larger with greater retinal eccentricities. Under mesopic conditions (i.e., luminance levels where both rods and cones are responding), perceptive fields are found to be smaller at 10° along the horizontal meridian (nasal and temporal retina) than at 10° along the

vertical meridian (superior and inferior retina) of the peripheral retina (Volbrecht, Clark, Nerger, and Randell, 2009).

The smaller receptive fields may be due in part to the higher density of cone photoreceptors along the horizontal meridian of the peripheral retina than along the vertical meridian (Curcio et al., 1990). Cone density alone, however, does not tell the whole story, as the perceptive field sizes measured in superior retina are similar to those measured in the nasal and temporal (Volbrecht et al., 2009). Rod signals may also play a role, as conditions designed to minimize rod activity (e.g., bleach condition), decrease perceptive field sizes relative to conditions where rod activity is maximized (e.g., no bleach condition) (Troup et al., 2005; Volbrecht et al., 2009). The best predictor of perceptive field size for the majority of the elemental hue terms (the exception being green) may be the rod:cone ratio at various locations in the retina. At 10° in the temporal, nasal, inferior, and superior retina, the rod:cone ratios are approximately 15:1, 16:1, 19:1, and 21:1, respectively (Curcio et al., 1990), and the correlation coefficients comparing rod:cone ratios to perceptive field sizes are .99 for blue and red hues, .79 for yellow, and .58 for green in a no-bleach condition (Volbrecht et al., 2009). Perceptive fields for three of the four elemental hues (blue, yellow, and red) under no-bleach (maximal rod input) and mesopic conditions are filled once stimuli reach approximately 1° in the temporal, 2° in the nasal, 5° in the superior, and 3° in the inferior retinas. The perceptive field sizes for green increase to approximately 2°, 7°, 8°, and 15° for the temporal, nasal, superior, and inferior retinas, respectively (Volbrecht et al., 2009).

Even when perceptive fields have been filled, there are still differences in the perception of hue between bleach (minimal rod input) and no-bleach (dark adapted) conditions, as well as when those areas are compared to the fovea (Angel, 2003). There are many studies which

suggest rods may impact the perception of hue (Ambler, 1974; Stabell and Stabell, 1976; Stiles and Burch, 1958; Troup et al., 2005; Volbrecht et al., 2009). As mentioned above, the presence of rod photoreceptor input into chromatic signals have been shown to desaturate (i.e., add an achromatic component) the appearance of chromatic stimuli (Lie, 1963; Stabell and Stabell, 1976). Additionally, many studies have noted an increase in blueness/yellowness in dark adapted conditions (maximal rod contribution) when compared with conditions where rod input has been minimized (Ambler, 1974; Boynton et al., 1964; Moreland and Cruz, 1959; Nerger, Volbrecht, Ayde, and Imhoff, 1998; Trezona, 1970). Stabell and Stabell (1999) have demonstrated that these changes in hue due to rod intrusion are greatly diminished with larger stimuli presented for longer durations (i.e., 500 ms). Researchers (Buck and Knight, 2003; Buck, Thomas, Conner, Green, and Quintana, 2008; Knight and Buck, 2002) have investigated the effect of stimulus duration on the magnitude of perceptual shifts occurring due to rod input and have identified what they have termed "rod biases": for shorter duration stimuli (< 20 ms) presented at longer wavelengths, rod input pushes hue perception toward greenness (as opposed to redness). At longer durations (100 ms to 5 s), middle wavelength stimuli appear more blue (as opposed to yellow) and shorter wavelength stimuli appear more red (as opposed to green). These findings suggest that there is not only a spatial component to rod influence, but there is a temporal component to rod influences on hue perception.

Color Spreading – Filling-in and Filling-out

Color vision research has traditionally focused on very specific regions and receptors of the retina. Through this research, many things have been discovered with respect to photoreceptor interactions and their functions (e.g., Gouras and Link, 1966), as well as

photoreceptor distribution (e.g., Curcio et al., 1990), and the resulting perceptual differences across various regions of the retina (e.g., Boynton et al., 1964). This research has produced a wealth of information explaining these perceptual microcosms in controlled laboratory settings, but tend to avoid discussing how we view color in our natural environments. For most of us, it is probably not often that we encounter 8° monochromatic stimuli placed specifically at 10° in the temporal retina; however, we often encounter visual scenes that are made up of large blocks of hues that are uniform in appearance and cover a large portion of our retina. This is rather interesting since the variety of retinal photoreceptors are not distributed uniformly across the retina (Curcio et al., 1990); and consequently, the same, relatively small stimuli presented to different regions of the retina often yield different percepts (Opper et al., 2014; Troup et al., 2005; Volbrecht et al., 2009). If we know that small stimuli placed in different retinal locations can yield different color percepts, the question remains as to how we perceive large fields as uniform in color appearance, as opposed to mottled, as our retinal mosaics might suggest would be the case.

Despite these differences in the retinal mosaic (e.g., Curcio et al., 1990; Nerger and Cicerone, 1992; Roorda and Williams, 1999) and perceptive field sizes (e.g., Abramov et al., 1991; Troup et al. 2005, Volbrecht et al., 2009), the real world perceptions remain the same: we perceive hue to be uniform across large visual fields. The ability of our visual system to maintain uniform perceptions is demonstrated with the "filling-in" of our natural blind spot. The blind spot is the location in the nasal retina where axons of the retinal ganglion cells leave the retina from the optic disk to transmit information to the cortex. There are no photoreceptors in this area of the retina, yet we do not see an interruption in our perception of a stimulus (Spillmann, Otte, Hamburger, Magnussen, 2006). Similarly, we do not notice a blue stimulus appearing non-

uniform even though there is a lack of S-cones in the very center of our fovea (Williams, MacLeod, and Hayhoe, 1981).

Perceptual filling-in has also been reported in texture perception (Motoyoshi, 1999), brightness perception (Cornsweet, 1970; Paradiso and Nakayama, 1991), and color perception, although the color effects are generally considered a "filling-out" or color-spreading phenomena (O'Neil and Webster, 2014). One such effect is the neon-color spreading effect, where replacing portions of black lines of a simple 2-dimensional image (e.g. a matrix of black lines) with another color (e.g. blue) to create a "subjective contour" causes the white space surrounding the colored lines to take on that same colored appearance (see Figure 1.2; van Tuijl, 1975).

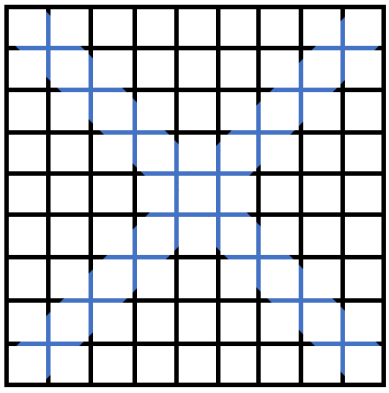

Figure 1.2. Adapted from van Tuijl's (1975) study on neon color spreading effects. See text for details.

The watercolor effect (Pinna, Brelstaff, and Spillmann, 2001) similarly describes the perceptual experience of color spreading to the white spaces of an image that contains two complimentary colored "winding" lines drawn immediately adjacent to one another. One such example is demonstrated in Pinna et al. (2001), where purple lines are surrounded by an orange line of a similar thickness, resulting in the appearance of light orange in the space between the

contours (see Figure 1.3). Pinna et al. (2001) demonstrated that the higher the contrast between these two lines, the greater the effect of the illusory coloration. If the two lines have any white space between them, the effect disappears (Pinna et al., 2001). For many studies describing neon and watercolor spreading effects, little attention is given to the region of the retina and underlying retinal mosaic where the stimuli are placed, and instead focus on the cortical contributions to color-spreading effects (e.g., Pinna et al., 2001; van Tuijl, 1975).

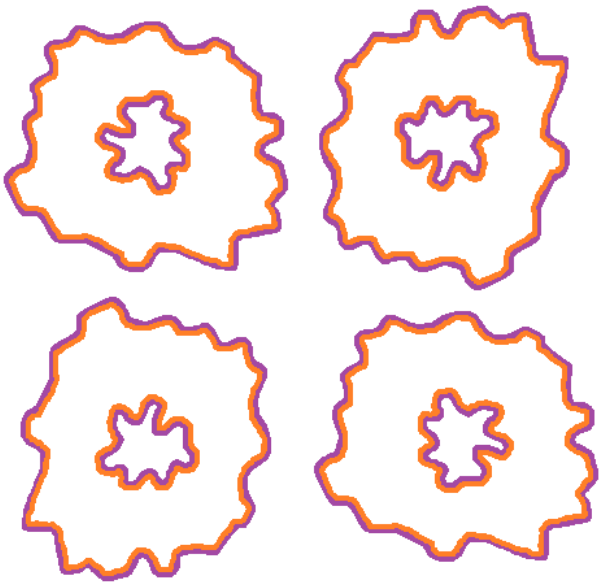

Figure 1.3. Adapted from Pinna et al.'s (2001) study on the watercolor effect. See text for details.

Balas and Sinha (2007) were interested in investigating whether one portion of the visual field was more likely to produce the color-spreading effect, and did so by creating achromatic regions in either the center or peripheral region of an image. Their results indicated that participants saw the whole image as colored in both conditions: first, when the center of the image remained colored and the peripheral portion was grey in appearance, and second, when the center of the image was grey and the peripheral portion remained colored. Balas and Sinha's

(2007) results suggest that one region of the retina is not more responsible than any other for creating the fully colored appearance, and instead suggested that the higher cortical functions that process many aspects of a visual scene (such as contours, luminance statics, or recognizable objects) are responsible for the "filling-out" effect. What is not addressed is whether 1) the retina accurately encodes the chromatic information of the visual scene (i.e., photoreceptor firing rates are a direct reflection of the hues impinging on them) and high-level cortical processing drives the illusion of color in the achromatic portions of the image, or, 2) if local processes within the retina (e.g., horizontal cells) modulate the firing rates of the photoreceptor signals to contribute to the filling-out effect.

More recent research has investigated lower-level processes, like the retina, as explanations for uniform hue perception. O'Neil and Webster (2014) were interested in determining which portion of the retina was responsible for the hue appearance of large fields, and did so by comparing a 1° purple stimulus presented at 8° retinal eccentricity to a purple stimulus of slightly different hue presented in the fovea that increased in size from 1° to 16°. Their results indicated that once the foveally presented stimulus reached 8° in size, its hue appearance was similar to that of the 1° stimulus presented to the peripheral retina and stayed that way as the stimulus increased up to 16°, thus suggesting that the peripheral retina was responsible for dictating the hue appearance of large fields. They concluded that the edges of the stimuli had little role in determining color appearance (since edges play a large role in the neon and watercolor effects), as the peripheral retina still determined the hue of the field when the edges were softened with a Gaussian function. Since varying the contrast of the edges of the stimuli did not have much of an effect on color appearance, O'Neil and Webster (2014) suggested that the hue of large fields is not mediated by the same mechanisms as the neon and

watercolor spreading effects. O'Neil and Webster (2014) speculated that an averaging of the percept from the underlying retinal areas might account for the hue of the large fields, a possibility which the present study examines. While the peripheral retina is part of the equation of determining the hue of large fields, the local gain changes (e.g., adaptation of photoreceptors, ganglion cells, or other retinal cells) are not enough to account for all the compensation necessary to produce a uniform field; therefore, O'Neil and Webster (2014) suggested that cortical processing must also play a role. It is unlikely, in the O'Neil and Webster (2014) study, that the 1° stimulus presented at 8° in the peripheral retina filled the perceptive fields (Volbrecht et al., 2009) for the four elemental hues (blue, green, yellow, and red) and may not be an appropriate comparison of foveal versus peripheral color percepts, since the periphery is known to become more fovea-like with increases in stimulus size (Abramov et al., 1991). Because O'Neil and Webster (2014) did not study the full complement of hues, instead focusing only on purple, it makes it hard to compare their results to other studies (e.g., Opper et al., 2014) where differences were not seen between the periphery and fovea for purple hue percepts, but differences were seen in the green-yellow (i.e., middle wavelength) portion of the spectrum.

The Present Experiment

The present experiment investigates the perceptual mechanism(s) and retinal locations responsible for the determination of the hue appearance of large fields across the visible spectrum. The stimulus sizes used in this study were chosen specifically to fill the perceptive fields of the four elemental hues at 10° retinal eccentricity (Volbrecht et al., 2009), as well as to provide a comparison of hue perceptions between the fovea and peripheral retina. One of the stimuli chosen for this study, an annulus with a 3˚ wide ring, filled the perceptive fields for most

hue terms (blue, yellow and red) at most retinal locations (i.e., inferior, nasal, and temporal); however, an annular stimulus with a 15˚ wide ring was used as well to ensure perceptive fields were filled for all hues and retinal locations (especially green). A 1˚ foveally placed stimulus was used to compare hue perceptions in the fovea to hue perceptions of full-field stimuli covering both the fovea and peripheral areas, and with annular stimuli which are devoid of foveal input. The goal of this study was to determine whether 1) signals from the fovea dominate the signals from the peripheral retina, or 2) the signals from the peripheral retinal dominate the fovea, or 3) the uniform appearance is the result of an averaging of the signals across the retina.

CHAPTER 2: METHODS

Participants

Observers were AIW, a 23-year old male; JO, a 35-year old female; KY, a 28-year old female; and VV, a 57-year old female. All observers were assessed for normal color vision in their right eye using the Farnsworth-Munsell 100-hue panel test, D-15 and desaturated D-15 panel tests, and a Neitz anomaloscope (Neitz OT-II). Before commencing the study, each observer participated in one practice session for each stimulus condition with the "4+1" hue-naming task (described below).

Apparatus

A three-channel Maxwellian-view optical system with a 300 W (5500 K) xenon arc lamp (Oriel, model 66065) regulated by a 290 W dc power supply (Oriel, model 68811) supplied the stimuli for this experiment. A schematic for this system is presented in Figure 2.1.

Light leaving the exit port of the lamp housing passed through a heat-absorbing filter (H1) before being collimated by a lens (L1). Using L2, light was focused, passed through a beamsplitter (BS1), such that the focal point was just beyond the reflective plane within the beamsplitter), to form channel 1 and create a second path of light.

Light in channel 1 was collimated by L3, passed through a field stop (FS1) that defined the size of the bleaching field, and was focused by L4 on a shutter (S1), controlled by a driver system (Uniblitz, model T132). The light was again collimated by L5, passed through a filter box holding neutral density filters (FB1; Ealing Electro-Optics) that controlled the intensity of the bleaching field, and then reflected at a 90-deg angle by a mirror (M1).

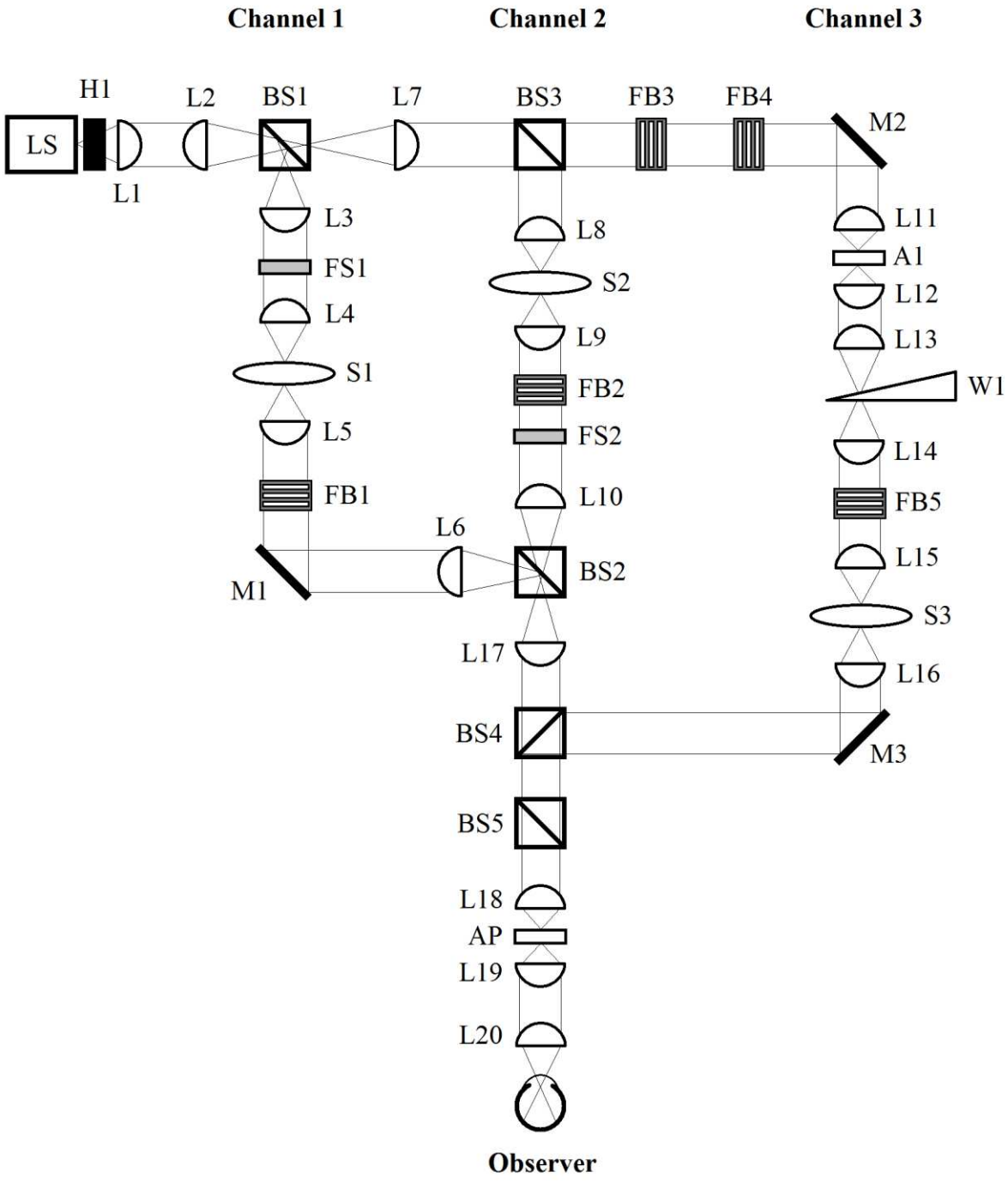

Figure 2.1. Schematic of the three-channel Maxwellian-view optical system. Components are as follows: LS = Light Source; H = Infrared Heat Absorbing Filter; L = lens; BS = Beamsplitter; M = Mirror; W = Neutral Density Wedge; FS = Field Stop; FB = Filter Box; S = Shutter; AP = Artificial Pupil, A = Aperture. The observer's position is indicated at the bottom of the figure.

This collimated light was then focused by L6 on BS2, which combined light from channels 1 and 2.

Light passing through BS1 was collimated by L7 before passing through a second beamsplitter (BS3), which formed channels 2 and 3. Light coming from BS3 that formed channel 2 was focused by L8 onto a driver-controlled shutter (S2, Uniblitz, model T132) and then collimated by L9. The collimated light passed through FB2 and a field stop (FS2) that controlled the light intensity and defined the fixation array, respectively, before being refocused by L10 and passed through BS2 that combined light from channels 1 and 2.

Light passing through BS3 formed channel 3. The collimated light then passed through FB3 and FB4, which were used to hold the 35 mm film stimulus slides (Digi-graphics, Fort Collins), a 1.3 log-unit neutral density filter (Ealing Electro-Optics) for reducing the intensity of the light, and the interference filters (420-660 nm, in 20 nm steps) that defined the spectral composition of the stimuli. The collimated light was reflected at a 90-deg angle by M2 before being focused by L11 and passed through an aperture to reduce stray light. It was then re-collimated by L12. The collimated light was re-focused by another lens, L13, and passed through a two log-unit circular neutral density wedge (W1, Ealing Electro-Optics) that controlled the retinal illuminance of the stimuli by means of a computer. The focused light was re-collimated by L14, passed through FB5, which contained a filter that controlled the intensity of the stimulus during observer-alignment before the start of the experiment. Light in Channel 3 was re-focused by L15 onto the blades of a driver-controlled shutter (S3, Uniblitz, model T132) and collimated by L16 before being reflected 90-degrees by M3 and directed through BS4. BS4 combined light from all three channels (light from BS2 combined focused light from channels 1 and 2, which was collimated by L17 before passing through BS4).

The collimated light passing though BS5 was re-focused by L18 onto an artificial pupil (AP) that defined the final size of the Maxwellian image as 1.8 mm in diameter. Light exiting the AP was collimated by L19 before being focused on the pupil of the right eye by L20. Each observer aligned to the optical system by means of a dental-impression bite-bar, which permitted alignment in three orthogonal directions, ensuring the Maxwellian image was focused on the plane of the pupil and thereby passed through the pupil unobstructed and stimulus intensity was maintained.

Stimuli

As in past experiments from the vision laboratory (e.g., Opper et al., 2014; Volbrecht et al., 2009), stimuli were equated at a retinal illuminance of 20 photopic trolands (tds). The stimuli were centered with respect to a single, centrally located, pin-sized fixation point, with the fixation intensity set by the observer to be slightly above absolute threshold to minimize adaptation effects (Jameson and Hurvich, 1967). Test stimuli were presented for 500 ms, and the shutter drivers for channels 2 and 3 were synchronized so that the fixation-point shutter closed simultaneously to the opening of the shutter for the test stimulus. Test stimuli ranged from 420 nm to 660 nm in 20 nm steps, which were generated using interference filters placed in the filter box in channel 3. Stimuli were created by means of 35 mm film recordings (Digi-graphics, Fort Collins); the opaque portion of the slide blocked light, while the exposed sections of the film allowed light to transmit through the Maxwellian-view optical system.

In the first portion of the experiment, two stimuli were utilized: a full-field stimulus and an annular stimulus. Full-field stimuli were circular and 1°, 23°, and 35° in size (visual angle). The first annular stimulus, depicted in the left-hand portion of Figure 2.2, was defined by a 3°

wide annulus with an outer stimulus diameter of 23° and an inner, diameter of 17°. The 3° wide annulus bisected 10° retinal eccentricity and filled the perceptive fields for the four elemental hues (blue, green, yellow, and red) in the temporal retina at 20 tds, and three of the elemental hues (blue, yellow, and red) in the nasal and inferior retinas, and yellow in the superior retina (Troup et al., 2005; Volbrecht et al., 2009). The second annular stimulus, depicted in the right-hand portion of Figure 2.1, was defined by a 15° wide annulus with an outer stimulus diameter of 35° and an inner diameter of 5°. The 15° wide annulus filled all of the perceptive fields in the temporal, nasal, superior and inferior retinas for the four elemental hues (Troup et al., 2005; Volbrecht et al., 2009).

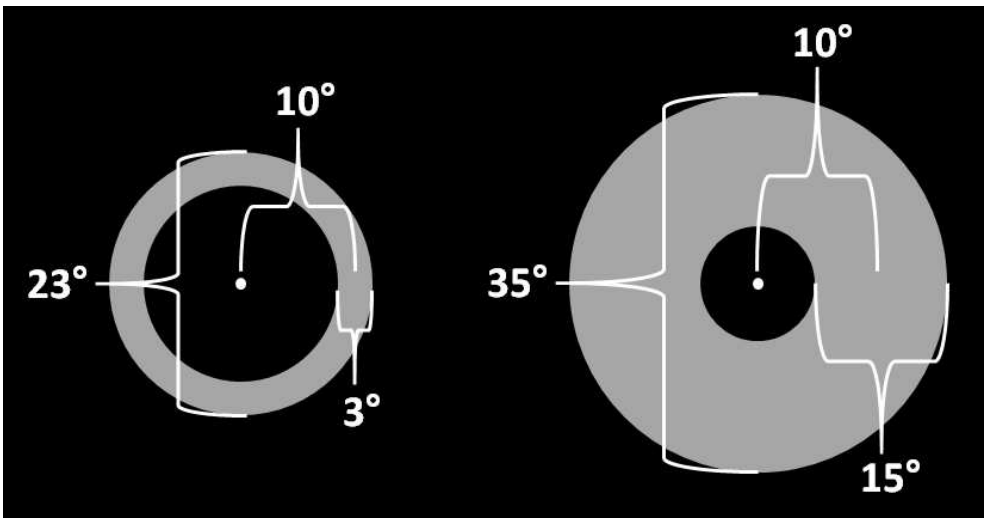

Figure 2.2. The schematic on the left depicts the 23° annular stimulus and the schematic on the right depicts the 35° annular stimulus. The grey portion corresponds to the annular area where the chromatic stimulus was present; the white dot in the center of each stimulus is the fixation point.

In the second experiment, data were collected on hue perception at four retinal locations (i.e. inferior, superior, nasal, temporal), with 3° stimuli centered at 10° from the fovea. A depiction of these stimuli in relation to the annulus are shown in Figure 2.3 – it should be noted

that stimuli were only presented at one retinal location within each data-collection session. The goal was to compare data from the 23° annulus to each of the individual retinal locations that have been previously investigated (Abramov et al., 1991; Volbrecht et al., 2009), as well as to compare the annular data to the mean across all four retinal locations.

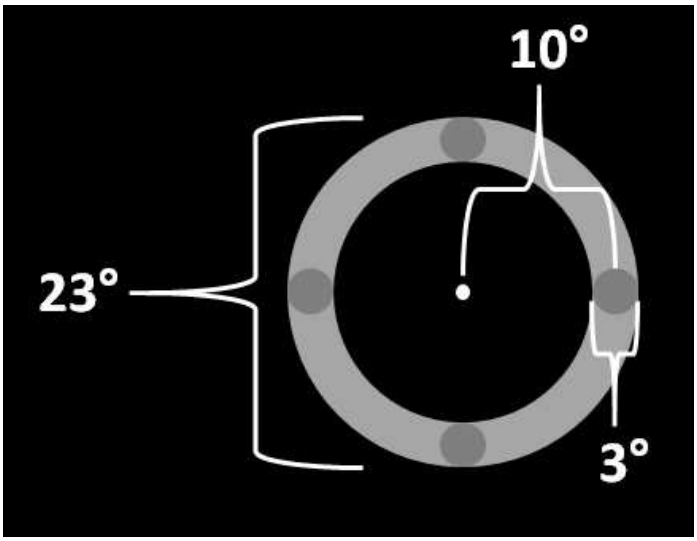

Figure 2.3. Dark-gray circles represent the positioning of the 3° stimuli relative to the 23° annular stimulus. 3° stimuli were centered at 10° in the nasal, temporal, inferior, and superior retinas. The white dot in the center represents the fixation point, which allowed the stimuli to be positioned at 10° eccentricity. Note: the annulus and 3° stimuli were not presented at the same time.

As a control, data were collected under a bleaching condition to minimize rod input for the 1° (foveal), 23° full-field, and 23° annular stimuli. In this control condition, observers were exposed to a 49.3°, 6.14 log scotopic troland bleaching field centered over the fovea for 20 seconds. Under these conditions, the bleaching field was calculated to bleach approximately 95% of rod photopigment (Alpern, 1971; Rushton and Powell, 1972)

Calibrations

The neutral density filters and wedge were calibrated by taking radiometric measurements (UDT Instruments Radiometer, Model S370) from 420-660 nm in 20 nm steps. A photometric measurement (Minolta Chroma Meter, Model CS-100) was taken for channel 3 at a reference wavelength of 560 nm (peak spectral sensitivity of the photopic luminosity function) to enable conversion of radiometric measurements from 420 to 660 nm to photometric measurements. A photometric measurement was also obtained for the bleaching field using the method of Westheimer (1966) and converted to scotopic trolands (Wyszecki and Stiles, 1982). A spectral radiometer (Photo Research SpectraScan PR650) was used to verify the spectral distribution of the interference filters, which took measurements in 4 nm steps from 380 nm to 780 nm. Due to the 4 nm step size, exact measurements were not available at the specified/expected peak transmission wavelength of every filter (i.e., 410 nm, 430 nm, etc), so the peak transmission wavelength was estimated by taking the mean of the two highest irradiance levels for those filters. Half-bandwidth was calculated by finding the two values of the spectral distribution that were half of the peak transmission and calculating the absolute value of the difference between these two values. Figure 2.4 illustrates the peak transmission and half bandwidth for the 500 nm interference filter. Half-bandwidth and peak energy are listed for each of the interference filters used in the present study in Table 2.1. With the exception of the 440 nm filter (with peak transmission at 442 nm), the interference filters demonstrated peak transmission at the manufacturer's nominal values.

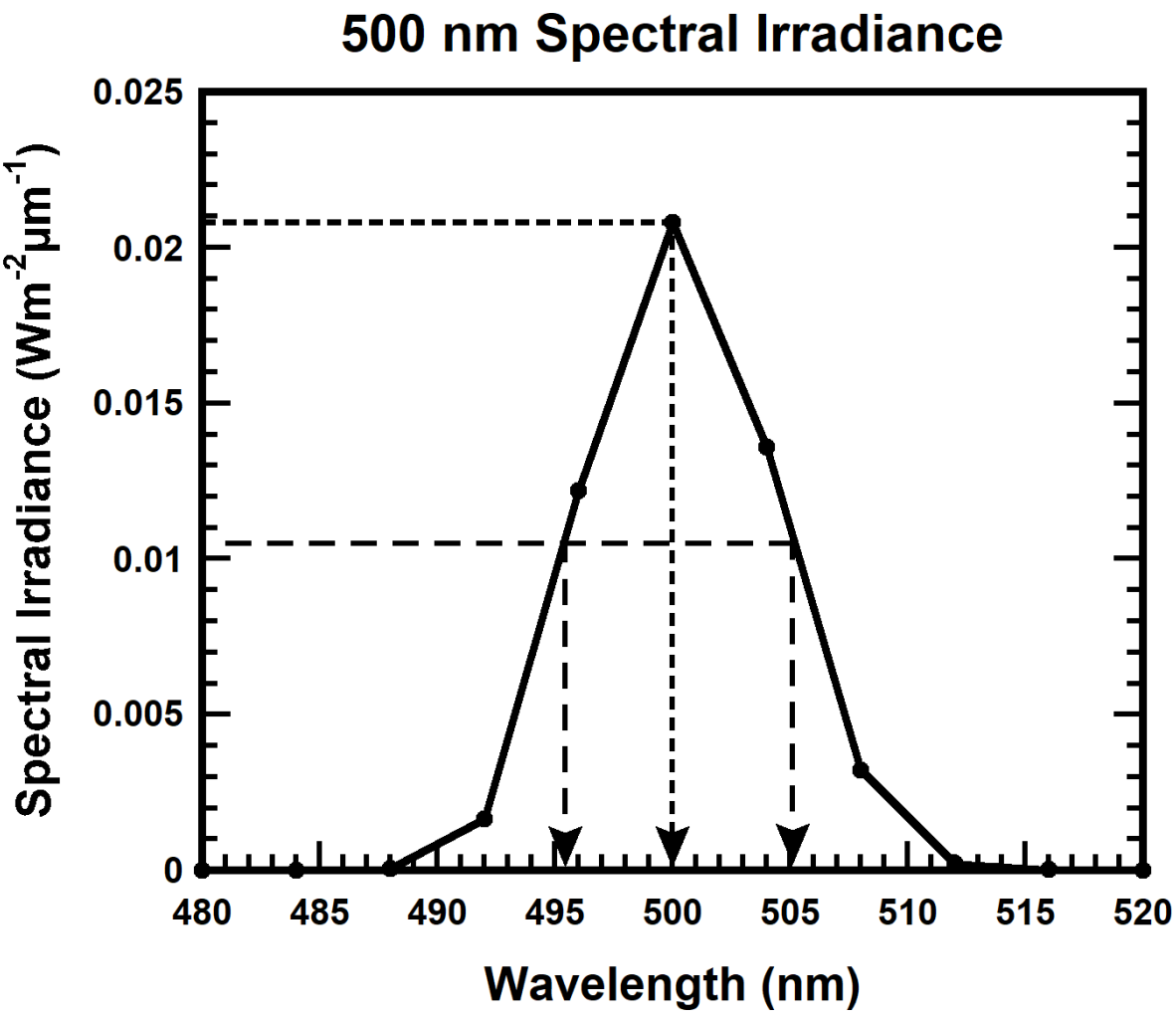

Figure 2.4. Energy output across wavelengths for the 500-nm interference filter. The shorter-dashed horizontal and vertical lines indicate the wavelength corresponding to peak energy transmission. The longer-dashed horizontal and vertical lines show the two wavelengths associated with the half-bandwidth range.

Table 2.1. Wavelengths of peak energy transmission and half-bandwidth of interference filters

Filter (nm)	Peak (nm)	Half-Bandwidth (nm)	Filter (nm)	Peak (nm)	Half-Bandwidth (nm)
400	400	5.4	540	540	5.5
410	410	5.7	550	550	5.8
420	420	5.1	560	560	5.2
430	430	4.9	570	570	6
440	442	4.9	580	580	5.5
450	450	4.8	590	590	6.3
460	460	5	600	600	5.4
470	470	4.8	610	610	5.9
480	480	5.3	620	620	5.6
490	490	5.4	630	630	6.5
500	500	4.9	640	640	5.9
510	510	5.5	650	650	6.9
520	520	5	660	660	6.4
530	530	6			

Procedure

Prior to data collection, one stimulus was pseudorandomly chosen for presentation. Observers aligned to the system and then adapted to the dark for 30 minutes, for maximal rod input, before making hue judgments. After the 500-ms presentation of the stimulus, the observers made hue responses using the "4+1" hue-scaling procedure described by Abramov et al. (1991). With the hue-scaling procedure, observers described the stimulus by assigning percentages to one to two of the four elemental hue terms (blue, green, yellow, and red), with the condition that the percentage(s) totaled 100%. Observers were not permitted to use opponent terms to describe a single stimulus (i.e. blue-yellow or green-red). Additionally, observers also described how saturated the stimulus appeared on a scale from 0 to 100%, with 0% corresponding to stimuli that appeared completely achromatic and a value of 100% corresponding to stimuli that appeared entirely chromatic.

Each session of data collection terminated after collecting four responses to each of the 13 different wavelengths for a given stimulus condition. The first set of responses obtained in a session was practice, with each of the 13 wavelengths randomly presented once. After the practice set, three responses were obtained for each wavelength, which was achieved by randomly selecting a wavelength from the 39 possible responses still to be collected (13 wavelengths x 3 responses). The session terminated when all 39 responses were recorded. Data for each stimulus were collected across three experimental sessions, yielding three practice responses and nine responses per wavelength. Means were calculated from the nine responses to yield a grand mean for each of the hue and saturation terms at each wavelength.

In the first experiment, data were collected with four observers (AIW, JO, KY, and VV) for five different stimuli to assess the differences and similarities between hue scaling with a foveal stimulus (1°), annular stimuli (23° and 35°), and full-field stimuli (23° and 35°). In a follow-up experiment, data were collected on three observers (AIW, KY, and VV) for another set of stimuli to assess if spatial integration could explain the results from the large field stimuli. The stimuli used for this investigation were the 23° annuli and 3° fields that were placed at 10° retinal eccentricity in the inferior, superior, nasal, and temporal retinas. The goal was that data from the 23° annulus could be compared to each of the individual retinal locations to determine if responses from one specific retinal location mediated the appearance of the larger stimuli or if spatial integration across retinal locations accounted for hue perception in a large field.

Lastly, a control condition was used for three observers (AIW, KY, and VV) to assess the role of rod input on hue appearance. In order to reduce rod input, the observer's eye was exposed to a relatively brief, bright white light (20 s, 6.14 log scot tds, 5500K), rendering the rod photopigment less sensitive than the cone photopigment for approximately 10 minutes post

bleach (Alpern, 1971; Rushton and Powell, 1972). Hue-naming data were collected on the 1° foveal stimulus, 23° annular stimulus, and 23° full-field stimulus for the duration known as the cone plateau, which is 4 to 10 minutes post bleach. During the cone plateau, cone photopigment has regenerated and the cones have a lower threshold for detecting light than rods, so hue data collected during this period reflects diminished rod input. By bleaching the fovea, even though there are no rods in the fovea, you can control for extraneous variables (e.g., cone adaptation) that the bleaching field might introduce. Troup et al. (2005) used a similar procedure and concluded that bleaching fields did not differentially adapt the cone photoreceptors. The larger 35˚ fields were not included in this comparison, as Volbrecht et al. (2009) demonstrated that perceptive fields were filled at much smaller stimulus sizes under bleaching (2˚ or less) than in no-bleach conditions (up to 15˚).

CHAPTER 3: RESULTS

Data Analysis

For each response, hue values were scaled to saturation, a procedure commonly used for experiments of this nature (e.g. Abramov et al., 1991; Opper et al., 2014; Troup et al., 2005). As a result, the total hue percentage for a given wavelength is equivalent to the percent saturation reported for that wavelength and provides an indication of the strength of the chromatic response(s) at that wavelength. For example, if we were comparing two blue hue responses at 460 nm, but with different stimulus configurations, an observer might describe the first stimulus as 90 percent blue, 10 percent green, and 70 percent saturation, while the second stimulus might be described as 90 percent blue, 10 percent green, and 50 percent saturation. While the ratio of the two hue responses is the same for both stimuli, the overall strength of the blue responses after scaling to saturation is weaker with the second stimulus than the first stimulus (45% blue versus 63% blue). Means and standard error of the means (SEM) across experimental sessions for each observer were computed for each wavelength and stimulus combination, and this mean data can be found in the appendix.

Hue-Naming Functions

Mean hue-naming functions were plotted for each individual observer. Figures 3.1 – 3.5 depict percent hue or saturation plotted as a function of wavelength for each of the four observers (columns) for the 1° stimuli (solid line and circular symbols), 23° annular stimuli (long-dashed line with square symbols), and 23° full-field stimuli (short-dashed line with diamond symbols). The 1° stimulus excites the fovea, the 23° annulus excites the peripheral retina, and the 23° full-field stimulus excites both fovea and peripheral retinas. The top row of panels compares the hue-

scaling responses to the 1° stimulus with those obtained during the 23° annulus conditions (included to highlight similarity between both 23° stimuli, in contrast to the 1° stimuli), the middle row of panels compares responses to the 1° stimulus and 23° full-field stimulus conditions, and the bottom row of panels compares responses to the 23° annulus and 23° full-field stimulus conditions. Error bars represent ±1 SEM.

For each of the panels in the figures, a corresponding Table (3.1 – 3.5) lists the results of calculating the mean absolute difference across wavelengths between the hue percent of the 23° full-field stimulus and the 1° foveal stimulus, as well as between the hue percent of the 23° full-field stimulus and the 23° annular stimulus. The higher the mean value, the larger the difference between the hue responses of those from the 23° full-field stimulus. Comparisons with the lowest mean absolute difference values were considered more perceptually similar to the 23° full-field stimulus than those with higher values. When mean absolute difference values between comparisons were within ±1% of each other (i.e., 2% or smaller overall difference between comparison values listed in the tables), these comparisons were considered to be similar to one another. This ±1% criterion value was determined by examining median SEM values across wavelengths within each hue term and observer and noting that conditions with the observers' lowest median SEM values were approximately 1%. Additionally, data from Volbrecht, Nerger, and Trujillo (2011) suggests a 1% shift in hue percentage may be enough to produce a just-noticeable difference. One of the caveats of comparing these absolute mean deviation tables to the hue-naming function figures is that the tables are consolidating data across wavelengths and large differences that may exist at a single wavelength between conditions is not clearly reflected in the mean data. Additionally, because absolute values are used, it is possible for two conditions to have similar deviation values yet have hue percents moving in opposite directions in the

conditions being compared. For example, an absolute mean deviation of 4% seen in both comparisions (i.e., full-field versus annulus and full-field versus fovea) could mean that a 450 nm stimulus was reported as 90% blue in the full-field condition, 86% blue in the annular condition, and 94% in the foveal condition.

Overall, for the perception of blue (Figure 3.1), the 23° annular stimuli are more similar to the 23° full-field stimuli across all four observers and less like the 1° foveal stimuli. Across observers, there are notable differences between the 1° stimulus and the 23° stimuli at the longer wavelengths (i.e., ≥ 480 nm) where blue was reported. In particular, percent blue was higher in the fovea (1°) than for stimuli which excited the peripheral retina (23° annulus and full-field). Overall, all four observers showed differences (i.e., ±1 SEM error bars do not overlap) between the 1° and 23° annular stimuli at 500 nm, and three of the four observers showed differences between the 1° and 23° full-field stimuli between 460 - 500 nm. One or two observers showed small differences between the 23° annulus and 23° full-field stimulus, but the direction of these differences were inconsistent across observers. As confirmed in Table 3.1, all of the observers demonstrated smaller mean absolute differences between the 23° full-field and 23° annulus when compared to the 23° full field and 1° foveal stimulus. KY's mean absolute difference comparisons were within ±1% of each other, although the foveal data were approximately 9% less blue than the full-field data at 440 nm and 13% more blue at 500 nm than the full-field data.

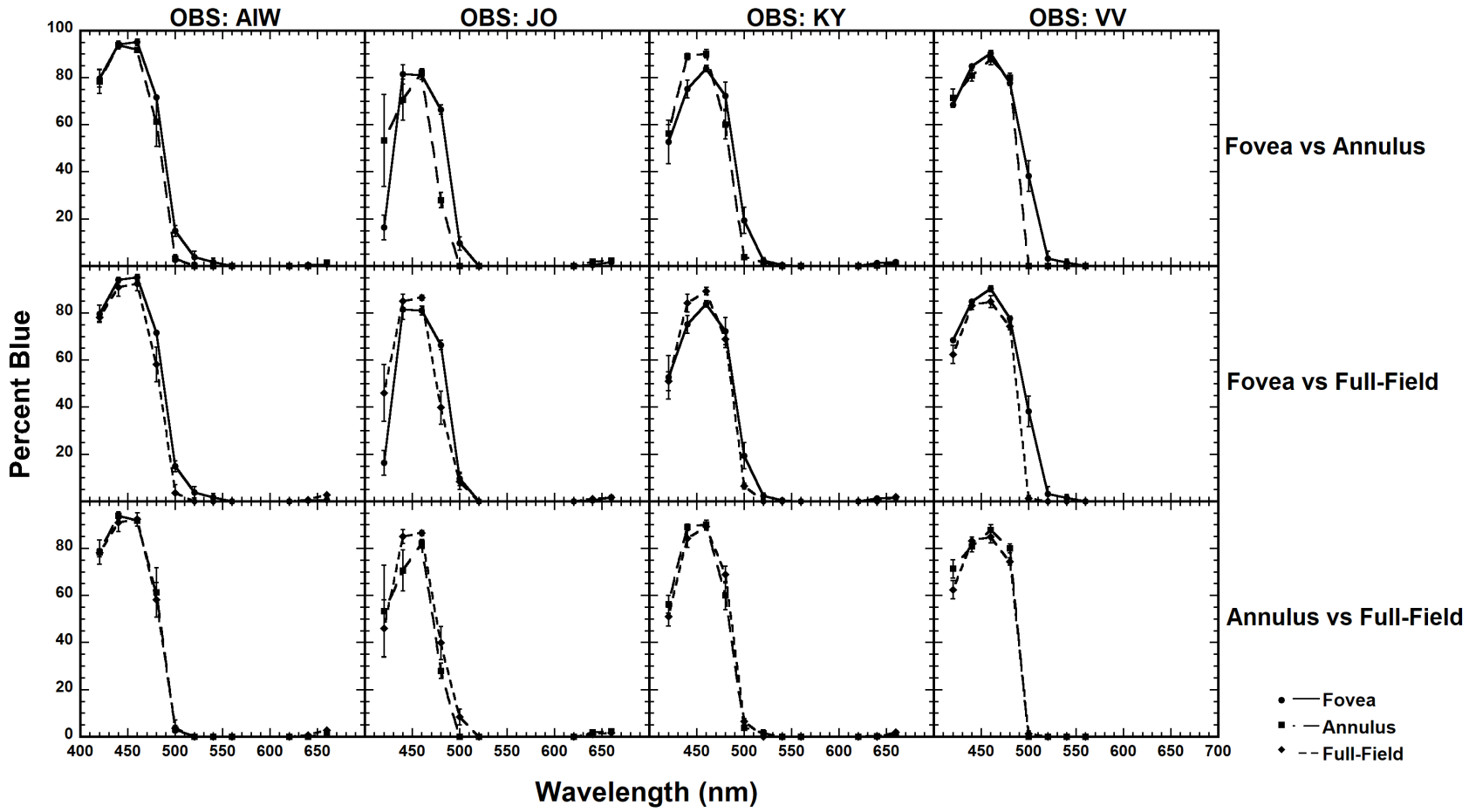

Figure 3.1. Percent blue is plotted as a function of wavelength for the 1° foveal (solid line and circle symbols), 23° annular (long-dashed line and square symbols), and 23° full-field (short-dashed line and diamond symbols) conditions. The error bars represent ±1 standard error of the mean (SEM) across sessions. The top row of panels compares percent blue obtained with the 1° fovea stimulus to that obtained with the 23° annulus for each observer, the middle row of panels compares percent blue obtained with the 1° fovea to that obtained with the full-field, and the bottom panel row of panels compares percent blue obtained with the 23° annulus to that obtained with the 23° full-field stimulus.

Table 3.1. Sum and mean absolute deviations of percent blue between two stimulus conditions for each observer.

Observer	Comparison	N*	Sum	Mean
	Blue Hue:			
AIW	23° Full Field - 1° Fovea	9	39.64	4.40
	23° Full Field - 23° Annulus	7	8.98	1.28
JO	23° Full Field - 1° Fovea	7	67.37	9.62
	23° Full Field - 23° Annulus	7	47.79	6.83
KY	23° Full Field - 1° Fovea	9	36.07	4.01
	23° Full Field - 23° Annulus	8	24.75	3.09
VV	23° Full Field - 1° Fovea	7	58.02	8.29
	23° Full Field - 23° Annulus	5	21.15	4.23

*N denotes the number of wavelengths at which there were hue-scaling responses for both stimulus conditions.

Similar to Figure 3.1, Figure 3.2 (percent green) shows that the 23° annular stimuli appear similar to the 23° full-field stimuli, and less like the 1° foveal counterpart. For all four observers, there was a portion of the spectrum around 500 nm where both 23° stimuli conditions generate a higher percent green than the 1° foveal stimulus. Overall, three of the four observers (AIW, KY, VV) show non-overlapping SEM values between the foveal stimulus and annulus for 500 and 520 nm. At least three observers show this between the foveal and full-field stimuli from 460 to 500 nm. Between the two 23° stimuli at 520 nm, three observers (AIW, KY, VV) show non-overlapping values; however, unlike the comparison to the foveal stimulus, there is no agreement across these three observers for which stimulus (annulus or full-field) appears most green. In Table 3.2, the absolute mean deviations are smaller between the 23° full-field stimulus and the 23° annulus than the absolute mean deviation between the 23° full-field stimulus and 1° foveal conditions across participants. Mean absolute differences between comparisons are within ±1% for JO and KY, although the full-field stimuli appeared approximately 30% more green than the fovea at 480 nm for JO and 18% more green at 500 nm for KY.

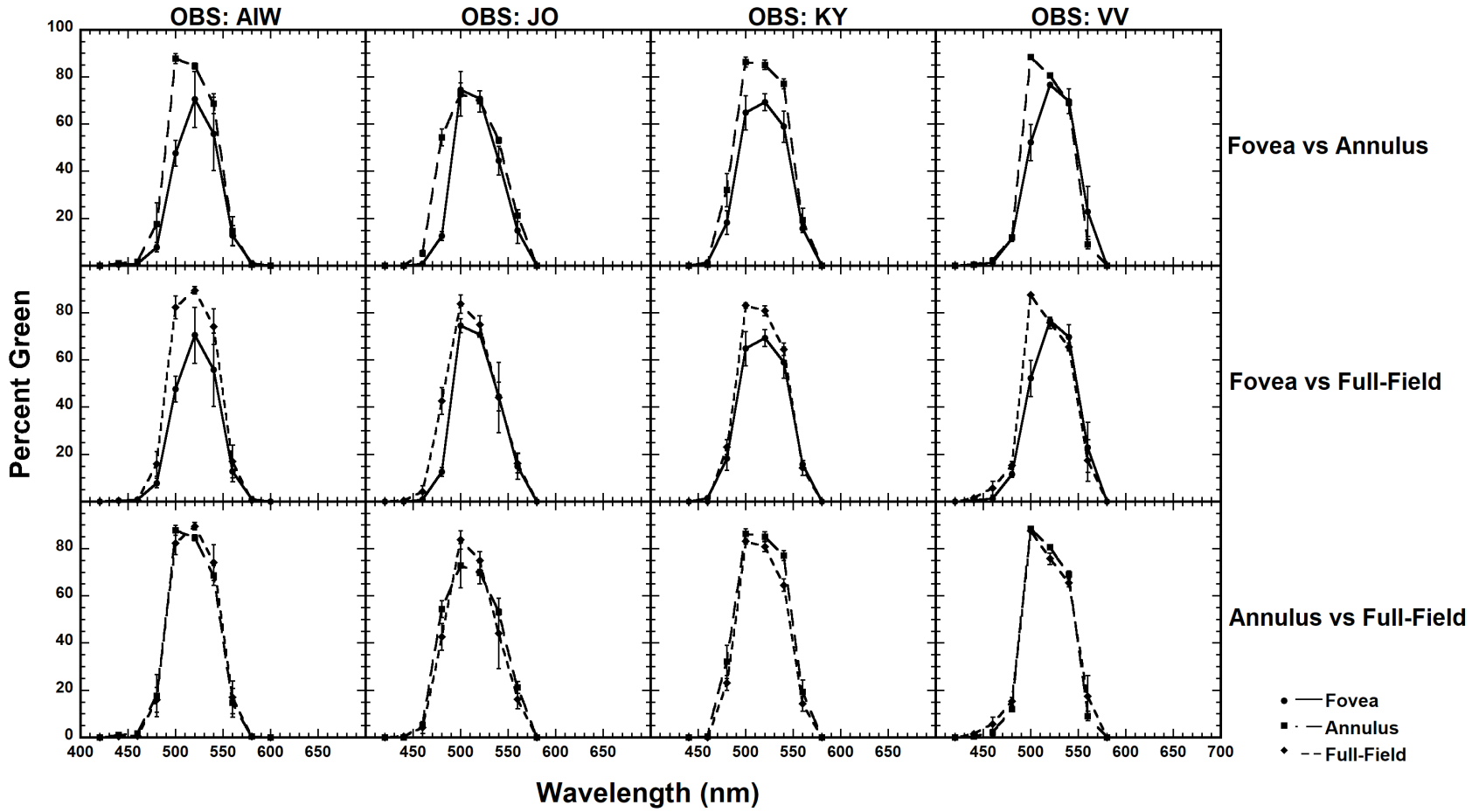

Figure 3.2. Same as Figure 3.1, except for percent green.

Table 3.2. Sum and mean absolute deviations of percent green between two stimulus conditions for each observer.

Observer	Comparison	N*	Sum	Mean
	Green Hue:			
AIW	23° Full Field - 1° Fovea	8	85.11	10.64
	23° Full Field - 23° Annulus	8	21.46	2.68
JO	23° Full Field - 1° Fovea	7	48.92	6.99
	23° Full Field - 23° Annulus	7	43.11	6.16
KY	23° Full Field - 1° Fovea	6	42.93	7.16
	23° Full Field - 23° Annulus	6	34.34	5.72
VV	23° Full Field - 1° Fovea	7	55.09	7.87
	23° Full Field - 23° Annulus	7	25.9	3.70

*N denotes the number of wavelengths at which there were hue-scaling responses for both stimulus conditions.

For percent yellow (Figure 3.3), there is less agreement across observers than there was for percent blue or green between the two 23° stimuli. For two observers (AIW and JO), longer wavelengths (only 600 nm for JO) appeared more yellow for stimuli that activated the peripheral retinal than those that activated just the fovea; however, the fovea had a greater peak percent yellow than the annulus condition. For the VV, the shorter wavelengths appeared more yellow for stimuli that activated the peripheral retina than the foveal stimulus. Overall, the only condition where data were not overlapping for at least three observers was at 500 nm between the foveal stimulus (lower percent yellow) and both of the 23° stimuli (higher percent yellow). With the exception of observer JO, all of the observers demonstrated smaller mean absolute differences between the 23° full-field and 23° annulus conditions than between the 23° full field and 1° foveal conditions (see Table 3.3). AIW, JO, and KY show mean absolute difference values within ±1% between both comparison values. Overall, the data for yellow are inconclusive whether one region of the retina determines hue appearance.

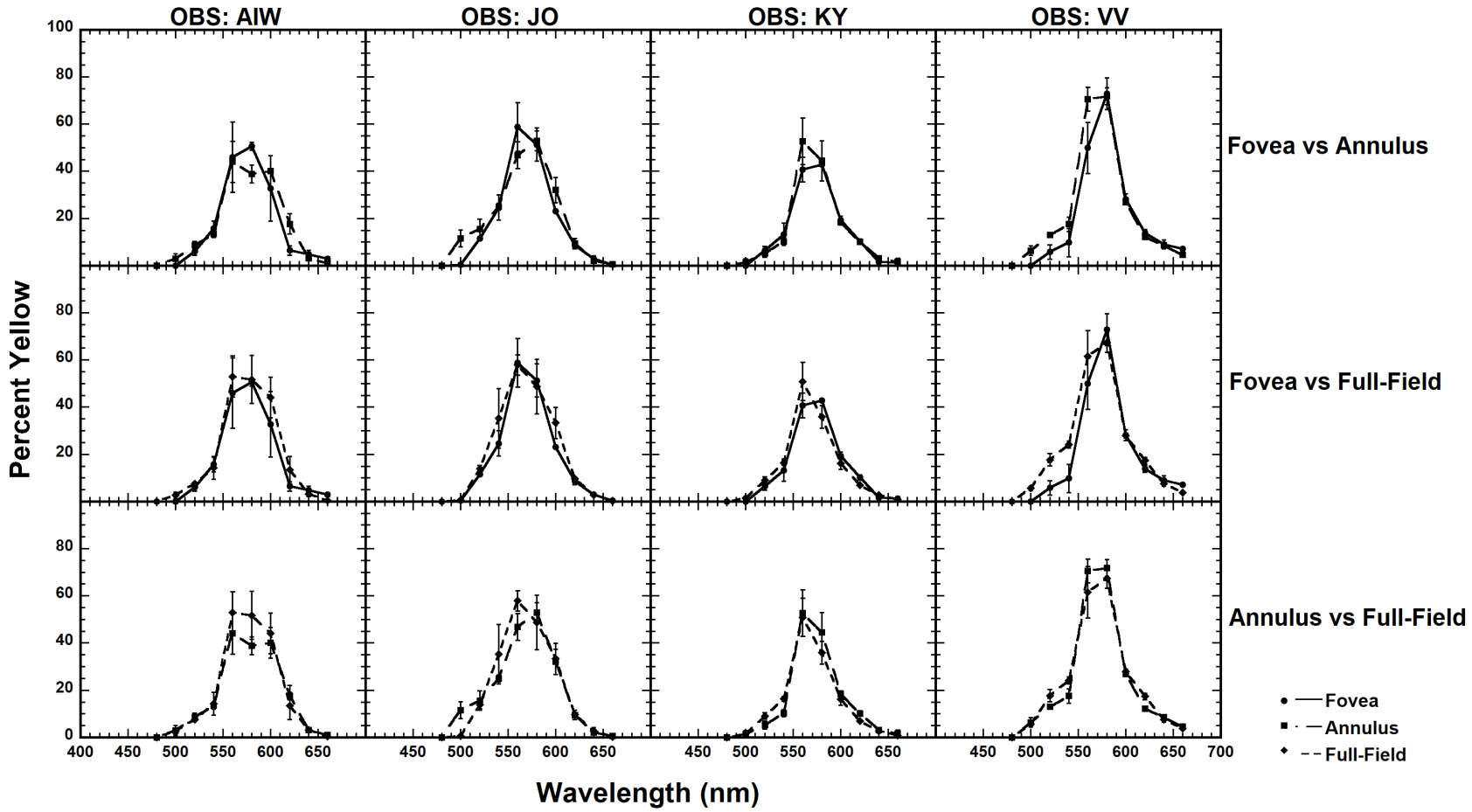

Figure 3.3. Same as Figure 3.1, except for percent yellow.

Table 3.3. Sum and mean absolute deviations of percent yellow between two stimulus conditions for each observer.

Observer	Comparison	N*	Sum	Mean
	Yellow Hue:			
AIW	23° Full Field - 1° Fovea	9	36.4	4.04
	23° Full Field - 23° Annulus	9	33.2	3.69
JO	23° Full Field - 1° Fovea	9	28.34	3.15
	23° Full Field - 23° Annulus	9	40.72	4.52
KY	23° Full Field - 1° Fovea	9	32.09	3.57
	23° Full Field - 23° Annulus	9	27.01	3.00
VV	23° Full Field - 1° Fovea	9	57.61	6.40
	23° Full Field - 23° Annulus	9	33.65	3.74

*N denotes the number of wavelengths at which there were hue-scaling responses for both stimulus conditions.

In Figure 3.4, for all four observers, the 23° stimuli were more similar to each other than the 1° foveal stimulus for percent red. While there were no trends across observers in the differences between hue values of the 1° stimulus and the 23° stimuli, there were individual differences. Overall, the only condition where three of the four observers did not have overlapping data was for the 1° condition compared to the 23° full-field condition. Mean absolute differences of percent red were highest between the 23° full-field stimulus and the 1° foveal stimulus for all observers compared to the 23° annulus and 23° full-field stimulus (see Table 3.4), although the two comparison values were within ±1% of each other for all observers.

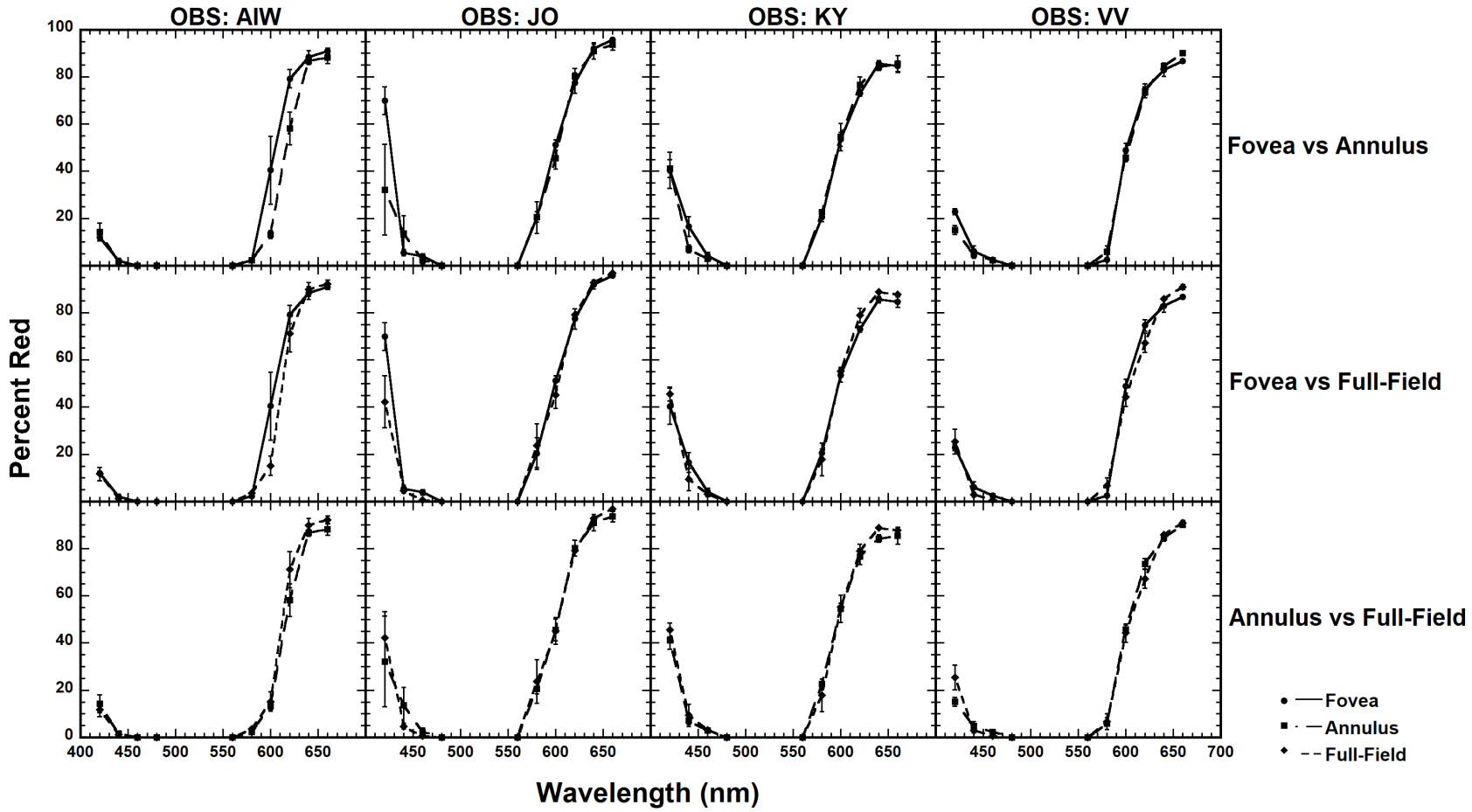

Figure 3.4. Same as Figure 3.1, except for percent red.

Table 3.4. Sum and mean absolute deviations of percent red between two stimulus conditions for each observer.

Observer	Comparison	N*	Sum	Mean
	Red Hue:			
AIW	23° Full Field - 1° Fovea	8	38.5	4.81
	23° Full Field - 23° Annulus	8	26.48	3.31
JO	23° Full Field - 1° Fovea	8	44.94	5.62
	23° Full Field - 23° Annulus	8	30.51	3.81
KY	23° Full Field - 1° Fovea	8	30.11	3.76
	23° Full Field - 23° Annulus	8	21.44	2.68
VV	23° Full Field - 1° Fovea	8	31.26	3.91
	23° Full Field - 23° Annulus	8	24.99	3.12

*N denotes the number of wavelengths at which there were hue-scaling responses for both stimulus conditions.

In terms of saturation perception (Figure 3.5), the 23° annulus follows a similar pattern as the 23° full-field stimulus, while the 1° foveal stimulus appears different from the 23° stimuli. For two of the observers (AIW and KY), it appears there are differences between the annulus and full-field stimulus in Figure 3.5; however, many of these have overlapping values (i.e., error bars overlap). The only wavelengths where three or more observers have non-overlapping values are 460 to 540 nm when comparing the fovea to the annulus condition, and 460, 500, 520, and 540 nm when comparing the fovea to the full-field condition. At individual wavelengths, there are no consistent patterns where three or more observers show differences between the annulus and full-field stimulus conditions; however, all four observers show a mean absolute deviation of percent saturation that is smaller for the 23° full-field versus 23° annulus conditions, as opposed to the larger deviations for the 23° full-field versus 1° foveal conditions (see Table 3.5). With the exception of VV, all other observers show mean absolute difference values within ±1% between both comparisons.

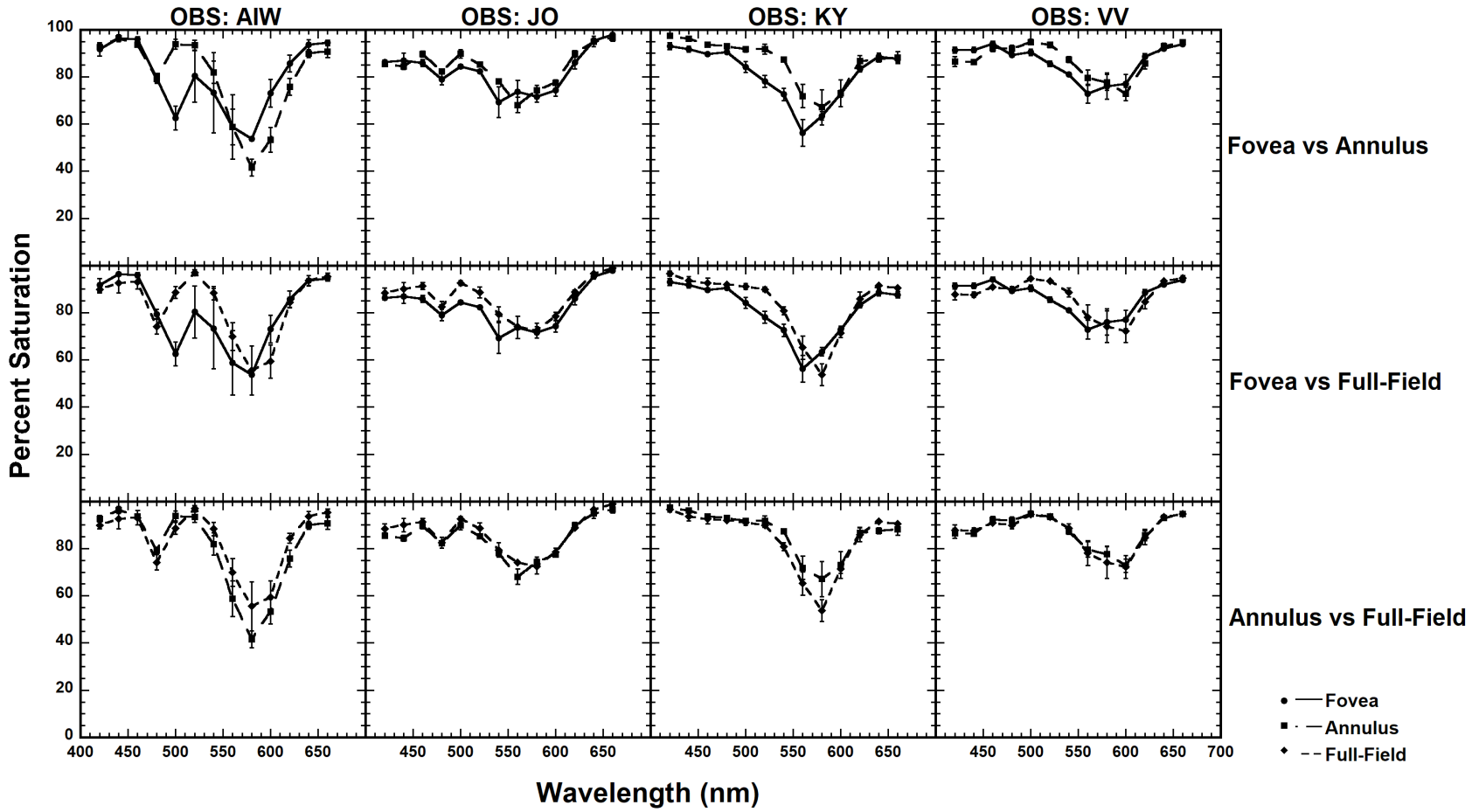

Figure 3.5. Same as Figure 3.1, except for percent saturation.

Table 3.5. Sum and mean absolute deviations of percent saturation between two stimulus conditions for each observer.

Observer	Comparison	N*	Sum	Mean
	Saturation:			
AIW	23° Full Field - 1° Fovea	13	100.45	7.73
	23° Full Field - 23° Annulus	13	75.45	5.80
JO	23° Full Field - 1° Fovea	13	48.99	3.77
	23° Full Field - 23° Annulus	13	31.45	2.42
KY	23° Full Field - 1° Fovea	13	65.13	5.01
	23° Full Field - 23° Annulus	13	43.34	3.33
VV	23° Full Field - 1° Fovea	13	49.01	3.77
	23° Full Field - 23° Annulus	13	14.99	1.15

*N denotes the number of wavelengths at which there were hue-scaling responses for both stimulus conditions.

Figures 3.6 – 3.10 and Tables 3.6 – 3.10 use the same format as Figures 3.1 – 3.5 and Tables 3.6 – 3.10, but present data from the 1° fovea, 35° annulus, and 35° full-field conditions. Percent blue reported with the 35° stimuli in Figure 3.6 are very similar to the 23° data in Figure 3.1, although the error bars are smaller. Two observers show that the foveal stimulus appears more blue than the 35° stimuli; JO shows this specifically at 480 nm, whereas VV shows this at 460 and 500 nm. KY shows the opposite of this, with 440 and 460 nm appearing more blue for the 35° stimuli. Overall, three of the four observers show non-overlapping values at 460 and 480 nm for the 1° stimulus compared to the 35° annulus, and at least three observers have non-overlapping data from 460 to 500 nm when the foveal condition is compared to the 35° full-field condition. Table 3.6 shows that for three of the observers (except AIW, whose comparison values are within ±1% of each other), the mean absolute deviation was smaller between the 35° stimuli and higher between the 35° full-field and 1° stimuli.

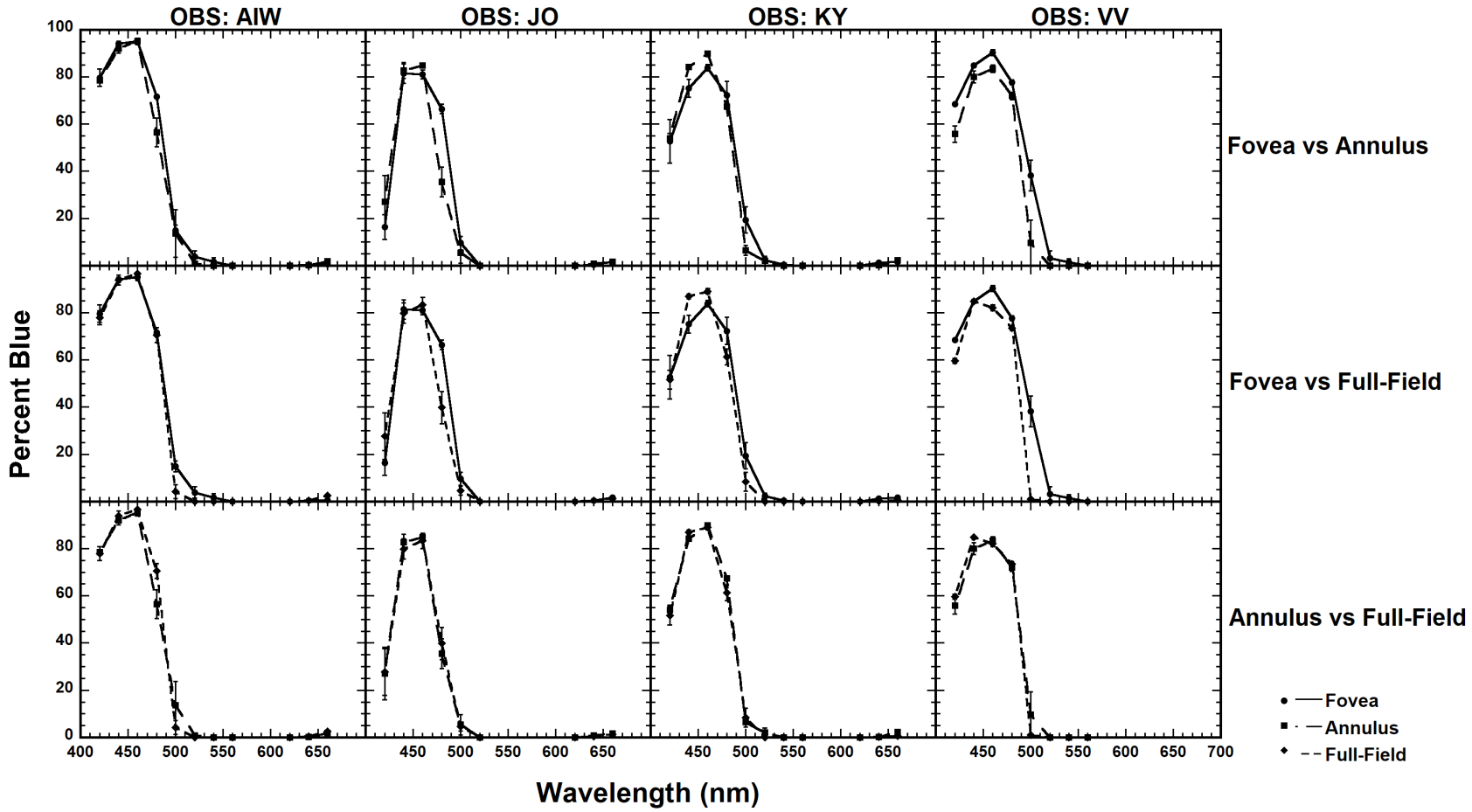

Figure 3.6. Percent blue is plotted as a function of wavelength for the 1° foveal (solid line and circle symbols), 35° annular (long-dashed line and square symbols), and 35° full-field (short-dashed line and diamond symbols) conditions. The error bars represent ±1 standard error of the mean (SEM) across sessions. The top row of panels compares percent blue obtained with the 1° fovea stimulus to that obtained with the 35° annulus for each observer, the middle row of panels compares percent blue obtained with the 1° fovea to that obtained with the full-field, and the bottom panel row of panels compares percent blue obtained with the 35° annulus to that obtained with the 35° full-field stimulus.

Table 3.6. Sum and mean absolute deviations of percent blue between two stimulus conditions for each observer.

Observer	Comparison	N*	Sum	Mean
	Blue Hue:			
AIW	35° Full Field - 1° Fovea	8	22.7	2.84
	35° Full Field - 35° Annulus	8	29.2	3.65
JO	35° Full Field - 1° Fovea	7	47.03	6.72
	35° Full Field - 35° Annulus	7	10.73	1.53
KY	35° Full Field - 1° Fovea	9	44.54	4.95
	35° Full Field - 35° Annulus	7	17.48	2.50
VV	35° Full Field - 1° Fovea	7	63.03	9.00
	35° Full Field - 35° Annulus	5	20.05	4.01

*N denotes the number of wavelengths at which there were hue-scaling responses for both stimulus conditions.

For percent green, (Figure 3.7), there are many individual differences, especially compared to the patterns seen in Figure 3.2 with the 23° stimuli. One aspect that was generally consistent for at least three of the four observers is that the 35° conditions had a higher percent green from approximately 480 to 540 nm than the foveal condition. Additionally, three observers (except KY) showed that the full-field stimulus appeared more green than the annulus at 500 nm. When looking closer at the SEM overlap, at least three observers show no overlap between the 1° stimulus and the 35° annulus for 480 and 520 nm. Four observers show no overlapping data points from 480 to 520 nm between the 1° and 35° full-field stimuli, and at least three observers show no overlap between the annulus and full-field stimuli at 480, 500, and 540 nm. Table 3.7 demonstrates that the mean absolute deviation between the 35° full-field and 35° annulus is smaller than the mean absolute deviation between the 35° full-field and the 1° stimulus for all four observers, with no comparison values within ±1%.

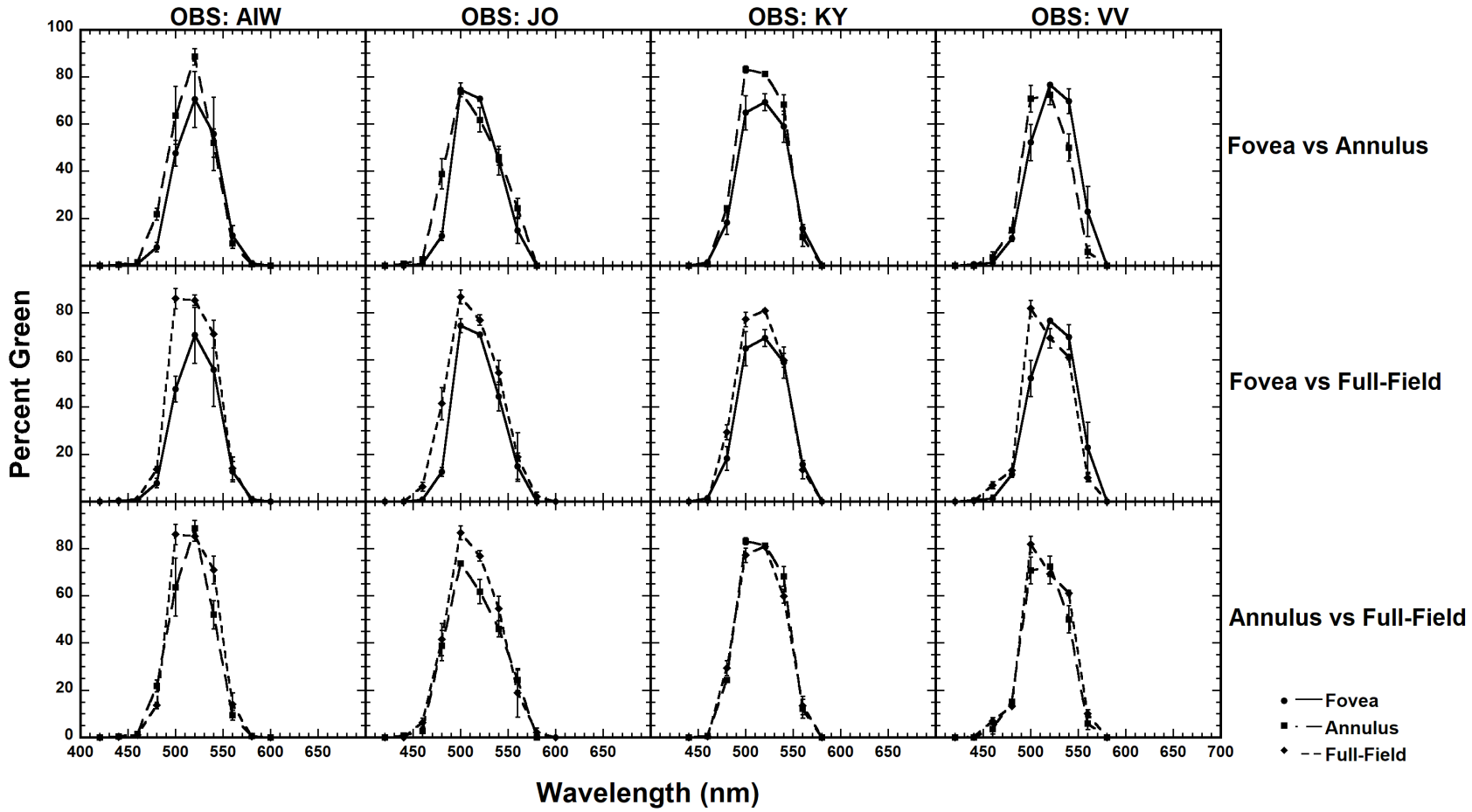

Figure 3.7. Same as Figure 3.6, except for percent green.

Table 3.7. Sum and mean absolute deviations of percent green between two stimulus conditions for each observer.

Observer	Comparison	N*	Sum	Mean
	Green Hue:			
AIW	35° Full Field - 1° Fovea	8	76.22	9.53
	35° Full Field - 35° Annulus	8	58.05	7.26
JO	35° Full Field - 1° Fovea	7	68.7	9.81
	35° Full Field - 35° Annulus	8	51.1	6.39
KY	35° Full Field - 1° Fovea	6	39.2	6.53
	35° Full Field - 35° Annulus	6	21.5	3.58
VV	35° Full Field - 1° Fovea	7	66.15	9.45
	35° Full Field - 35° Annulus	7	35.11	5.02

*N denotes the number of wavelengths at which there were hue-scaling responses for both stimulus conditions.

For the 35° stimuli that appeared yellowish (Figure 3.8), there were differences between all three stimulus comparisons. For three of the four observers (except KY), the foveal stimulus had a higher percent yellow than the annulus at around 560 to 580 nm. For those same three observers, the full-field stimulus appeared more yellow than the annulus from a range of approximately 500 to 600 nm, depending on the individual observer. Table 3.8 shows that for three of the four observers (except JO), mean absolute difference values were lower between the 35° stimulus conditions than between the 35° full-field and foveal stimulus. Both comparison values were within ±1% for KY, although the full-field stimulus appeared approximately 12% more yellow at 560 nm than the foveal stimulus.

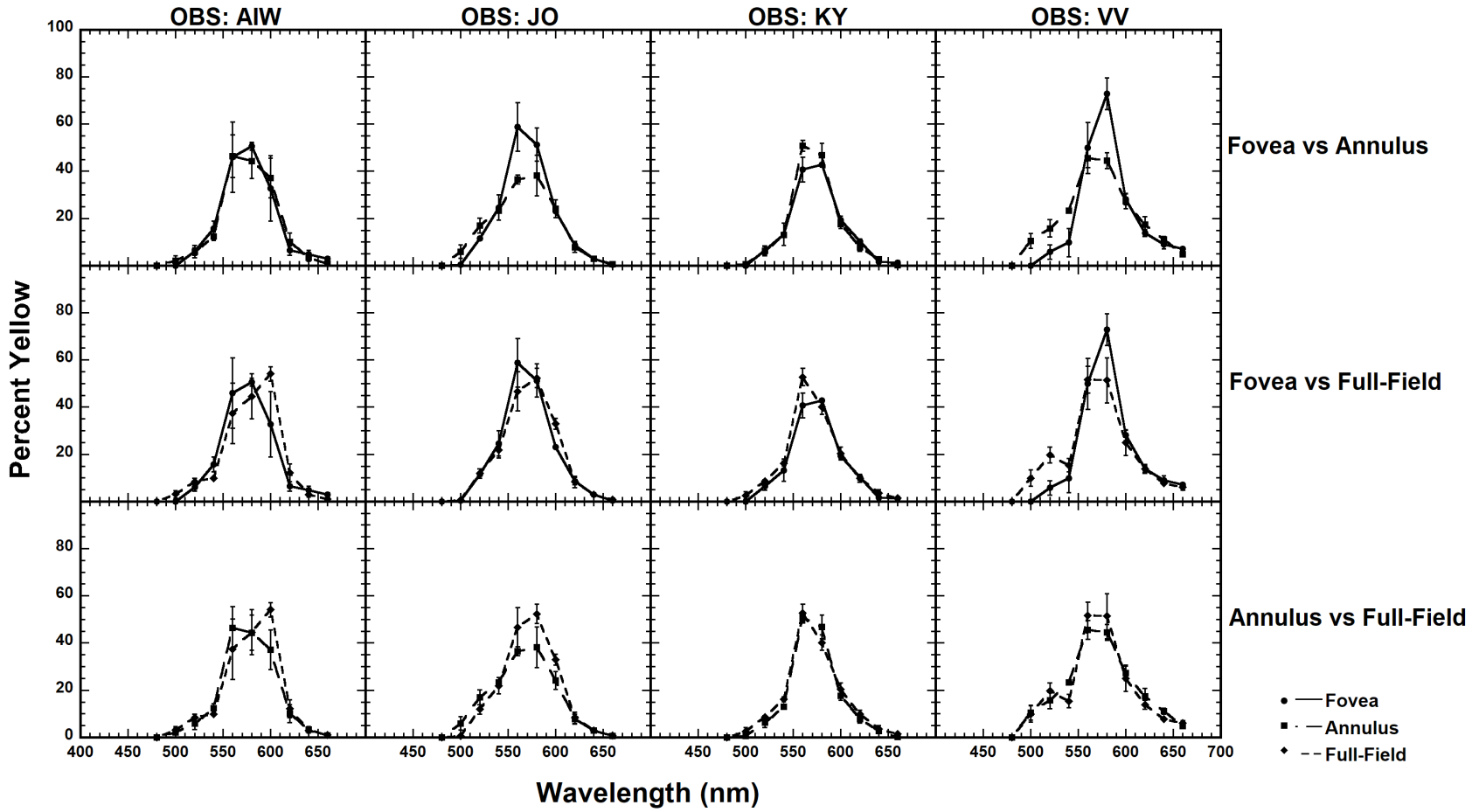

Figure 3.8. Same as Figure 3.6, except for percent yellow.

Table 3.8. Sum and mean absolute deviations of percent yellow between two stimulus conditions for each observer.

Observer	Comparison	N*	Sum	Mean
	Yellow Hue:			
AIW	35° Full Field - 1° Fovea	9	56.7	6.30
	35° Full Field - 35° Annulus	9	34.8	3.86
JO	35° Full Field - 1° Fovea	9	27.1	3.01
	35° Full Field - 35° Annulus	9	45.8	5.09
KY	35° Full Field - 1° Fovea	9	25.72	2.86
	35° Full Field - 35° Annulus	9	23.09	2.57
VV	35° Full Field - 1° Fovea	9	58.26	6.47
	35° Full Field - 35° Annulus	9	35.63	3.96

*N denotes the number of wavelengths at which there were hue-scaling responses for both stimulus conditions.

For the red 35° stimuli (Figure 3.9), there are few differences between the conditions among observers. Figure 3.9 shows that there are only two comparisons where three of the four observers had data that were non-overlapping – 600 nm (35° full-field vs 1°) and 580 nm (35° full-field and 35° annulus). Table 3.9 shows the mean absolute deviations were lowest for three observers (except KY) between the 35° full-field and 35° annulus, while the mean absolute deviation between the 35° full-field and 1° fovea were higher across observers. For all observers, comparison values were within ±1% of each other.

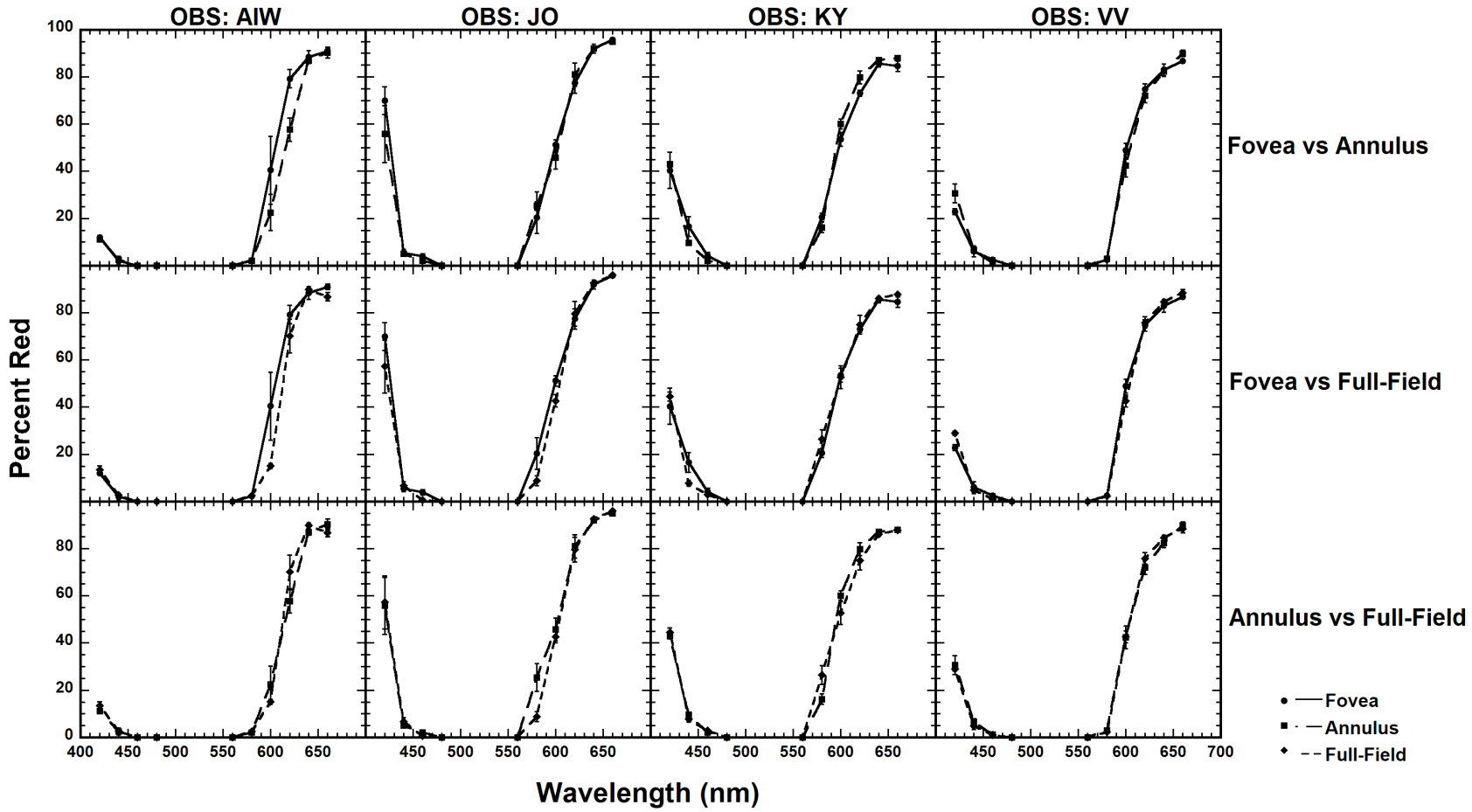

Figure 3.9. Same as Figure 3.6, except for percent red.

Table 3.9. Sum and mean absolute deviations of percent red between two stimulus conditions for each observer.

Observer	Comparison	N*	Sum	Mean
	Red Hue:			
AIW	35° Full Field - 1° Fovea	7	42.4	6.06
	35° Full Field - 35° Annulus	7	29.2	4.17
JO	35° Full Field - 1° Fovea	8	40.1	5.01
	35° Full Field - 35° Annulus	8	27.6	3.45
KY	35° Full Field - 1° Fovea	8	26.63	3.33
	35° Full Field - 35° Annulus	8	28.11	3.51
VV	35° Full Field - 1° Fovea	8	19.96	2.50
	35° Full Field - 35° Annulus	8	12.73	1.59

*N denotes the number of wavelengths at which there were hue-scaling responses for both stimulus conditions.

In general, consistent patterns emerged for at least three of the four observers (except KY) for percent saturation (Figure 3.10) across the various experimental conditions. Three of the four observers (except KY) showed a range of wavelengths (from approximately 540 to 600 nm) where the 1° foveal stimulus was more saturated than the 35° annulus. In the comparison between the 1° foveal stimulus and the 35° full-field stimulus, this dip in saturation was still observed, although the wavelength range was slightly reduced across observers. With the 35° full-field stimulus, all four observers showed a portion of the visible spectrum where there is a bump in percent saturation (from approximately 480 to 540 nm) that exceeds that of the 1° foveal stimulus. This saturation bump is present in the 35° annulus condition as well, but is much less pronounced than in the 35° full-field condition. Between the two 35° stimuli, all four observers show that the annulus is less saturated than the full-field stimulus in the area associated with the minimum (approximately 520 to 600 nm). Overall, at least three observers had non-overlapping data between the 1° stimulus and 35° annulus at 420, 460, and 520 nm. Non-overlapping data (i.e., error bars ±1 SEM do not overlap) was present for at least three observers at 460, 500, 520,

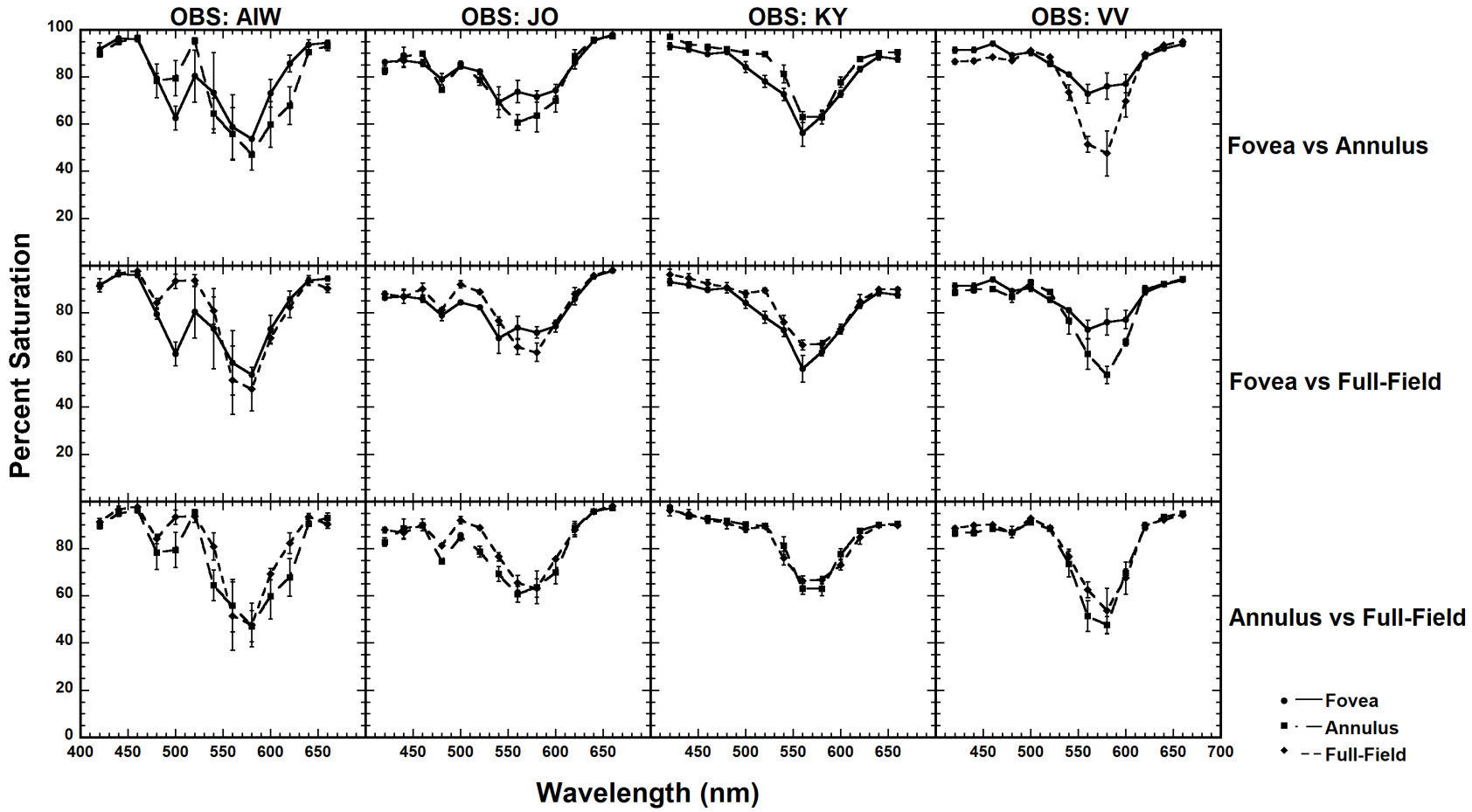

Figure 3.10. Same as Figure 3.6, except for percent saturation.

and 560 nm between the 1° stimulus and 35° full-field stimulus. All four observers had non-overlapping data at 500 nm for the comparison between the 35° annulus and full-field stimuli. With the exception of JO, the other three observers show lower mean absolute difference values (Table 3.10) between the 35° full-field stimulus and 35° annulus, and higher mean absolute difference values between the 35° full-field and 1° foveal stimuli. AIW, JO, and KY show comparison values within 1% of each other, although AIW shows foveal stimuli appeared approximately 31% less saturated than full-field stimuli at 500 nm.

Table 3.10. Sum and mean absolute deviations of percent saturation between two stimulus conditions for each observer.

Observer	Comparison	N*	Sum	Mean
	Saturation:			
AIW	35° Full Field - 1° Fovea	13	83.66	6.44
	35° Full Field - 35° Annulus	13	76.9	5.92
JO	35° Full Field - 1° Fovea	13	50.32	3.87
	35° Full Field - 35° Annulus	13	51.22	3.94
KY	35° Full Field - 1° Fovea	13	46.32	3.56
	35° Full Field - 35° Annulus	13	25.34	1.95
VV	35° Full Field - 1° Fovea	13	65.42	5.03
	35° Full Field - 35° Annulus	13	33.89	2.61

*N denotes the number of wavelengths at which there were hue-scaling responses for both stimulus conditions.

Spatial Integration

The main purpose of this study was to investigate which region(s) of the retina is (are) responsible for determining the color appearance of large fields. The majority of the data, as presented in the previous figures, indicates that the peripheral retina determines full-field hue perception. The question remains, however, as to whether a particular area in the peripheral retina determines hue perception or if the visual system is averaging/integrating across the retina. To investigate this, participants viewed 3° test stimuli placed at 10° retinal eccentricity in either

the temporal, nasal, inferior or superior retinas. In Figures 3.11 – 3.14 (3.15), percent hue (saturation) is plotted as a function of wavelength for three observers (AIW, KY, VV). As with the previous figures, each row of panels represents a different comparison. In the top row of panels, hue responses from 3° stimuli located on the vertical meridian (inferior and superior retinas) are compared with hue responses from the 23° annulus. The middle row of panels represents 3° stimuli hue responses obtained from the horizontal meridian (nasal and temporal retina) compared with hue responses obtained from the 23° annulus condition, and the bottom row of panels represents hue responses obtained with the 23° annulus compared to the mean of the 3° stimuli at all four retinal locations (inferior, superior, nasal, and temporal retinas). Error bars represent ±1 SEM. Similar to above, Tables 3.11– 3.15 provide a closer look at the similarities between retinal locations and the 23° annular stimulus by showing mean absolute differences between various stimulus conditions.

In Figure 3.11, VV shows that the 3° superior percent blue is lower than the 3° inferior and 23° annulus percent blue values at short wavelengths (i.e., 400 to 420 nm), while the other two observers show very little difference between stimuli on the vertical meridian. On the horizontal meridian, both AIW (400 to 420 nm) and KY (420 to 440 nm) show that percent blue is lower in the temporal retina, while VV (400 to 420 nm) shows that percent blue is lower for the nasal condition. When comparing the mean of the four 3° locations, all three observers show the four location mean as being less blue at some point (varies for each observer) in the visible spectrum than the 23° annulus. While Table 3.11 shows the lowest mean absolute deviation values are between the annulus and nasal retina for AIW, superior retina for KY, and temporal retina for VV, many comparison values are within ±1% of the lowest mean absolute deviations for all observers (except VV's superior, nasal, and 4-location mean).

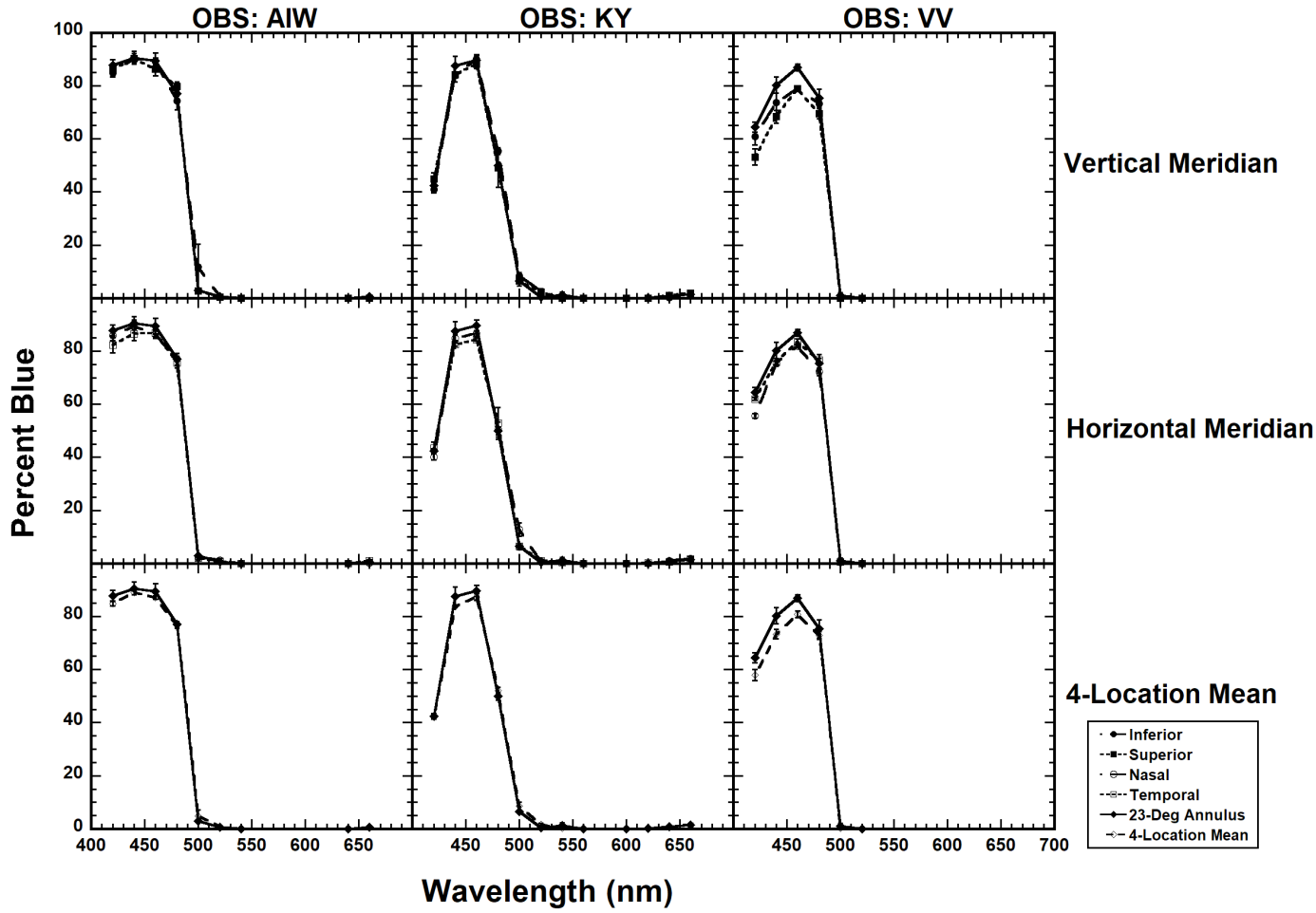

Figure 3.11. Percent blue is plotted as a function of wavelength for the 23° annulus (solid line and diamond symbols), 3° inferior (long-dashed line and circle symbols), 3° superior (short-dashed line and square symbols), 3° nasal (long-dashed line and open circle symbol), 3° temporal (short-dashed line and open square symbols), and mean of the four 3° locations (dashed line and open diamond symbols). The error bars represent ±1 SEM.

Table 3.11. Sum and mean absolute deviations of percent blue between two stimulus conditions for each observer.

Observer	Comparison	N*	Sum	Mean
	Blue Hue:			
AIW	Annulus - Inferior	7	15.63	2.23
	Annulus - Superior	7	8.57	1.22
	Annulus - Nasal	7	7.77	1.11
	Annulus - Temporal	7	15.15	2.16
	Annulus - 4 Location Mean	7	9.27	1.32
KY	Annulus - Inferior	10	17.09	1.71
	Annulus - Superior	10	12.12	1.21
	Annulus - Nasal	10	16.87	1.69
	Annulus - Temporal	10	16.16	1.62
	Annulus - 4 Location Mean	10	12.76	1.28
VV	Annulus - Inferior	5	21.2	4.24
	Annulus - Superior	5	38.12	7.62
	Annulus - Nasal	5	22.12	4.42
	Annulus - Temporal	5	11.93	2.39
	Annulus - 4 Location Mean	5	22.7	4.54

*N denotes the number of wavelengths at which there were hue-scaling responses for both stimulus conditions.

For stimuli where the perception of greenness was reported (Figure 3.12), KY (500 to 540 nm) and VV (520 to 660 nm) show the 3° stimulus in the superior retina appeared the least green in comparison to the inferior retina and annulus. On the horizontal meridian, all three observers show a portion of the visible spectrum (approximately 540 nm) where the lowest percent of green is reported in the temporal retina condition. AIW and KY show the four location mean percent green to be lower from 500 to 540 nm than the annulus, and VV shows this from 520 to 560 nm. Table 3.12 shows that the lowest absolute mean difference values occur between the annulus and superior stimulus for AIW, and between the annulus and inferior retina for KY and VV. The lowest mean absolute deviations are within ±1% of other comparisons for AIW (annulus vs. superior, temporal, and 4-location mean), KY (annulus vs. inferior, superior, and 4-location mean), and VV (annulus vs. inferior, nasal, temporal, and 4-location mean).

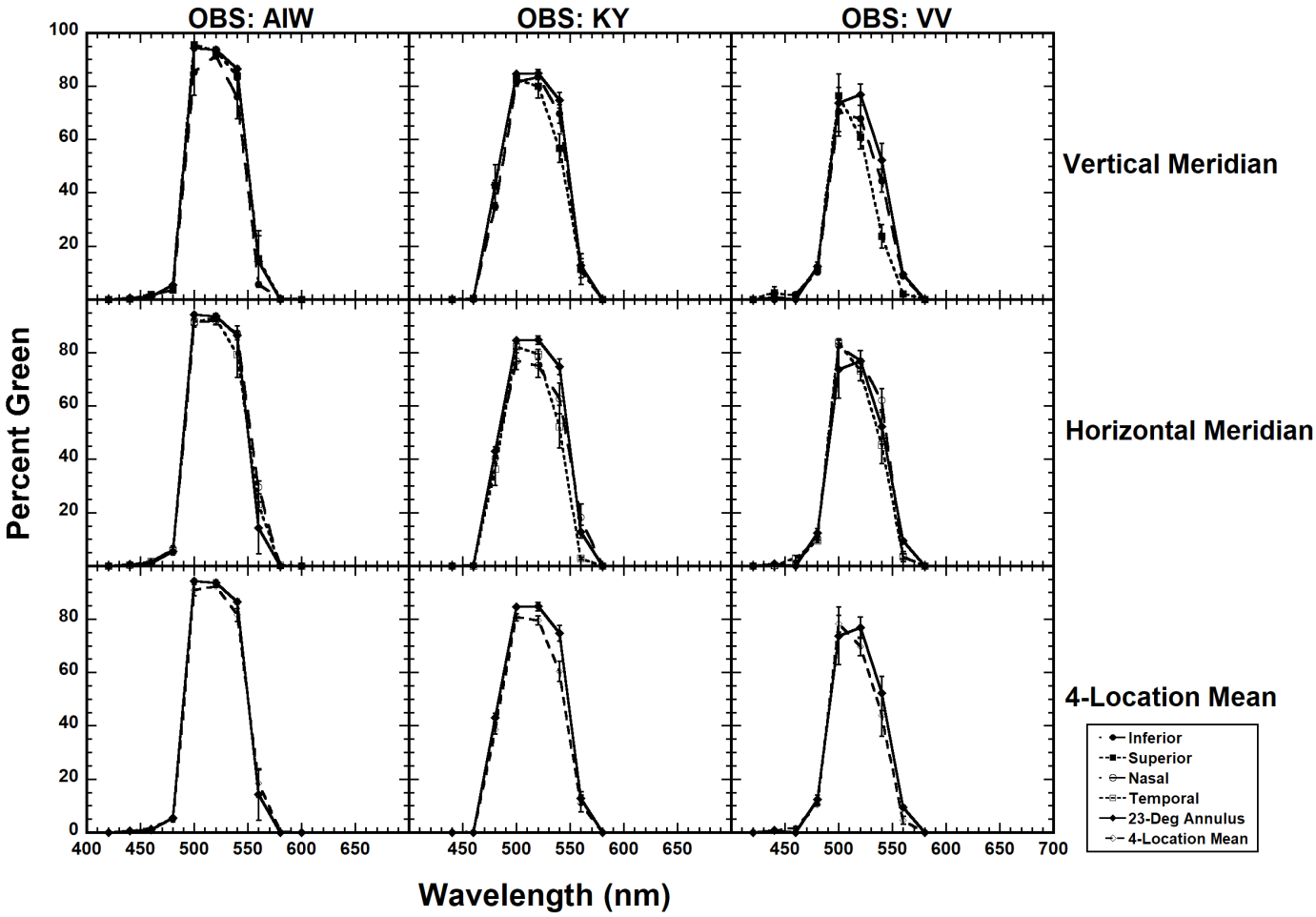

Figure 3.12. Same as Figure 3.11, except for percent green.

Table 3.12. Sum and mean absolute deviations of percent green between two stimulus conditions for each observer.

Observer	Comparison	N*	Sum	Mean
	Green Hue:			
AIW	Annulus - Inferior	8	33.25	4.16
	Annulus - Superior	8	8.75	1.09
	Annulus - Nasal	7	21.92	3.13
	Annulus - Temporal	8	20.88	2.61
	Annulus - 4 Location Mean	8	15.35	1.92
KY	Annulus - Inferior	5	19.26	3.85
	Annulus - Superior	6	26.68	4.45
	Annulus - Nasal	6	37.11	6.19
	Annulus - Temporal	5	46.83	9.37
	Annulus - 4 Location Mean	6	29.84	4.97
VV	Annulus - Inferior	7	25.07	3.58
	Annulus - Superior	7	58	8.29
	Annulus - Nasal	7	28.54	4.08
	Annulus - Temporal	7	32.88	4.7
	Annulus - 4 Location Mean	7	28.75	4.11

*N denotes the number of wavelengths at which there were hue-scaling responses for both stimulus conditions.

In Figure 3.13, VV reports the highest percent yellow with the 3° superior stimulus from 500 to 580 nm when compared to the inferior and annular stimuli (top row). KY shows this as well, at 540 nm. At 560 nm, AIW perceived the stimulus in the inferior retina to have the highest percent yellow compared to the superior and annular stimulus. In the horizontal meridian, all observers report the smallest percent of yellow in the nasal retina when compared to the annular and temporal stimuli, ranging from approximately 540 to 580 nm. KY and VV show that the four location mean is less yellow than the 23° annulus at 560 nm, while AIW shows this at 540 nm. For all observers at shorter wavelengths (540 nm for KY and VV, 520 nm for AIW), the four location mean appears more yellow than the annulus. In Table 3.13, the lowest mean absolute difference value occurred for the superior stimulus for AIW and KY and the temporal stimulus for VV; however, the lowest mean absolute deviations are within ±1% of other comparisons for

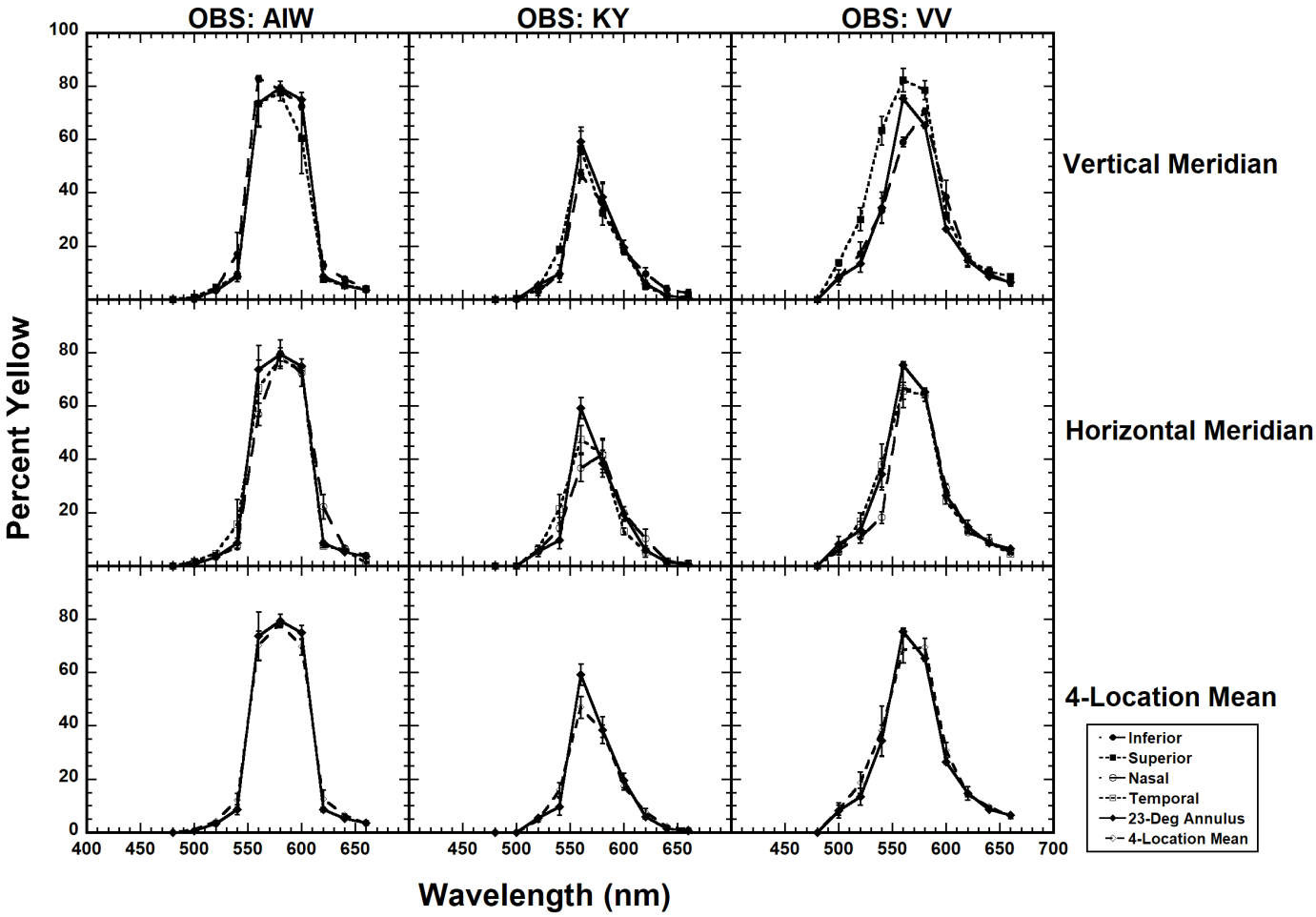

Figure 3.13. Same as Figure 3.11, except for percent yellow.

Table 3.13. Sum and mean absolute deviations of percent yellow between two stimulus conditions for each observer.

Observer	Comparison	N*	Sum	Mean
	Yellow Hue:			
AIW	Annulus - Inferior	9	29.13	3.24
	Annulus - Superior	9	19.8	2.2
	Annulus - Nasal	9	37.29	4.14
	Annulus - Temporal	9	24	2.62
	Annulus - 4 Location Mean	9	19.96	2.22
KY	Annulus - Inferior	8	26.21	3.28
	Annulus - Superior	9	21.52	2.39
	Annulus - Nasal	8	36.25	4.53
	Annulus - Temporal	8	34.72	4.34
	Annulus - 4 Location Mean	9	25.22	2.8
VV	Annulus - Inferior	9	39.92	4.44
	Annulus - Superior	9	80.83	8.98
	Annulus - Nasal	9	37.96	4.22
	Annulus - Temporal	9	25.11	2.79
	Annulus - 4 Location Mean	9	27.06	3.01

*N denotes the number of wavelengths at which there were hue-scaling responses for both stimulus conditions.

AIW (all comparisons), KY (all except nasal), and VV (all except superior), suggesting no one location determines the hue experience.

In Figure 3.14, for AIW (640 to 660 nm) and KY (620 to 660 nm) the inferior stimulus appears the least red in comparison to the annulus and superior stimulus. For stimuli on the horizontal meridian, AIW and KY show the nasal stimulus to appear the least red at 620 nm in comparison to the annulus and temporal stimulus, and as a result, they also show the four location mean to appear less red than the 23° annulus from 640 to 660 nm for AIW and from 620 to 660 nm for KY. Table 3.14 shows that AIW and VV had lowest absolute mean deviations between the temporal and annulus conditions, while KY had the lowest between the superior and annulus conditions. The lowest mean absolute deviations are within ±1% of other comparisons for AIW (all but nasal), KY (all but nasal), and VV (all comparisons).

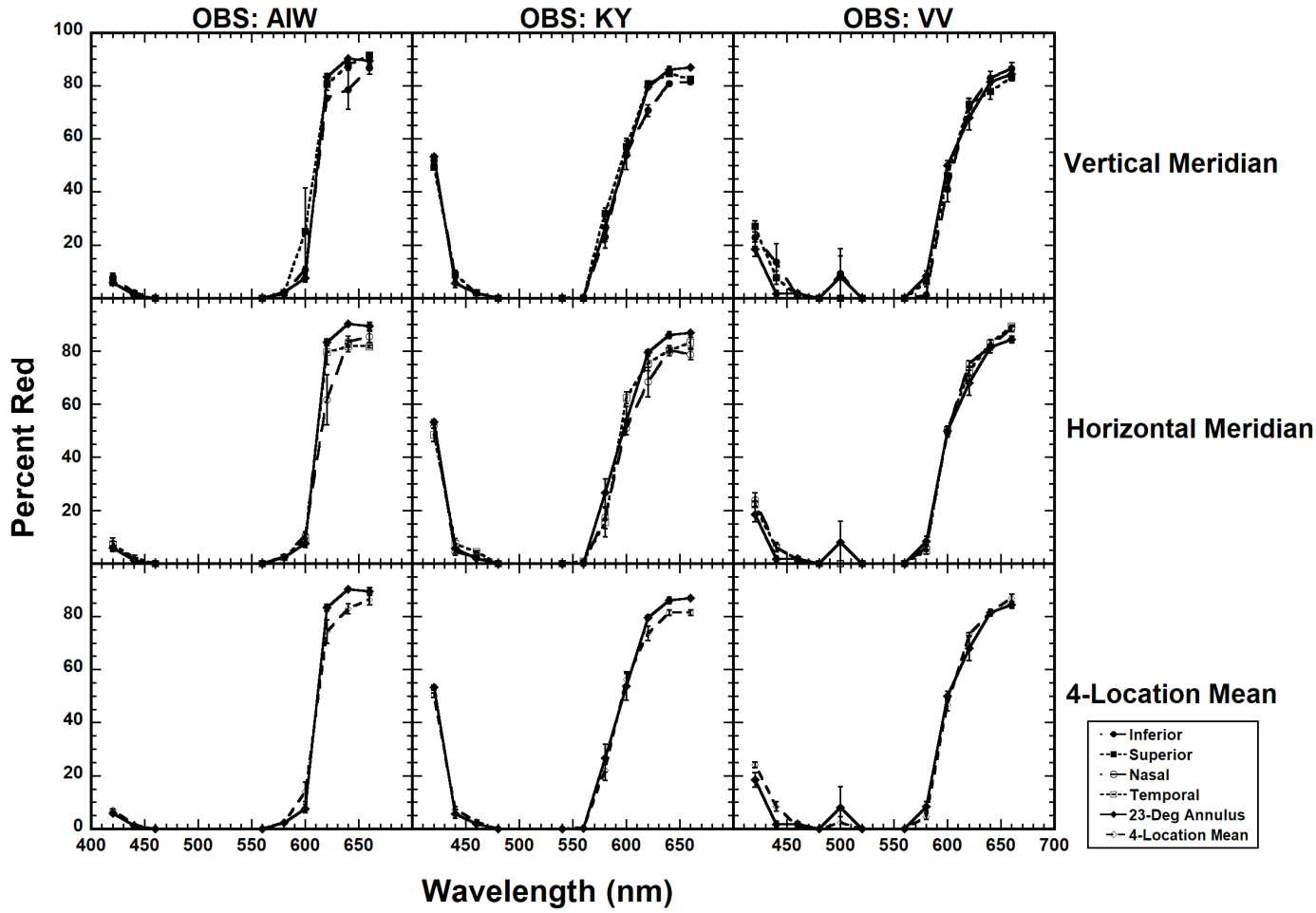

Figure 3.14. Same as Figure 3.11, except for percent red.

Table 3.14. Sum and mean absolute deviations of percent red between two stimulus conditions for each observer.

Observer	Comparison	N*	Sum	Mean
	Red Hue:			
AIW	Annulus - Inferior	7	28.82	4.12
	Annulus - Superior	7	25.74	3.68
	Annulus - Nasal	6	37.11	6.19
	Annulus - Temporal	7	24	3.43
	Annulus - 4 Location Mean	6	27.56	4.59
KY	Annulus - Inferior	9	28.7	3.19
	Annulus - Superior	9	22.82	2.54
	Annulus - Nasal	9	40.95	4.55
	Annulus - Temporal	9	43.47	4.83
	Annulus - 4 Location Mean	9	28.62	3.18
VV	Annulus - Inferior	10	42.59	4.26
	Annulus - Superior	10	39.83	3.98
	Annulus - Nasal	10	33.29	3.33
	Annulus - Temporal	10	31.49	3.15
	Annulus - 4 Location Mean	10	33.87	3.39

*N denotes the number of wavelengths at which there were hue-scaling responses for both stimulus conditions.

Figure 3.15 shows that on the vertical meridian, each observer experienced different conditions which elicited the highest saturation values. AIW shows very little difference between conditions, KY shows that the 23° annular stimulus was generally the most saturated, and VV shows that the 23° annulus was most saturated up until 540 nm, after which point the superior stimulus appeared most saturated. On the horizontal meridian, each observer shows that at different points along the visible spectrum, the 23° annulus appeared most saturated (AIW at longer wavelengths, KY throughout the spectrum, and VV around 560 nm). When comparing the mean of the four retinal locations to the annulus, the annulus appears more saturated for AIW at 620 to 660 nm, KY throughout the visible spectrum, and VV from 440 to 580 nm. In Table 3.15, the lowest mean absolute difference occurred between the 23° annulus and stimuli placed in the

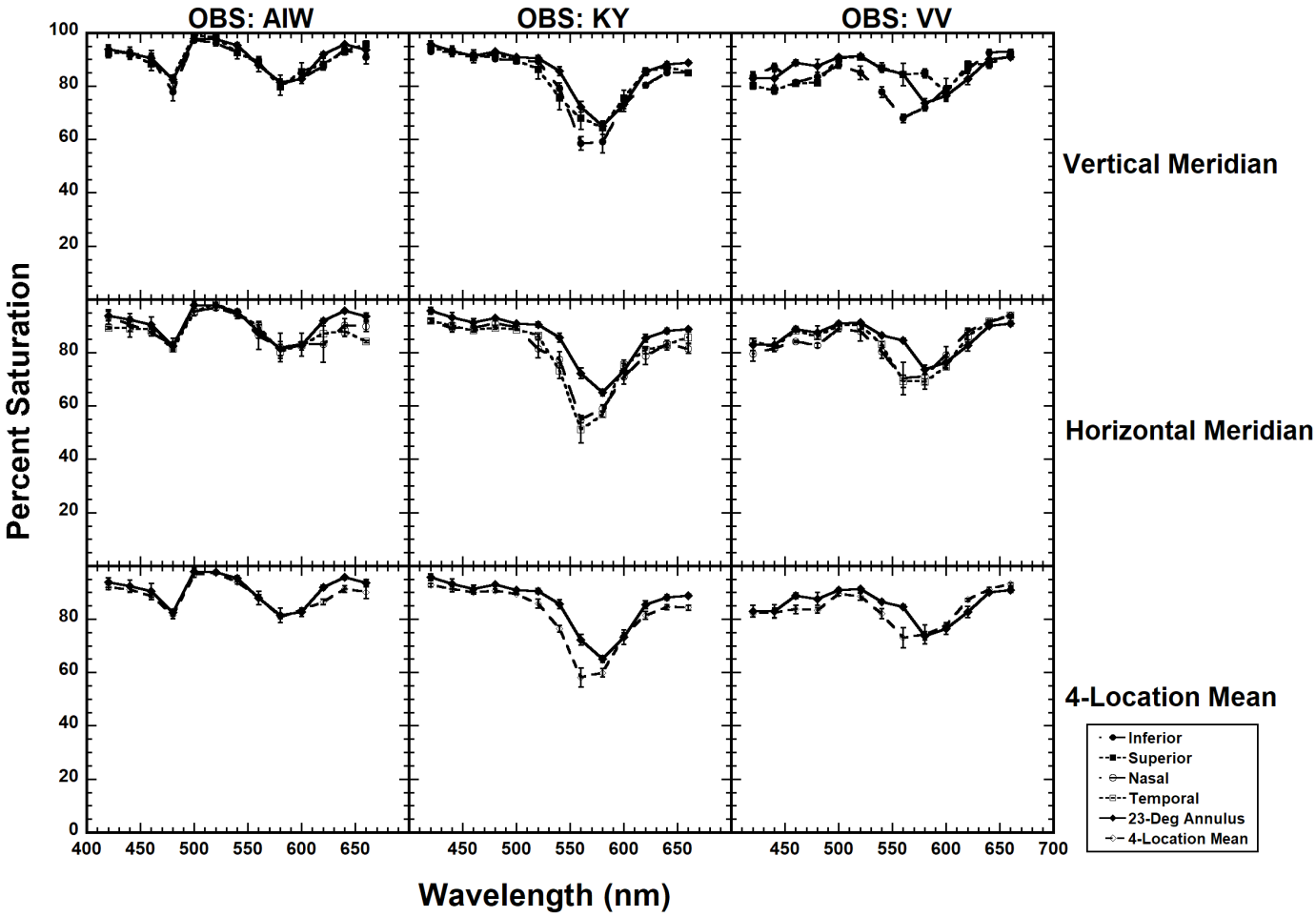

Figure 3.15. Same as Figure 3.11, except for percent saturation.

inferior (AIW), superior (KY), and temporal (VV) retinas; although, the lowest mean absolute deviations are within ±1% of other comparisons for AIW (all comparisons) , KY (all but nasal and temporal), and VV (all comparisons).

Table 3.15. Sum and mean absolute deviations of percent saturation between two stimulus conditions for each observer.

Observer	Comparison	N*	Sum	Mean
	Saturation:			
AIW	Annulus - Inferior	13	21.46	1.65
	Annulus - Superior	13	22.9	1.76
	Annulus - Nasal	13	29.79	2.29
	Annulus - Temporal	13	39.11	3.01
	Annulus - 4 Location Mean	13	23.96	1.84
KY	Annulus - Inferior	13	47.44	3.65
	Annulus - Superior	13	31.1	2.39
	Annulus - Nasal	13	75.21	5.79
	Annulus - Temporal	13	76.66	5.9
	Annulus - 4 Location Mean	13	56.06	4.31
VV	Annulus - Inferior	13	64.01	4.92
	Annulus - Superior	13	43.21	3.32
	Annulus - Nasal	13	54.66	4.2
	Annulus - Temporal	13	40.01	3.08
	Annulus - 4 Location Mean	13	40.62	3.12

*N denotes the number of wavelengths at which there were hue-scaling responses for both stimulus conditions.

CHAPTER 4: DISCUSSION

Fovea vs Peripheral Stimuli

Stimuli in this study were chosen to selectively stimulate the fovea (1° stimulus), the peripheral retina (annular stimuli), and both the fovea and peripheral retina (23° and 35° full field stimuli). The size of the foveal stimulus was the same as that used in previous studies (e.g., Abramov et al., 1991; Nerger et al., 1998; O'Neil and Webster, 2014; Volbrecht and Nerger, 2012) for the purpose of comparison. Two different annular stimuli were used. The 23° outer diameter annulus consisted of a 3° ring of light, which others have shown fills the perceptive fields for blue, yellow and red at 10° retinal eccentricity with rod input. The 35° outer diameter annular stimulus comprised a 15° ring of light which filled the perceptive fields for all four hues at 10° retinal eccentricity with rod input (Volbrecht et al., 2009). The 23° and 35° full-field stimuli served as the large uniform fields that covered both the fovea and the peripheral retina and allowed comparisons between the stimuli positioned purely in the fovea and those in the peripheral retina.

In the present study, the annular stimuli were described by the observers as being more similar to the full-field stimuli than they were to the foveal stimulus. This was most apparent with hues in the short-wavelength region of the visible spectrum (i.e. perceptions of blue and green), where there was more overlap in data points between the annulus and full-field stimuli than there was between the full-field stimuli and the foveal stimulus, indicating the annular stimuli appeared more similar in hue to the full-field stimuli. In the longer wavelength regions of the visible spectrum (i.e. yellows and reds), the differences between the foveal stimulus and the full-field stimuli were less pronounced perhaps due to rods being less sensitive in this portion of the visible spectrum and exerting less of an influence on these hue perceptions. Percent

saturation was also more similar between the annular and full-field stimuli as compared to the 1° foveal stimulus, with 480 – 560 nm stimuli appearing more saturated with the 23° and 35° stimuli than in the fovea, which is consistent with findings from Opper et al. (2014). Other than the range of wavelengths associated with the perception of green (i.e., blue-green, green, and yellow-green), hue percepts in the fovea were more saturated than the full-field and peripheral stimuli, especially at the extremes of the visible spectrum. For the annular stimuli, this is consistent with the findings of Stabell and Stabell (1976) and Abramov et al. (1991), which suggest that stimuli placed in the peripheral retina tend to be less saturated than stimuli in the fovea and near-periphery; however, it does not explain why the large full-field stimuli would share this desaturation effect if the assumption is true that the fovea is responsible for determining the saturation and uniform appearance of stimuli. One plausible explanation for this effect is that rod photoreceptors, which are activated when viewing the full-field and annular stimuli, are contributing to a desaturation effect to the stimuli. One concern is that this desaturation effect observed in the data was exacerbated by the transformation (i.e., scaling to saturation).

Impact of Scaling to Saturation

Since the present study shows differences between saturation values between differing stimulus conditions, one concern is that the differences between hue percents may have been due to the data being scaled to saturation values. The purpose of scaling to saturation is to maintain the hue ratios, while also giving a sense of the chromatic strength of the appearance of the stimuli. For example, if an observer describes a 420 nm stimulus as 80 percent blue and 20 percent red (i.e., a 4:1, blue:red ratio), the plotted hue value depends on the saturation values

reported by the observer. If the observer noted the stimulus appeared 80 percent saturated in one condition, the scaled to saturation values would be 64 percent blue and 16 percent red. If, in another condition, the observer reported the stimulus as 60 percent saturated, the values when scaled to saturation would be 48 percent blue and 12 percent red. While both stimuli have the same raw hue values and hue ratio, the hue values after being scaled to saturation clearly differ. Again, the reason for scaling to the saturation values is to equate for the overall chromatic experience – a hue that is 100 percent red could appear a vibrant red (i.e., 100% saturated), or a dull pink (i.e. 20% saturated), and the differences in chromatic strength would be quite apparent regardless of those stimuli sharing the same hue ratio. In order to investigate whether scaling to saturation was a primary factor in the differences seen between conditions (1° versus both 23° stimuli), figures 4.1 – 4.4 display data that were not scaled to saturation and are comparable to the scaled data that are shown in Figures 3.1 – 3.4. Following each figure (Figures 4.1 – 4.4), a table is included (Tables 4.1 – 4.4) that lists the mean absolute difference between the hue percent of the 23° full-field stimulus and the 1° foveal stimulus, as well as between the hue percent of the 23° full-field stimulus and the 23° annulus for the non-scaled data.

The differences that were present between conditions for percent blue in Figure 3.1 are still present between those same conditions when the data have not been scaled to saturation (Figure 4.1). As would be expected, there is some variability in the magnitude of those differences between conditions when the data are scaled versus not scaled; however, it is clear that scaling to saturation was not responsible for those differences. As with the scaled data (Table 3.1), non-scaled mean absolute deviations (Table 4.1) are smaller for the full-field versus annulus comparisons than for the full-field versus foveal comparisons for all observers and none of the comparison values are within ±1% of each other.

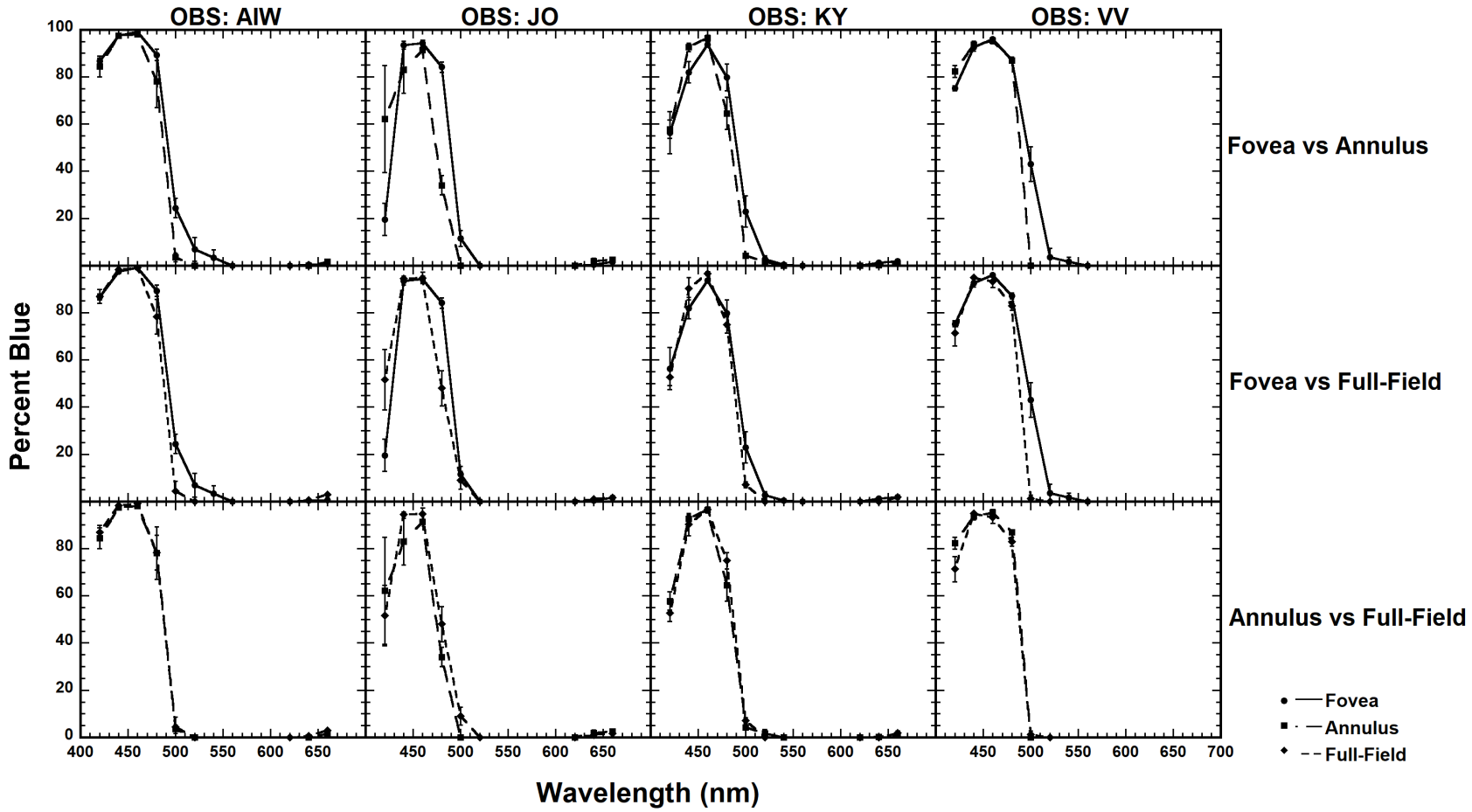

Figure 4.1. Percent blue is plotted as a function of wavelength for the 1° foveal stimulus (solid line and circle symbols), 23° annulus (long-dashed line and square symbols), and 23° full-field stimulus (short-dashed line and diamond symbols) for data that has not been scaled to saturation. The error bars represent ±1 SEM.

Table 4.1. Sum and mean absolute deviations of non-scaled percent blue between two stimulus conditions for each observer.

Observer	Comparison	N*	Sum	Mean
	Blue Hue:			
AIW	23° Full Field - 1° Fovea	8	44.89	5.61
	23° Full Field - 23° Annulus	7	7.33	1.05
JO	23° Full Field - 1° Fovea	7	73.11	10.44
	23° Full Field - 23° Annulus	7	51.22	7.32
KY	23° Full Field - 1° Fovea	8	40.00	5.00
	23° Full Field - 23° Annulus	8	23.44	2.93
VV	23° Full Field - 1° Fovea	7	60.11	8.59
	23° Full Field - 23° Annulus	5	19.67	3.93

*N denotes the number of wavelengths at which there were hue-scaling responses for both stimulus conditions.

For percent green, the impact of scaling to saturation was more pronounced (in terms of reducing the distance between data points of each condition) than it was for percent blue. Figure 4.2, specifically observers AIW and KY, shows that the large differences between the foveal stimulus and the 23° stimuli from 500 to 560 nm are no longer differing by approximately 20% as they were with the data that was scaled to saturation (Figure 3.2). AIW and KY show a pronounced difference between saturation functions (Figure 3.5) in that same region of the visible spectrum (500 to 560 nm). Comparing the data that has been scaled (Figure 3.2) to data that has not been scaled to saturation (Figure 4.2) shows that some of those differences between conditions still exist regardless of scaling; however, the magnitude of those differences is greatly reduced. Some of these differences are apparent in the mean absolute deviation values between scaled data (Table 3.2) and non-scaled data (Table 4.2), where an additional observer (KY) showed less than ±1% difference between comparisons with non-scaled data.

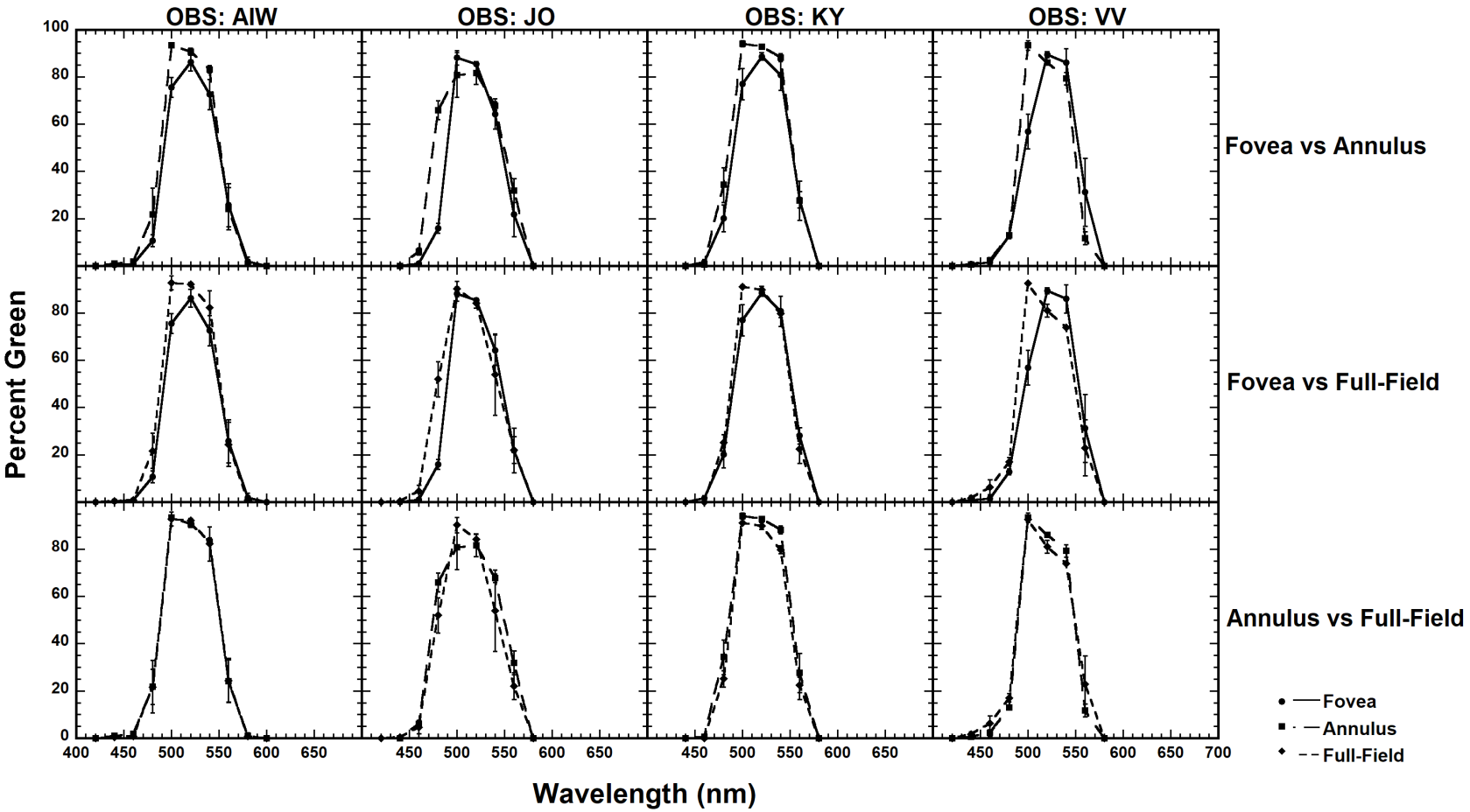

Figure 4.2. Same as figure 4.1, but for percent green.

Table 4.2. Sum and mean absolute deviations of non-scaled percent green between two stimulus conditions for each observer.

Observer	Comparison	N*	Sum	Mean
	Green Hue:			
AIW	23° Full Field - 1° Fovea	7	46.22	6.60
	23° Full Field - 23° Annulus	8	5.56	0.69
JO	23° Full Field - 1° Fovea	7	54.00	7.71
	23° Full Field - 23° Annulus	7	51.22	7.32
KY	23° Full Field - 1° Fovea	6	28.44	4.74
	23° Full Field - 23° Annulus	6	29.00	4.83
VV	23° Full Field - 1° Fovea	7	74.44	10.63
	23° Full Field - 23° Annulus	7	31.56	4.51

*N denotes the number of wavelengths at which there were hue-scaling responses for both stimulus conditions.

For percent yellow, not scaling data to saturation (Figure 4.3) reduces the differences observed between conditions for data that has been scaled to saturation (Figure 3.3). This is most apparent for observers AIW and KY, who showed differences between the peak of the yellow functions for foveal and peripheral stimuli for scaled data (Figure 3.3), but not for non-scaled data (Figure 4.3). The patterns of differences between conditions remains similar between scaled data (Figure 3.3) and non-scaled data (Figure 4.3) for observers JO and VV. Mean absolute deviation values are similar between scaled (Table 3.3) and non-scaled data (Table 4.3), except AIW shows more of a difference and JO shows less of a difference between the comparisons with the non-scaled values (i.e., more than a ±1% difference between comparisons for AIW and less than a ±1% difference for JO, which did not exist with the scaled data).

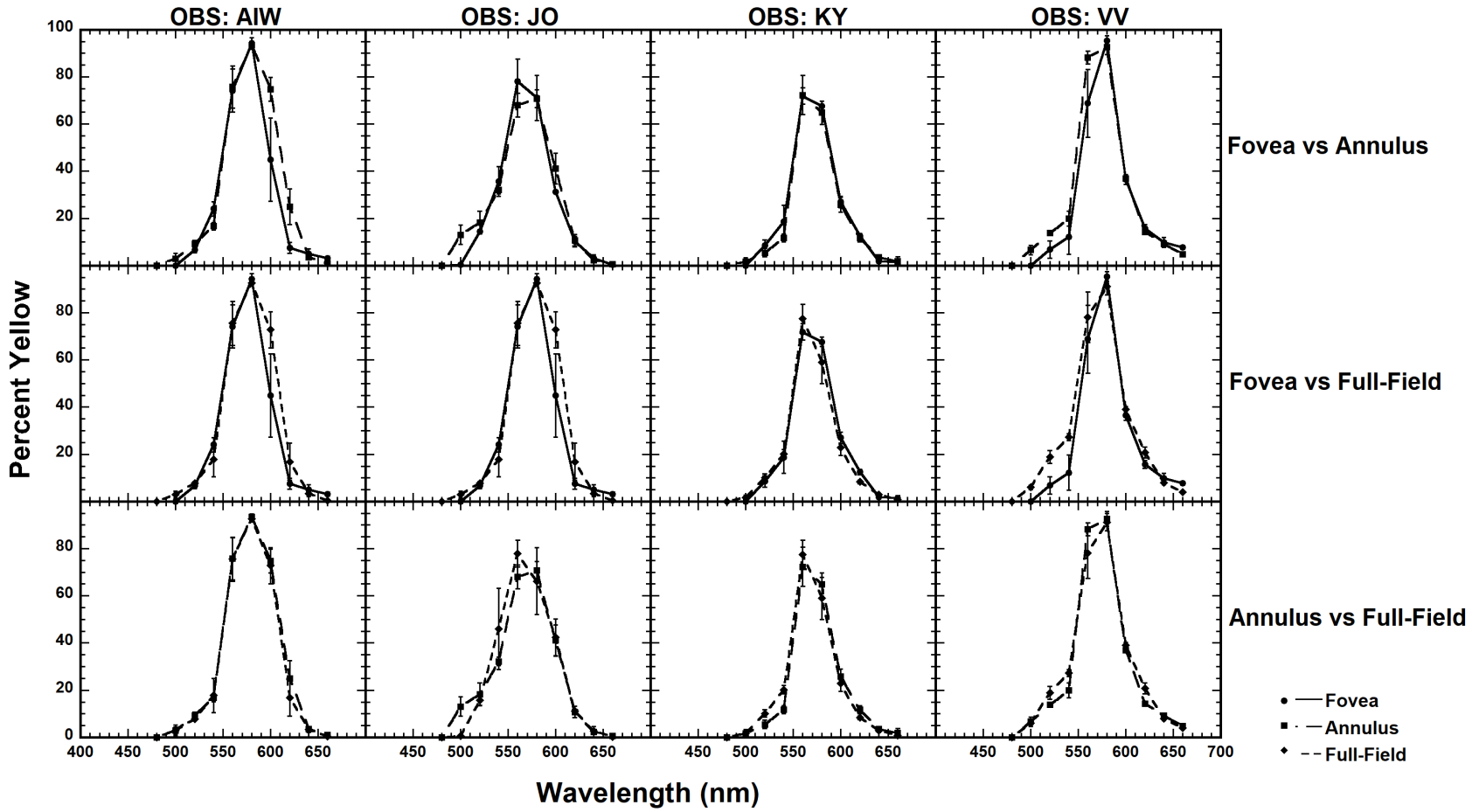

Figure 4.3. Same as figure 4.1, but for percent yellow.

Table 4.3. Sum and mean absolute deviations of non-scaled percent yellow between two stimulus conditions for each observer.

Observer	Comparison	N*	Sum	Mean
	Yellow Hue:			
AIW	23° Full Field - 1° Fovea	9	54.89	6.10
	23° Full Field - 23° Annulus	9	14.56	1.62
JO	23° Full Field - 1° Fovea	9	29.67	3.30
	23° Full Field - 23° Annulus	9	45.44	5.05
KY	23° Full Field - 1° Fovea	9	28.78	3.20
	23° Full Field - 23° Annulus	9	32.11	3.57
VV	23° Full Field - 1° Fovea	9	59.56	6.62
	23° Full Field - 23° Annulus	9	34.89	3.88

*N denotes the number of wavelengths at which there were hue-scaling responses for both stimulus conditions.

For percent red, there are few differences between scaled data (Figure 3.4) and data that has not been scaled to saturation (Figure 4.4). While there were not many differences between conditions, the small patterns of differences within each observer are still present in the non-scaled data (Figure 4.4). The patterns seen with mean absolute deviation values displayed in the scaled data (Table 3.4) are the same patterns present in the non-scaled data (Table 4.4); however, AIW and JO shows more of a difference between the comparisons with the non-scaled values (i.e., more than a ±1% difference between comparisons for both observers, which did not exist with the scaled data).

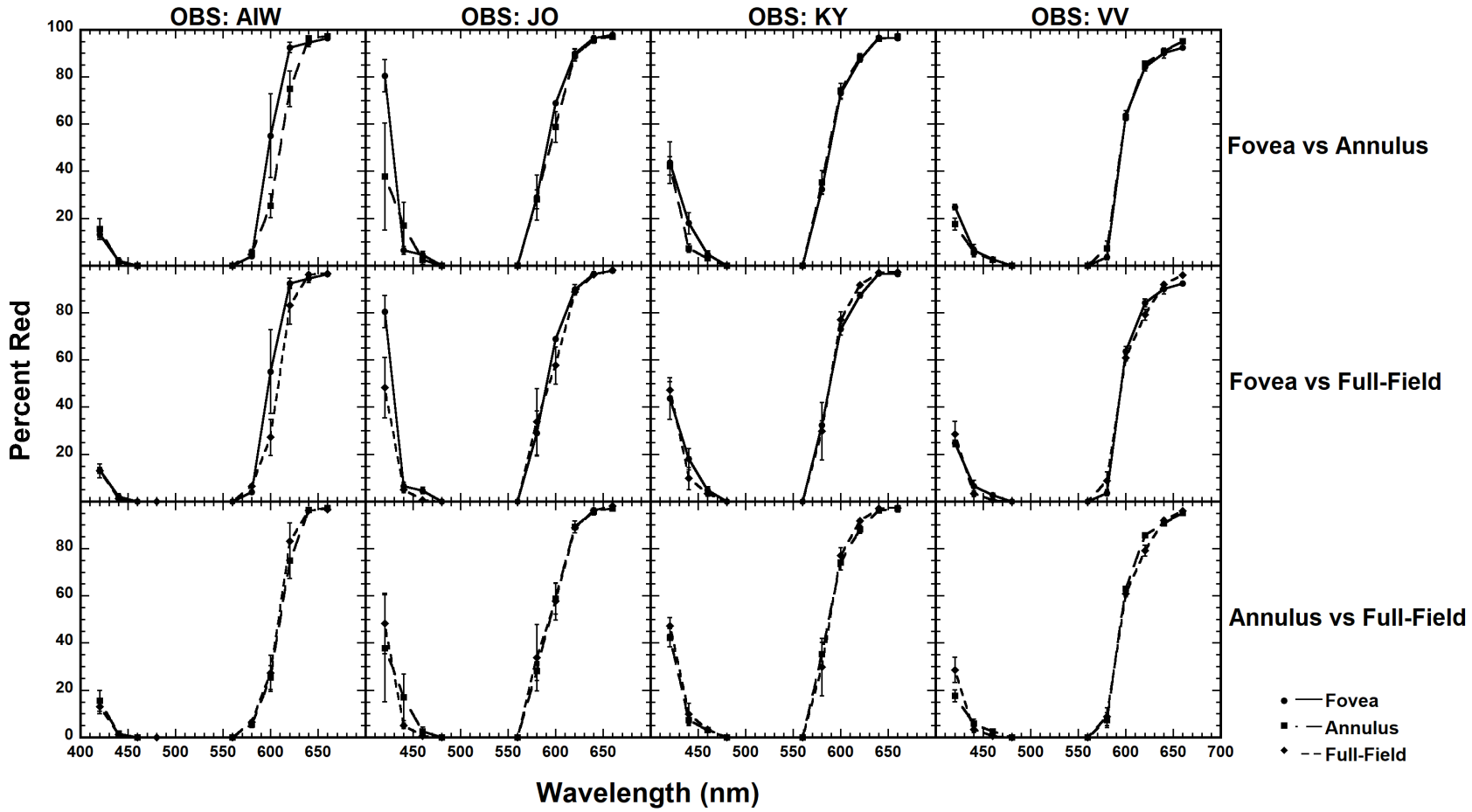

Figure 4.4. Same as figure 4.1, but for percent red.

Table 4.4. Sum and mean absolute deviations of non-scaled percent red between two stimulus conditions for each observer.

Observer	Comparison	N*	Sum	Mean
	Red Hue:			
AIW	23° Full Field - 1° Fovea	8	43.11	5.39
	23° Full Field - 23° Annulus	8	15.00	1.88
JO	23° Full Field - 1° Fovea	8	55.00	6.88
	23° Full Field - 23° Annulus	8	33.11	4.14
KY	23° Full Field - 1° Fovea	8	25.00	3.13
	23° Full Field - 23° Annulus	8	20.33	2.54
VV	23° Full Field - 1° Fovea	8	27.44	3.43
	23° Full Field - 23° Annulus	8	27.22	3.40

*N denotes the number of wavelengths at which there were hue-scaling responses for both stimulus conditions.

In summary, the data show that differences between stimulus conditions continue to exist, regardless of whether the data has been scaled to saturation or not. Scaling to saturation remains an effective data transformation for this data-set, as it maintains the hue ratios and allows the data to also reflect the chromatic strength. This inclusion of chromatic strength information better summarizes the perceptual experience. As referenced in the example above, a hue that is reported as 100% red which varied in saturation (e.g., 100% versus 20%) between conditions would not appear the same (i.e., vibrant red versus dull pink) and is an important part of determining perceptual equivalencies for the present study.

Comparison to O'Neil and Webster (2014):

O'Neil and Webster (2014) investigated retinal influences on filling-in and filling-out and serve as a good comparison for the findings of the present study. The results of the present study agree with the results of O'Neil and Webster (2014), which is intriguing, considering the many differences between the two studies (e.g., retinal location, background hue, stimulus size and retinal illuminance, initial motivation for the study). O'Neil and Webster (2014) displayed their

stimuli on a uniform gray background in comparison to the present study's black background. Also, O'Neil and Webster viewed the stimuli binocularly on a CRT display, versus this study in which stimuli were viewed monocularly in a Maxwellian-view system. Additionally, the present study used stimuli ranging from 420 nm to 660 nm, while the design of O'Neil and Webster (2014) was such that only a bichromatic unique purple (i.e., the point at which a hue looks equally red as it does blue) was used as their stimulus. O'Neil and Webster (2014) used a stimulus with a luminance of 5 cd/m^2, which makes it difficult to directly compare to the 20 td photopically equated stimuli used in the present study. The ages of participants in O'Neil and Webster (2014) are not known, but if we assume the pupil sizes of the participants were approximately 5 mm in diameter on average (Watson and Yellott, 2012), then their stimuli would have been 98 trolands (Wyzecki and Stiles, 1982). Similar to this study, the majority of the experiments within O'Neil and Webster (2014) used a stimulus duration of 500 ms. For the present study, the hue of 23˚ (3˚ wide ring) and 35˚ (15˚ wide ring) annular stimuli were compared to a 1˚ foveally presented stimulus and 23˚ and 35˚ full-field stimuli in order to assess hue differences between the fovea and peripheral retina. The center of the rings from the annular stimuli bisected 10˚ retinal eccentricity on both horizontal and vertical meridians. O'Neil and Webster used stimuli ranging from 1˚ to 16˚ (presented centrally to the fovea, with measurements taken using a central fixation point and a fixation point on the left-edge of the stimulus); however, they compared the hue of the larger fields to the hue of a 1˚ field presented at 0˚ and 8˚ retinal eccentricity. It is possible their larger stimuli would account for perceptive field size changes; however, a 1˚ stimulus presented at approximately 10˚ in the nasal and inferior retinas would not have filled the perceptive fields for red/blue (i.e., "purple") hues used in their study (Volbrecht et al., 2009). Specifically, O'Neil and Webster (2014) noted that after

foveally placed stimuli exceeded 4˚, their appearance was similar to a 1˚ stimulus presented at 8˚ in the peripheral retina. O'Neil and Webster (2014) showed that a stimulus that appeared purple in the fovea appeared more blue in the periphery, which is opposite of what was observed in the present study. For the observers in the present study, the shorter wavelengths had a higher percentage of blue, and, blue was seen at longer wavelengths in the fovea than the full-field and annular stimuli. Despite the many differences between O'Neil and Webster (2014) and the present study, both arrive at the same conclusion; i.e., the peripheral retina appears to have a greater role in the hue appearance of a large field than does the fovea. This similar result, regardless of the varied stimulus conditions, adds to the robustness of the finding that the peripheral retina has greater weight in mediating the hue of large fields.

Spatial Integration

One of the speculated mechanisms behind the periphery determining the hue appearance of large fields is that hue signals may be averaged across the portions of the retina where the stimulus is placed. In order to investigate the averaging of signals across the retina, data were collected with 3° stimuli centered at 10° from the fovea in four retinal locations (i.e. inferior, superior, nasal, temporal). With this data, the 23° annulus was compared to hue responses from each of the individual retinal locations, as well as compared with the mean hue responses from all four retinal locations. Since the earlier portion of this experiment demonstrated that the annular stimulus was similar in appearance to the full-field stimulus, this portion of the experiment sought to explore if responses from one specific retinal location had more influence over the appearance of the annular stimuli.

The data for the spatial integration portion of the experiment showed that the retinal location that was most similar in appearance to the annular stimuli for each hue term varied

across observers. Table 4.5 lists the retinal locations that had the lowest mean absolute deviations when percent hue of the 3° fields were compared to the percent hue for the annulus across all wavelengths where each hue term was reported.

Table 4.5. Summary of lowest mean absolute difference data from Tables 3.10 – 3.15.

Hue Term:	**Lowest Mean Absolute Difference Relative to Annulus**		
	AIW	**KY**	**VV**
Blue	Nasal (ALL)	Superior (ALL)	Temporal (I)
Green	Superior (T, 4-LM)	Inferior (S, 4-LM)	Inferior (N, T, 4-LM)
Yellow	Superior (ALL)	Superior (I, T, 4-LM)	Temporal (I, N, 4-LM)
Red	Temporal (I, S, 4-LM)	Superior (I, 4-LM)	Temporal (ALL)
Saturation	Inferior (ALL)	Superior (I, 4-LM)	Temporal (ALL)

* Parentheses indicate comparison(s) within ±1% of the lowest mean absolute difference value. I = Inferior, N = Nasal, S = Superior, T = Temporal, 4-LM = 4 – Location Mean, ALL = all comparisons overlap.

When factoring in comparison values for other retinal locations which were within ±1% of the lowest mean absolute difference value (see Table 4.5), some trends across observers becomes more apparent. AIW and KY show for all hue terms the 3° field presented to the superior retina has one of the lowest mean absolute differences when compared to the annulus. VV shows the temporal retina has the lowest mean absolute difference when compared to the annulus for all but green hues. The 4-location mean value is within 1% of all other comparisons across observers (except blue hues for VV). Additionally, stimuli on the horizontal meridian were slightly more similar to one another compared to those on the vertical meridian, which may be due to general perceptive field size similarities between retinal locations on the same meridian (Volbrecht et al., 2009). According to Volbrecht et al.'s (2009) data, perceptive fields for all hue terms would have been filled by the 3˚ field placed in the temporal retina, and all but the green hue term for the nasal retina. On the vertical meridian, a 3˚ field would only fill the perceptive fields of yellow hue in the superior retina, while green is the only hue in the inferior retina not filling perceptive fields with a 3˚ field. Based on perceptive field sizes alone, it would have been

expected that percent green would have varied most between the 3˚ and 23˚ annulus, since the 3˚ wide annuluar ring would not be filling the perceptive fields of the majority of the retinal regions it passes through. Since the 3˚ ring of the 23˚ annulus would fill perceptive fields for the other hues (blue, yellow, and red) at most of the retinal locations, fewer differences would be expected between these individual retinal locations and the annulus.

The findings of the present study (see Table 4.5) suggest that the hue of the annulus might be most influenced by the retinal regions where the perceptive fields have not been filled. Across hue terms, perceptive field sizes are generally largest for the superior retina (Volbrecht et al., 2009), and, Table 4.10 demonstrates that two of the three observers (AIW and KY) show more similarities between the hue of the annulus and the small field presented to the superior retina. The remaining observer, VV, shows that small stimuli presented to the temporal retina appear more similar across hue terms to the annular stimulus. This is an interesting finding because the temporal retina is generally reported as having the smallest perceptive field sizes (Volbrecht et al., 2009) and VV's data would be more in line with the expectation that the annular stimulus would appear most like the 3° fields in the retinal regions and hue terms where perceptive field sizes had been filled. More consistent with the general idea demonstrated by AIW and KY that the region whose perceptive fields are not filled would be most similar to the annulus, both KY and VV show that a 3° field presented to the inferior retina appears more similar to the annulus for green hue terms; i.e., the inferior retina has the largest perceptive field sizes for green hues at 10° retinal eccentricity, Volbrecht et al. (2009).

In summary, data from the spatial integration portion of this experiment points to an interaction between perceptive field sizes and the retina region that influences the hue of the annulus. The initial expectation was that one retina region may have had a stronger influence

over the hue appearance than other retinal regions, assuming the stimulus presented to that specific region had filled the perceptive fields. The unexpected finding was that for many conditions, the retinal regions that did not have their perceptive fields filled by the transecting annular ring may have shaped the overall hue appearance. When taking the mean absolute deviation comparison values that were within ±1% of each other into account, the weight of the individual retinal regions are much less pronounced as the 4-location mean values are nearly the same as the retinal location with the lowest mean absolute deviation values.

These findings suggest that the size of underlying retinal area covered by stimuli may play a role in shaping the hue of the large fields. One of the issues still present in averaging the hue and saturation values across retinal locations is that each 3˚ field is presented in isolation, which covers far less surface area of the retina than the 23˚ annulus. Perhaps some of the overall hue appearance is shaped by averaging of signals across the retina, but also by how much of the retina is simultaneously covered by a stimulus. For example, in averaging 3° stimuli, it is a closer approximation to the hue experience of the larger fields; however, the differences that are unaccounted for may be due to those stimuli all being presented one at a time and not simultaneously, which would cover more of the retina at one time and perhaps be an even closer approximation of the hue and saturation experienced with the annulus. If this were true, it would be expected that hue and saturation values from presenting a 3˚ field to all four retinal locations simultaneously would differ from the mean of the four locations with individually presented 3˚ fields. This question could be addressed by having observers view a foveally placed fixation point and reporting hue of a stimulus in a given retinal region (e.g., temporal) in conditions with and without stimuli placed in the other retinal regions.

Stimulus Size

To investigate the effect of ever increasing stimulus size and the role of underlying retinal area activated by various stimuli, preliminary data were also collected for 3° and 5° stimuli (centered in the fovea). If stimulus size was a factor, then one might expect that the progression of hue change would be seen as stimuli increased from 1° to 35°. Two sessions worth of data were collected for KY for 3˚ and 5˚, which were compared to the three sessions of data for the 1˚, 23˚, and 35˚ full-field stimuli. Data were scaled to saturation. Figure 4.5 shows percent hue/saturation plotted as a function of wavelength for the four elementary hues and saturation for KY, the only observer with multiple sessions of data collected for this condition. In general, once stimuli reached 5°, they appeared similar to their larger counterparts (i.e., 23° and 35°). In the case of green, the 3° stimuli are similar in hue appearance to the larger stimuli, i.e., the differences observed between 500 – 540 nm have vanished. The saturation plot shows the 1° stimulus as generally being the least saturated, with the exception of the 23° stimulus at 580 nm, where KY experienced that stimulus as less saturated than any other stimulus at any wavelength. Overall, the larger the stimulus, the stronger the chromatic component of the hue percept; and in general, this effect plateaued by the time the stimulus reached 5° in diameter. Perhaps part of this shifting hue appearance between 3˚ and 5˚ is due to macular pigment filtering that tapers off just outside of the fovea (Wooten and Hammond, 2005). The 35° stimulus covers a substantial portion of the peripheral retina and a higher proportion of rods than the smaller stimuli, and yet, saturation is the highest with this stimulus. This suggests any desaturating effects from the rods

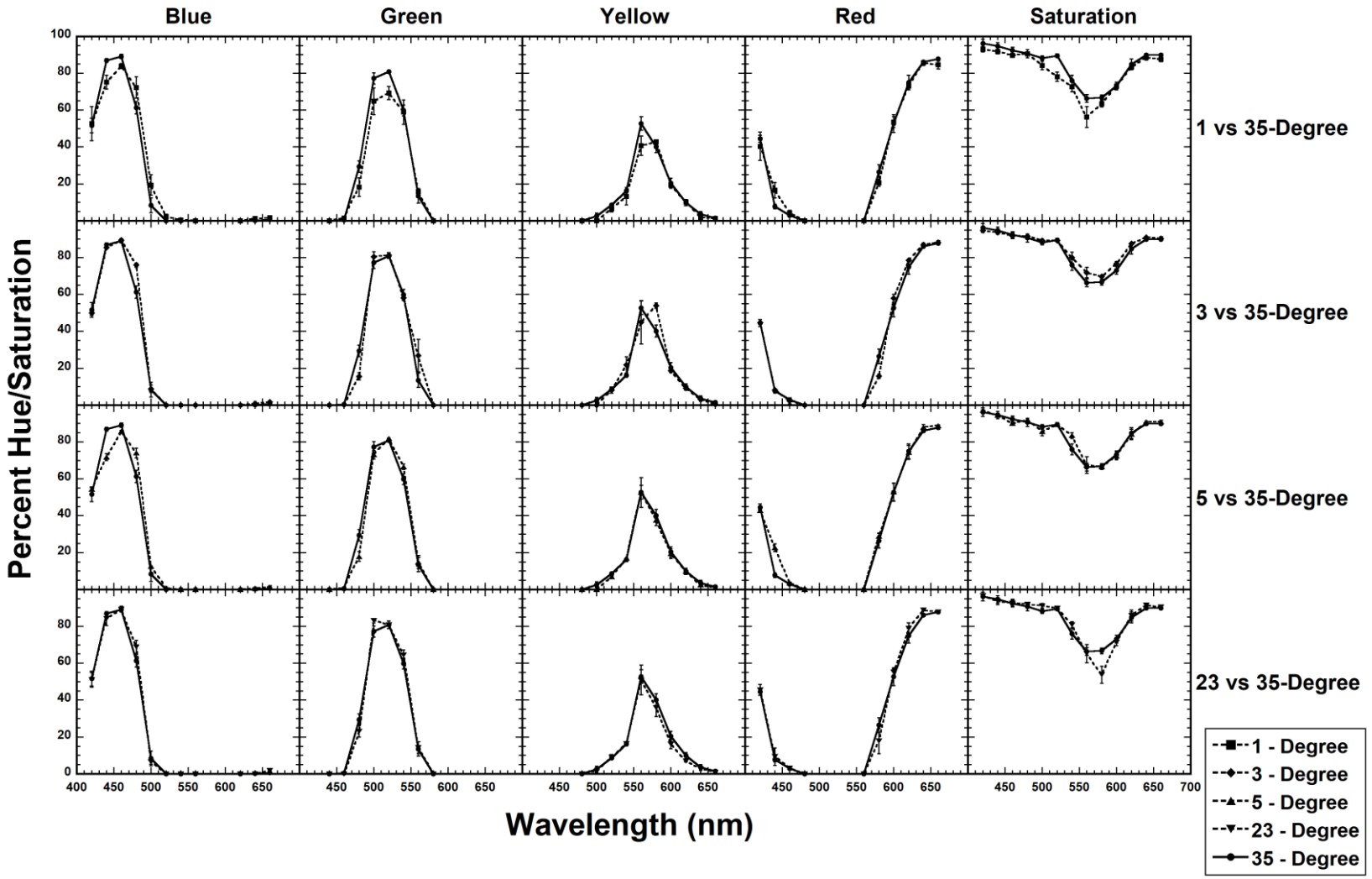

Figure 4.5. Five different stimulus sizes (1°, 3°, 5°, 23°, 35°) plotted as a function of percent hue/saturation and wavelength for KY. Each panel represents a different hue term (with the far right panel representing saturation).

have been suppressed, and the notion that large fields can exceed the saturation of a foveal stimulus (1°) is in agreement with previous studies (Moreland and Cruz, 1959; Opper et al., 2014; Stabell and Stabell, 1976).

Retinal Mechanisms Implicated in Findings of the Present Study

Previous research (e.g., Ambler, 1974; Stabell and Stabell, 1976; Stiles, 1962; Troup et al., 2005; Volbrecht et al., 2009) has already shown that rod photoreceptors can have an effect on hue perception. Studies note that rods change perceptive field sizes (e.g., Troup et al., 2005; Volbrecht et al., 2009), saturation of stimuli (e.g., Stabell and Stabell, 1976), and blue/yellow hue percepts (e.g., Ambler, 1974; Buck et al., 2000; Trezona, 1970). Because rods are located in the peripheral retina and not in the central fovea, they may potentially be responsible for the finding that annular stimuli in this study appear more similar to the full-field stimuli than the foveal stimuli. To investigate the impact of diminished rod input with respect to our findings, another experiment was conducted. In this experiment, the observer's eye was exposed to a relatively brief bright white light (bleach), which rendered the rod photopigment less sensitive than the cone photopigment for approximately 10 minutes after exposure to the bleaching field (Alpern, 1971; Rushton and Powell, 1972). Hue-naming data were collected with the 1°, 23° annulus, and 23° full-field stimuli for three observers (i.e. AIW, KY, and VV) for the duration known as the cone plateau, which is 4 to 10 minutes post bleach. During the cone plateau, cone photopigment has regenerated and the cones have a lower threshold for detecting light than the rods. Even though there are no rods in the central fovea, by bleaching before exposure to the 1˚ foveal stimulus, we can control for extraneous variables that the bleaching field might introduce. The 35˚ fields were not included in this comparison, as Volbrecht et al. (2009) demonstrated that perceptive fields for the four elemental hues are filled at much smaller stimulus sizes under

bleaching conditions (2˚ or less) than no-bleach conditions (up to 15˚for green). Figures 4.6 – 4.9 (4.10) show percent hue (saturation) as a function of wavelength. The solid line represents the 1° foveal stimulus, the dashed line represents the 23° annular stimulus, and the dotted line represents the 23° full-field stimulus. Each panel represents one of the three observers who participated in the bleach procedure. Tables 4.6 – 4.9 (4.10) list the mean absolute difference between the hue (saturation) percent of the 23° full-field stimulus and the 1° foveal stimulus, as well as between the hue (saturation) percent of the 23° full-field stimulus and the 23° annulus.

In Figure 4.6, all three observers show that the fovea is more blue at 520 nm, and the annulus appears less blue at 480 nm under bleach conditions. Two of the three observers (except KY) showed the lowest mean absolute difference values between the annulus and full-field stimulus (see Table 4.6). The mean difference between conditions is less than 1% for AIW, which is not surprising considering the foveal function closely mimics the annular and full-field hue functions with the exception of hue reported at 500 nm, where AIW reported the fovea appearing approximately 20% more blue than the annulus and full-field stimulus. KY also shows mean absolute difference values within 1% between both comparison values.

Table 4.6. Sum and mean absolute deviations of percent blue between two stimulus conditions for each observer.

Observer	Comparison	N*	Sum	Mean
	Blue Hue:			
AIW	23° Full Field - 1° Fovea	8.00	37.51	4.69
	23° Full Field - 23° Annulus	8.00	30.36	3.79
KY	23° Full Field - 1° Fovea	9.00	30.96	3.44
	23° Full Field - 23° Annulus	9.00	40.98	4.55
VV	23° Full Field - 1° Fovea	5.00	34.30	6.86
	23° Full Field - 23° Annulus	4.00	8.57	2.14

*N denotes the number of wavelengths at which there were hue-scaling responses for both stimulus conditions.

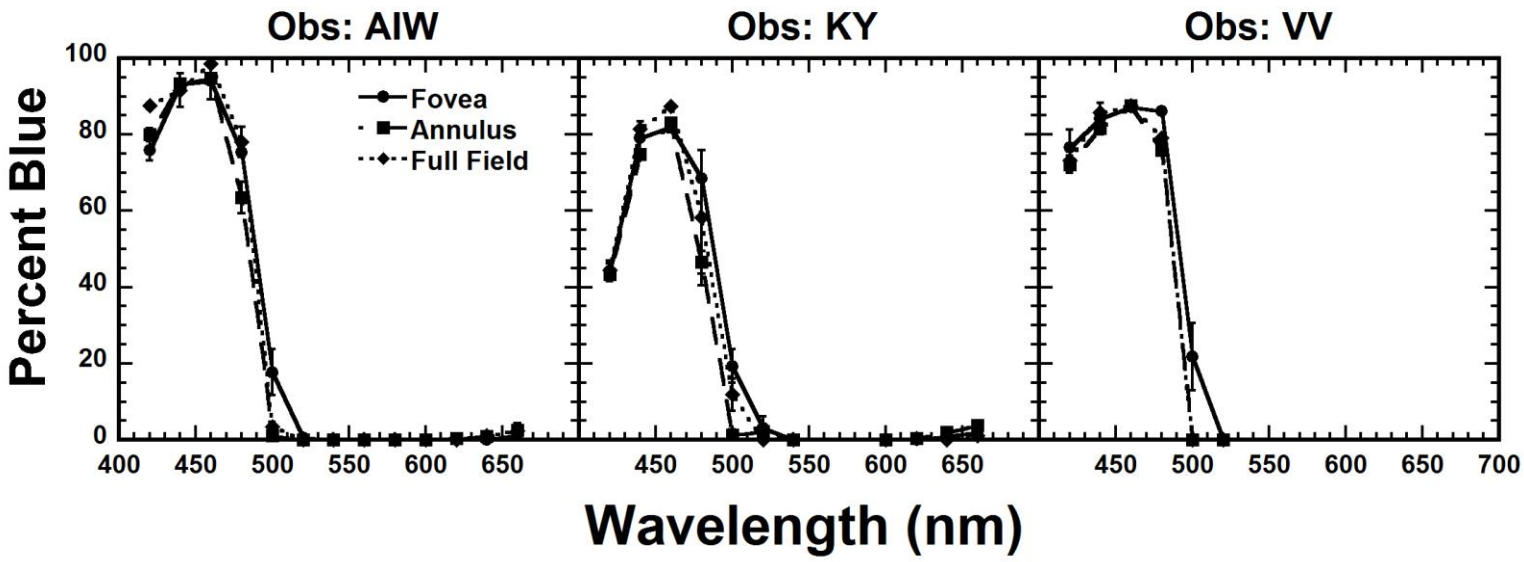

Figure 4.6. Percent blue is plotted as a function of wavelength for the 1° foveal stimulus (solid line and circle symbols), 23° annulus (long-dashed line and square symbols), and 23° full-field stimulus (short-dashed line and diamond symbols). Each panel represents data for each individual observer. The error bars represent ±1 SEM.

In Figure 4.7, all three observers show that the 23˚ stimuli appear more green at 480 nm than the foveal stimulus. AIW and KY also show this at 500 and 520 nm.. Two of the three observers (except VV) showed the lowest mean absolute difference values between the annulus and full-field stimulus (Table 4.7); however, mean deviation values for KY differ by less than ±1% between comparisons and would be considered perceptually similar.

Table 4.7. Sum and mean absolute deviations of percent green between two stimulus conditions for each observer.

Observer	Comparison	N*	Sum	Mean
	Green Hue:			
AIW	23° Full Field - 1° Fovea	8.00	48.44	6.05
	23° Full Field - 23° Annulus	7.00	14.27	2.04
KY	23° Full Field - 1° Fovea	5.00	52.24	10.45
	23° Full Field - 23° Annulus	5.00	36.19	7.24
VV	23° Full Field - 1° Fovea	6.00	38.58	6.43
	23° Full Field - 23° Annulus	6.00	48.53	8.09

*N denotes the number of wavelengths at which there were hue-scaling responses for both stimulus conditions.

In Figure 4.8, the yellow appearance of the stimuli differs for each observer. Mean absolute difference data (Table 4.8) show that AIW and VV have the lowest values between the foveal and full-field conditions, although VV's comparison values are within ±1% of each other. The lowest mean absolute difference value is between the full-field and annulus for KY, although mean deviation values differ by less than ±1% between comparisons and would be considered perceptually similar.

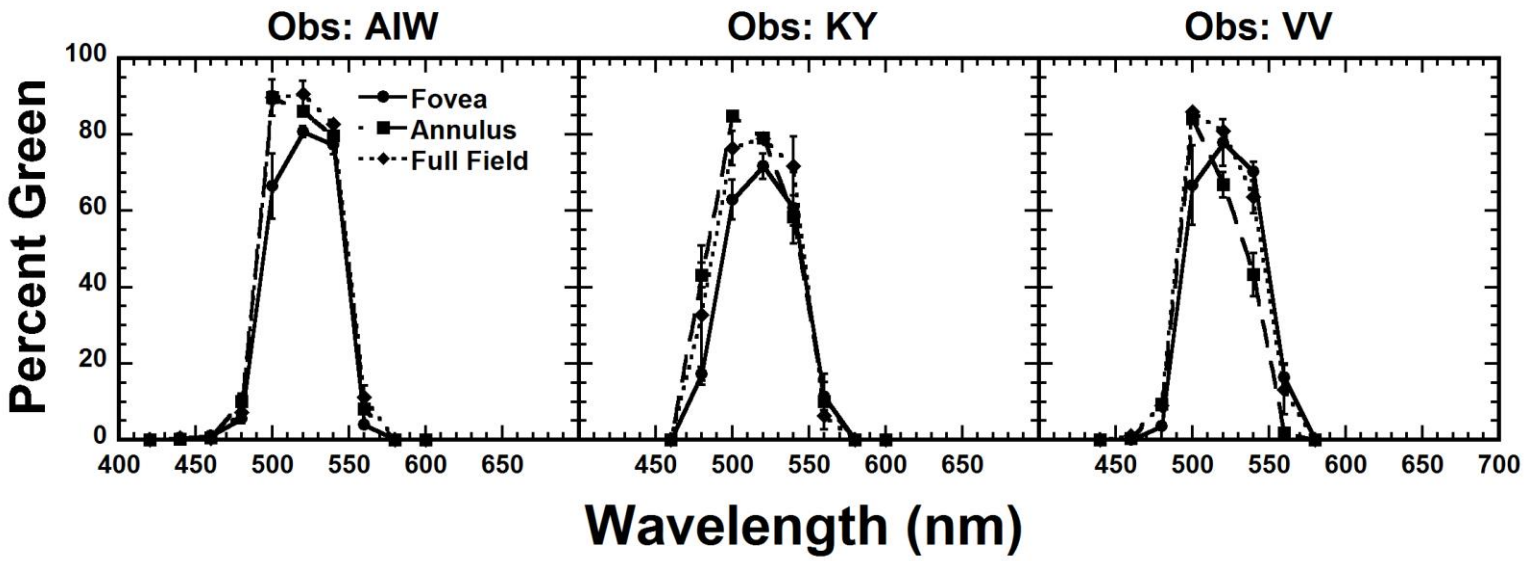

Figure 4.7. Same as figure 4.6, but for green hue.

Table 4.8. Sum and mean absolute deviations of percent yellow between two stimulus conditions for each observer.

Observer	Comparison	N*	Sum	Mean
	Yellow Hue:			
AIW	23° Full Field - 1° Fovea	9.00	26.30	2.92
	23° Full Field - 23° Annulus	9.00	76.51	8.50
KY	23° Full Field - 1° Fovea	9.00	40.80	4.53
	23° Full Field - 23° Annulus	9.00	37.96	4.22
VV	23° Full Field - 1° Fovea	9.00	48.62	5.40
	23° Full Field - 23° Annulus	9.00	58.36	6.48

*N denotes the number of wavelengths at which there were hue-scaling responses for both stimulus conditions.

Figure 4.9 shows that the annulus appeared more red at 580 nm for all three observers. Lowest mean absolute difference values (Table 4.9) were between the full-field and annulus for KY and VV, and the full-field and fovea for AIW. Similarly to KY's yellow data (Table 4.3), mean deviation values differed by less than ±1% between comparisons.

Table 4.9. Sum and mean absolute deviations of percent red between two stimulus conditions for each observer.

Observer	Comparison	N*	Sum	Mean
	Red Hue:			
AIW	23° Full Field - 1° Fovea	7.00	25.61	3.66
	23° Full Field - 23° Annulus	7.00	50.89	7.27
KY	23° Full Field - 1° Fovea	9.00	23.50	2.61
	23° Full Field - 23° Annulus	9.00	19.86	2.21
VV	23° Full Field - 1° Fovea	8.00	35.44	4.43
	23° Full Field - 23° Annulus	8.00	16.38	2.05

*N denotes the number of wavelengths at which there were hue-scaling responses for both stimulus conditions.

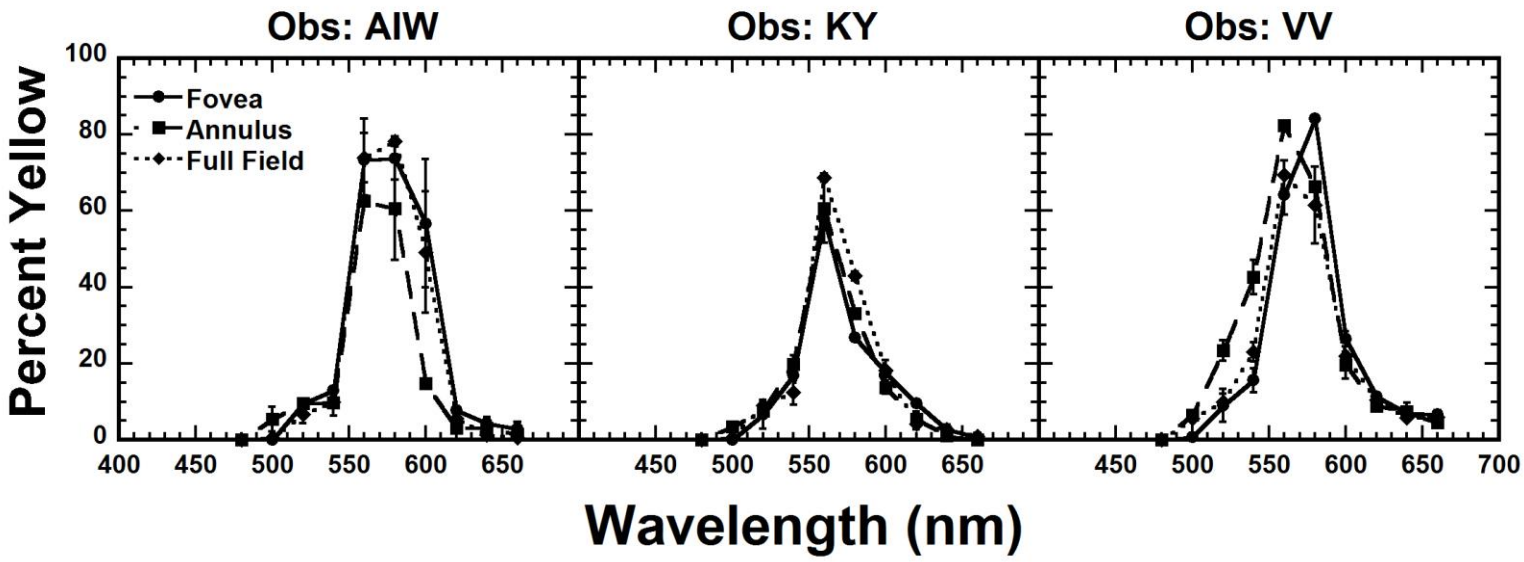

Figure 4.8. Same as figure 4.6, but for yellow hue.

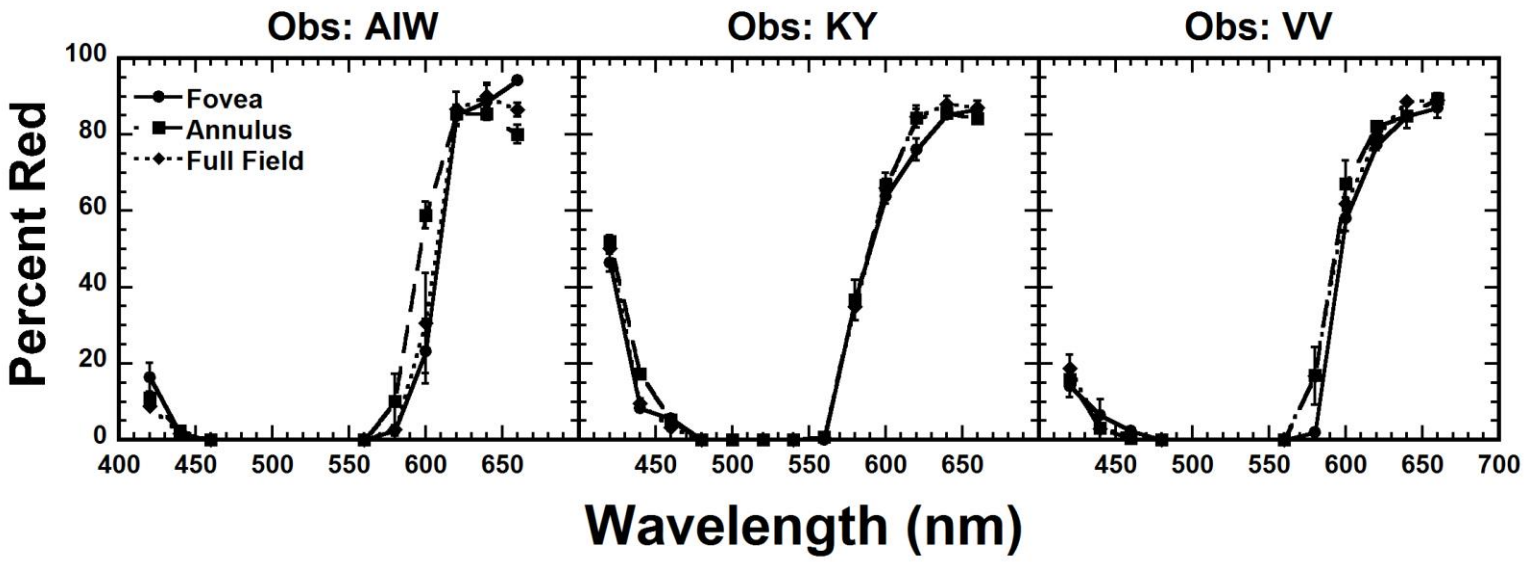

Figure 4.9. Same as figure 4.6, but for red hue.

Figure 4.10 shows that the full-field stimulus appeared most saturated for two observers (except VV) from 420 to 600 nm. Mean absolute difference values (Table 4.10) are lowest for AIW and VV between the foveal and full-field conditions and lowest for KY between the full-field and annular conditions; although, the mean deviation values differed by less than ±1% between comparisons for AIW and VV.

Table 4.10. Sum and mean absolute deviations of percent saturation between two stimulus conditions for each observer.

Observer	Comparison	N*	Sum	Mean
	Saturation:			
AIW	23° Full Field - 1° Fovea	13.00	54.33	4.18
	23° Full Field - 23° Annulus	13.00	72.83	5.60
KY	23° Full Field - 1° Fovea	13.00	63.33	4.87
	23° Full Field - 23° Annulus	13.00	33.17	2.55
VV	23° Full Field - 1° Fovea	13.00	28.17	2.17
	23° Full Field - 23° Annulus	13.00	28.83	2.22

*N denotes the number of wavelengths at which there were hue-scaling responses for both stimulus conditions.

Overall, the bleach condition appears to have reduced the perceptual gap between the different stimulus conditions when compared to the dark-adapted portion of this experiment. In the dark-adapted portion of this experiment that compared the 1° stimuli to the 23° annuli and full-field stimuli (See Chapter 3, Figures 3.1 – 3.5), all observers demonstrated lower mean absolute deviations between the annular and full-field stimuli (except JO with yellow, see Figure 3.3). When compared to the bleach conditions with these same stimuli, two of the three observers demonstrated lower mean absolute deviations between the annular and full-field stimuli for blue (except KY), green (except VV), and red (except AIW) hue terms (see Figures 4.6, 4.7, and 4.9). Two of the three observers demonstrated lower mean absolute deviations between the foveal and full-field stimuli for yellow hues (except KY) and saturation (except VV) (see Figures 4.8 and

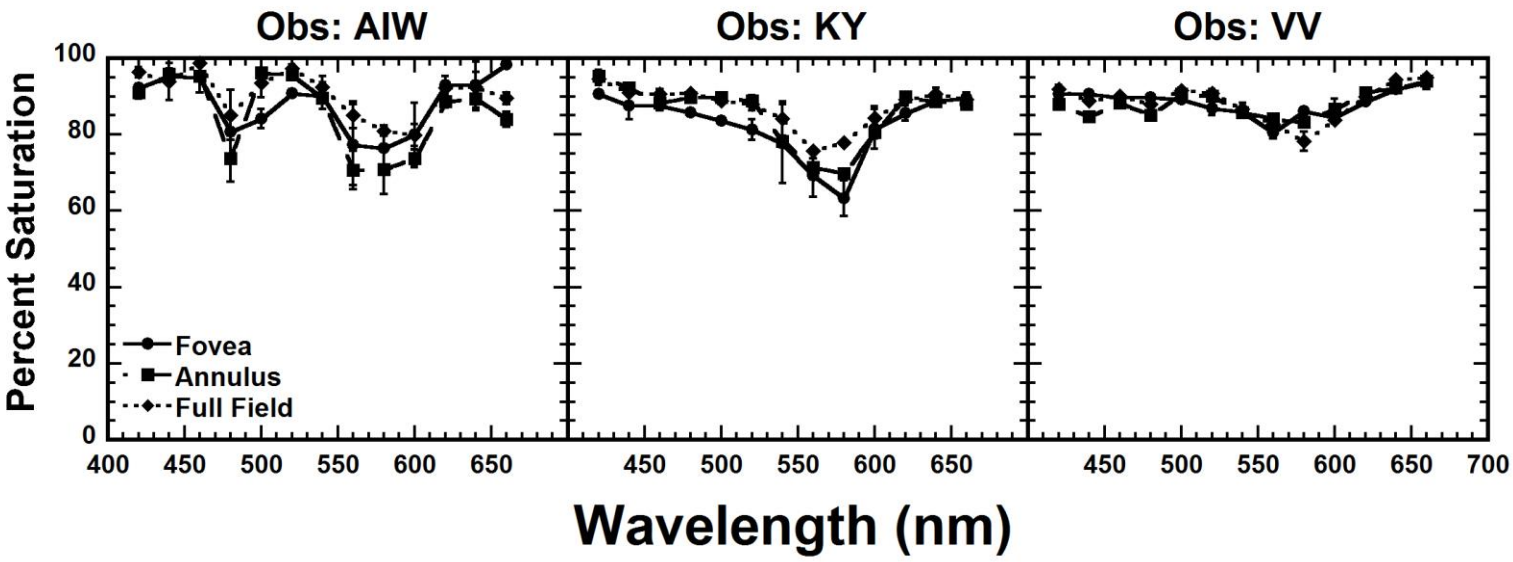

Figure 4.10. Same as figure 4.6, but for saturation.

4.10). Even after bleaching, large fields appeared more similar to stimuli presented to the periperhal retina (i.e., annulus) than stimuli presented to the fovea for the majority of observers and hue terms (except yellow).

While some of the previous literature points to cortical processing as being the primary determinant of hue for large uniform fields (Balas and Sinha, 2007; Breitmeyer and Jacob, 2012; Zweig, Zurawel, Shapley, and Slovin, 2015), other literature lends support to the idea that local retinal processes may influence the photoreceptor signals before they are sent to the cortex for processing (Bompas, Powell, and Sumner, 2013; O'Neil and Webster, 2014; Spillmann and Werner, 1996). As mentioned previously, rod photoreceptors are not found in the very center of the visual field (i.e., the fovea) and have generally been investigated in the peripheral retina; however, researchers (Buck, Thomas, Hillyer, and Samuelson, 2006; Thomas and Buck, 2006) have investigated if unstimulated rods outside of the fovea influences the hue of foveal stimuli. This is of interest to the present study, as hue differences were noted between bleach and no-bleach conditions for 1˚ stimuli (see Figures 3.1-3.5 compared to 4.6-4.10). This difference would be unexpected under the assumption that there is minimal rod input for 1˚, foveally placed stimuli. Buck et al. (2006) showed that 1˚ stimuli presented to the fovea could be affected by rods, as shifts of unique hue loci to longer wavelengths were reported under bleach conditions (minimal rod input) when compared to dark-adapted conditions (maximum rod input). These shifts of unique hue loci were consistent with what they had reported in the extrafoveal retinal areas (Thomas and Buck, 2006), which led them to speculate that the shifting loci were not due to remote suppression of the cones from nearby inactive rods. Instead, the shifts in unique hue loci were attributed to local rods that were stimulated by the 1˚stimulus. Even though 1˚ fields are generally regarded as a foveal stimuli, they are still large enough to stimulate some rod

photoreceptors. Buck et al. (2006) also speculated the shifts seen with the 1˚ stimuli were not due to bleaching aftereffects (i.e., physiological), as the hue loci of the two smallest stimuli used in their study (i.e., 0.2˚ and 0.6˚) showed minimal differences between their bleach (rod input minimized) and no-bleach (rod input maximized) conditions. In agreement with Buck et al. (2006), the shifts in hue experience between bleach and no-bleach conditions for all of the stimuli in the present study are due, at least in part, to rod input; however, this does not provide additional understanding as to why the peripheral retina appears to mediate the hue of large fields.

To get a better understanding of how stimulus placement affects rod influence on hue, and which portion of the retina influences overall hue appearance, Thomas and Buck (2006) presented foveally centered stimuli (2˚ and 7˚ full-fields, and a 7.4˚ annulus), and a 7.4˚ stimulus centered at 7˚ eccentricity during both bleach and no-bleach periods. They noted for larger stimuli which encompassed the fovea (especially for unique blue), rod biases were smaller than they were for an annulus (i.e., devoid of foveal input), and the hue appearance of the annulus differed the most from their other stimuli. Based on the specific rod hue biases seen in their study and the placement of stimuli and their edges, Thomas and Buck (2006) suggested that the perception of unique blue and green stimuli was dominated by the fovea. Their results suggest that the fovea would be more of an influence to the hue of large fields and it would be expected that the annulus would be dissimilar to the appearance of large fields; however, this is the opposite of the finding in the present study since the annular stimuli were more similar to the full-field stimuli. Perhaps the much larger sizes of the stimuli in the present study negate the effects seen with smaller extrafoveal stimuli in Buck et al. (2006), as 1) the rod:cone ratio would

be much higher with larger stimuli, and 2) it may be more likely that the chromatic system is suppressing the impact of rods on hue. These ideas are addressed in more detail below.

Some of the earlier work on rod intrusion suggested that rod input desaturates hue appearance (Gordon and Abramov, 1977; Stabell and Stabell, 1976) and shifts blueness in the peripheral retina (Ambler, 1974; Trezona, 1970); however, more recent studies suggest that is not always the case, as retinal areas containing rods have shown increased saturation in certain portions of the visible spectrum (Opper et al., 2014). Other studies (Frumkes and Eysteinsson, 1988; Stabell and Stabell, 1999; Volbrecht and Nerger, 2012; Volbrecht, Nerger, and Trujillo, 2011) have investigated how changing various stimulus dimensions (i.e., luminance, duration, size, and dark adaptation) affects the strength of the chromatic signal. Volbrecht et al. (2011) noted that increasing rod input (indicated by increasing dark adaptation time) appeared to reduce the effectiveness of the chromatic system. One of the concerns addressed by previous research was that by increasing the size of stimuli, the absolue number of rods that are responding to that particular stimulus increases and thus further desaturates its appearance (Abramov et al., 1991). This is not the case, however, as many studies demonstrate a reduced rod contribution with increasing stimulus size (Abramov et al., 1991; Frumkes and Eysteinsson, 1988; Stabell and Stabell, 1999). This may also explain the discrepancy between the present study and Thomas and Buck (2006), in terms of which retinal region appears to be mediating the hue of larger fields. There is evidence to suggest that once certain stimulus criteria have been met (i.e., retinal illuminance, stimulus size, stimulus duration), the cone system suppresses the effect of the rods on the chromatic system (Stabell and Stabell, 1999; Volbrecht and Nerger, 2012). Once some of these contraints have been met, few differences exist between conditions with maximal rod input (dark adaptation) and conditions with minimal rod input (bleach). Rod suppression could

partially explain why there was little difference between large full-field stimuli and the annular stimuli in the present study. Since the annular stimuli occupy a relatively large amount of retinal surface area, the chromatic system may be minimizing the rod system's influence on perceptual experience. If this is occurring, then the overall hue experience of large fields is primarily provided by the cones in the peripheral retina. A simple reductionist approach is not entirely satisfactory, as it discounts contributions from the fovea to the overall perceptual experience. While the peripheral retina appears to be the primary determinant of the hue experience, there are still slight differences in appearances between the full-field and annular stimuli. Unfortunately, rod influences alone do not explain why hues in the periphery appear different from hues in the fovea (especially for blueness and greenness). For example, large-fields and foveal stimuli still appear different if rod input is reduced by 1) rod suppression of the chromatic system, and 2) through use bleaching field. Additionally, while the hue experience was still most similar between the full-field and annular stimuli, regardless of bleach or no-bleach trials, it is clear that the bleaching field influenced the hue experience, thereby implicating retinal mechanisms beyond just rod input. With this in mind, it is reasonable to assume that cone photoreceptors might function differently between the fovea and periphery. It seems likely that the shifts in hue in the presence of a bleaching field are due in part to a reduction of rod input, as well as residual rod input, and also due to differences in cone system functioning in different portions of the retina. When dark-adapted, the combination of rod input and differential activity of the cones in the fovea versus those in the peripheral retina may be contributing to the similar hue appearance of the annulus and the large full-field stimuli.

The present study notes differences in blueness and greenness between the foveal and peripheral stimuli, and these results may be explained by rod-cone interactions and processing

occurring in the ganglion cells. While there are many different types of retinal ganglion cells (RGCs), three types are widely discussed because they establish the physiological basis for cone-opponency at the retinal level. Midget ganglion cells carry M and L cone signals (i.e., antagonistic) to the parvocellular layers of the LGN and visual cortex, creating a red-green opponent signal (Livingstone and Hubel, 1984). Parasol ganglion cells carry varying combinations of M- and L-cone signals (i.e., summative) to the magnocellular layers of the LGN and visual cortex, and are responsible for the white-black (luminance) signal (Shapley and Hawken, 2011). Bistratified ganglion cells encode for blue-yellow opponency by contrasting S-cone signals with both M- and L-cone signals, which are carried to the koniocellular layers of the LGN and visual cortex (Casagrande, 1994). Some psychophysics research suggests that rods must interface with S-cone pathways, namely due to findings that rods can influences perception of blueness (Buck, Knight, and Bechtold, 2000; Knight and Buck, 2002; Stabell and Stabell, 1994); however, physiologically, there is little evidence that rod signals are carried through the bistratified ganglion cells alongside blue and yellow information (Dacey and Lee, 1994: Lee, Smith, Pokorny, and Kremers, 1997). Lee et al. (1997) suggested that due to some of the psychophysical findings of blueness being affected by rod input, a lack of rod input into the bistratified ganglion cells does not necessarily mean that rods are not affecting the hue signal elsewhere in the visual system. Rod signals have been found to strongly influence the magnocellular (at photopic luminance levels, like those seen in the present study) and weakly influence the parvocellular pathways (at scotopic luminance levels) (Lee et al., 1997). Some studies have demonstrated that rods may enhance M-cone signals relative to L-cones and create changes in yellowness (Stabell and Stabell, 1996; Nerger et al., 1998); however, this research suggests this effect disappears once stimuli are large enough and bright enough (Nagy and

Doyal, 1993; Stabell and Stabell, 1996). The present study does not show any strong, clear patterns across observers for yellow stimuli between the foveal and large stimuli, further supporting the idea that the larger stimuli in this study are suppressing some of these rod effects noted in the previous literature. Nerger et al. (1995) demonstrated that unique green loci were reported at shorter wavelengths in the periphery when compared to the fovea, suggesting that rods were inhibiting S-cone activity (and thus, inhibiting blueness at the shorter wavelengths so stimuli would appear more green); however, the present study notes the opposite of this, with dark adapted conditions (i.e., with maximal rod input) pushing green perception to longer wavelengths compared to bleach conditions (refer to Figures 3.2 and 4.7). The caveats are that many of the stimuli used in Nerger et al.'s (1995) study were smaller than those used in the present study. They compared the foveal stimuli to stimuli at 20˚ temporal eccentricity, where stimuli were presented for 1000 ms (as opposed to 500 ms), and were considerably brighter at 250 tds (versus 20 tds in the present study).

Beside rod interaction with the cone signals, the cones themselves have interesting distributions across the retina that might affect local signal processing. As mentioned previously, S-cones are sparse in the center of the fovea and their peak distribution exists in a ring around the fovea (Ahnelt et al., 1987). Perhaps this aspect of the retinal mosaic explains why blueness appears different in the fovea when compared to the periphery. M- and L-cones are at their peak densities in the center of the fovea, but decline with eccentricity (Curcio et al., 1990). As retinal eccentricity increases, the ratio of L-cones relative to M-cones increases (Albrecht et al. 2002); however, the ratios are not consistent between individual observers (Roorda and Williams, 1999). These varying ratios may account for some of the differences seen in hue percentages across observers in the present study. Some researchers speculate that the decrease in overall

number of L- and M-cones reduces the quality of the chromatic signal (Martin, Lee, White, Solomon, and Ruttiger, 2001), even to the point where further increases in stimulus size cannot compensate for the reduced signal quality (Parry, McKeefry, and Murray, 2006). Because of this finding, it is possible that the large full-fields and annular stimuli look similar to one another, merely due to the same degradation of the signal from sparse M- and L-cones for both stimuli. Part of that signal degradation may be due to the increase in randomness of the connections of both M- and L- cones with increases in eccentricity (Crook, Manookin, Packer, and Dacey, 2011; Solomon, Lee, White, Rüttiger, and Martin, 2005), which decreases red-green sensitivity but leaves blue-yellow sensitivity relatively intact (Mullen and Kingdom, 2002), thereby increasing the blue-yellow contribution to perception.

It seems unlikely that a single type of photoreceptor (i.e., rods, or a specific cone type) would make the difference in mediating hue perception of large, uniform fields, especially because the perceptual experience occurs long after photoreceptor signals have been combined with and modulated by signals from other retinal cells (DeValois, 1965; Kaplan and Shapley, 1982; Derrington, Krauskopf, and Lennie, 1984). Some of this signal modulation occurs in the ganglion cells, which carry signals on to the lateral geniculate nucleus (LGN) and primary visual cortex (V1) for further processing. One of the questions the present study sought to explore was how large, full-field stimuli are uniform in appearance (as opposed to mottled), since small stimuli placed at different retinal locations yield different hue experiences. If the signals from the photoreceptors are uneven across the retina when viewing a uniform stimulus, as opposed to firing at the same rates and proportions across the stimulus, the subtle differences in chromatic signals might appear more like a low-spatial frequency pattern (i.e., a very subtle transition from brighter and dimmer portions of the stimulus) to the ganglion cells. Since the magnocellular

pathway is known for poor low-spatial frequency responses (Johnson, Hawken, and Shapley, 2004), perhaps it cannot encode the mottled appearance provided by the varied photoreceptor mosaic and instead encodes the experience as uniform in appearance by averaging the strength of the chromatic response, just as the contrast and pattern experience has been averaged to produce the perception of a uniform field. As the annular stimuli are subjected to the same mechanisms of signal degradation as the full-field stimuli in the peripheral retina (Martin et al., 2001; McKeefry et al., 2007; Mullen and Kingdom, 2002), it might be expected that the same compensatory mechanisms generating full-field uniform hue perception would be activated with the annular stimuli.

Other Mechanisms Implicated in Uniform Appearance of Stimuli

The present psychophysical study was not specifically designed to uncover whether one or more photoreceptor types were contributing to the uniform appearance of larger fields, and furthermore, some researchers have cautioned against using the knowledge of a varied retinal mosaic (Curcio et al., 1990) to make predictions of how it would impact the perceptual experience of hue, as variability of the photoreceptor ratios has little effect on normal color perception (Brainard et al., 2000; Miyahara, Pokorny, Smith, Baron, and Baron, 1998). Perhaps part of the reason why varying cone ratios have little impact on perceptual experience of uniform appearance is due to gain changes in the outputs of the cone photoreceptors. If the spectral sensitivity of small groups of photoreceptors are modulated (i.e., sensitivity of M- or L- cones was adjusted to compensate for varying receptor ratios), then a mottled appearance from the varied ratios could be reduced at the retinal level. One such example of gain changes at the retinal level is von Kries adaptation, which assumes spectral sensitivity of photoreceptors is

altered to accommodate slight changes in lighting of the environment and to keep the appearance of color consistent across multiple settings (Gordon and Abramov, 1977; Webster, Halen, Meyers, Winkler, and Werner, 2010). If the retina modulates the retinal signals to maintain color appearance across different environments, it seems plausible that those same mechanisms might influence the overall hue appearance of the stimulus. If gain mechanisms are in place for modulating photoreceptor activity within bounds of individual stimuli, that could explain how the 3˚ fields appear a slightly different hue from one another, as well as the annular ring, even though they are all placed at a similar eccentricity (i.e., 10°). Differing cone ratios across the retina are evident to be the primary factor responsible for why hue perception of the same physical stimulus varies across retinal quadrants (Volbrecht et al., 2009), so it would be expected that such a gain mechanism would be affected by the underlying retinal mosaic. Additionally, previous research (McKeefry, Murray, and Parry, 2007) shows that chromatic perceptual experience degrades with eccentricity, suggesting that gain mechanisms can only adjust for a limited range of deviation across retinal signals before overall hue appearance is affected. Some mechanisms that are partially responsible for the uniform appearance may involve local retinal gain changes to compensate for retinal physiology (i.e., varied cone ratios) and/or environmental changes (i.e., luminance changes), gain mechanisms driven by feedback from the visual cortex, or even higher-order learning processes adjusting the uniformity of the hue appearance (Bompas et al., 2013; Danilova and Mollon, 2006; Rensink, O'Regan, Clark, 1997; Webster et al., 2010).

Some researchers have investigated the effects of the macular pigment on uniform hue appearance and the mechanisms that compensate for its filtering effects (Bompas et al., 2013; O'Neil and Webster, 2014). Macular pigment is a yellow-colored filter, centered over the fovea, which has been shown to absorb short-wavelength light (approximately 400 – 580 nm), with

peak absorption occurring around 460 nm (Pease, Adams, and Nuccio, 1987). It might be expected that the differential filtering of short-wavelength light across the retina could contribute to some of the perceptual difference between the fovea (i.e., overlaid with macular pigment) and peripheral retinas (i.e., an absence of macular pigment). Bompas et al. (2013) suggested that macular pigment was the largest contributing factor of hue shifts classically seen between fovea and periphery. In the present study, the point at which the stimulus started appearing more like the large fields was between 3˚ and 5˚, which coincides with measurements that the macular pigment density tapers off at approximately 4˚ of retinal eccentricity (Wooten and Hammond, 2005). Macular pigment filtering could explain why the small foveally placed stimuli appear different than the annular stimuli in the present study, specifically in the shorter wavlengths where macular pigment filtering is most pronounced (i.e., 460 nm); yet, the full-field stimuli cover regions with and without macular pigment and appear most similar to the annular stimuli which were placed outside the macular pigment region. Also, for large full-field stimuli, observers reported the field as uniform in appearance, and do not report the central portion of the field covering the macular pigment region as appearing to be dimmer or of differing in hue; thus, suggesting a mechanism or some mechanisms compensate for the effects of macular pigment. Researchers have investigated the neural mechanisms maintaining the appearance of white (Webster and Leonard, 2008) and unique hues (Webster et al., 2010), taking into consideration the macular pigment differences between the fovea and peripheral retina. In both studies, the white field appeared uniform as it stimulated both the fovea and peripheral retina. Webster and Leonard's (2008) findings suggested that local cone gain mechanisms alone are enough to compensate for the short-wavelength filtering effect of the macular pigment, at least for constancy of white fields; however, Webster et al. (2010) found that chromatic fields must also

depend on gain mechanisms from the cortex in order to fully compensate for the filtering effects of macular pigment.

In addition to investigating the effect of macular pigment on hue perception, O'Neil and Webster (2014) were also interested in how the contrast of the edge of the stimulus played a role in the uniformity of large fields, based on the idea that much of the potency of the filling-in and filling-out effects reported in the literature depend on high contrast differences between the bordering stimuli (Broerse, Vladusich, O'Shea, 1999; Devinck, Delahunt, Hardy, Spillmann, and Werner, 2005; Pinna et al., 2001). For example, in general, the lower the luminance contrast between two boundaries, the less pronounced the watercolor effect (Devinck et al., 2005; see introduction for more discussion of the watercolor effect). If the neural mechanisms mediating the watercolor effect are also implicated in the hue appearance of large fields, the high contrast edges of the stimuli used in the present study would be likely to influence hue appearance. With the multitude of stimulus sizes used in the present study, there were high contrast edges on the outside and inside edges of the annular stimuli, as well as the outside edge of the full field stimuli. No clear patterns of differences emerged for hue appearance between the full-field and annular stimuli, suggesting that edge contrast differences that might exist for these two types of stimuli were not a factor in the present study. Additionally, O'Neil and Webster (2014) found no difference with the uniformity of the hue experience between stimuli with high and low spatial frequency edges, so the neural mechanisms proposed for color-spreading effects do not seem to apply to those for uniform color surfaces.

The role of stimulus edges in the filling-in process have also been investigated in the visual cortex. Huang and Paradisio (2008) found that V1 cells had faster and stronger responses to the outside portion of a full-field stimulus than to the interior portions, providing support for a

V1 neural mechanism for filling-in (rather than filling-out). von der Heydt, Friedman, and Zhou (2003) and Devinck et al. (2008) found that when perceptual filling-in was occurring, single-opponent neurons did not change their response rates to in the receptive fields where the induced color experience was occurring, suggesting that V1 cells respond differently to filled-in/induced portions of a stimulus than they do to physical stimuli. Similarly, Zweig et al. (2015) did not report a change in the response of V1 neurons to the interior portion of a chromatic stimulus where filling-in was occurring; however, they did see a change in double-opponent cell firing rates when filling-in occurred with achromatic stimuli. The findings of von der Heydt et al. (2003) and Devinck et al. (2008) would suggest it is not the V1 neurons themselves, but even higher-level processes (i.e., V4, or possibly more distributed conscious neural mechanisms) that are exerting some top-down influence on those cells in V1. Since V1 neurons fire at slower rates in response to the interior portion of the stimulus than the edges (Huang and Paradisio, 2008) and V1 neurons don't change their rate of responding to the interior portions of an induced/filled-in color experience (Zweig et al., 2015), this may be another part of the explantion for why the peripheral retina exerts more influence over the color appearance of large stimuli than the fovea does. If these mechanisms are applied to stimuli in the present study, it would be expected that the hue of large full-field stimuli would appear more similar to the hue of annular stimuli than to the hue of small foveally placed stimuli, especially since the outer edges of the full-field and annular stimuli were placed at identical positions in the retina. While the full-field stimulus includes the fovea and the annulus is stimulus-free at its center, the findings above (e.g., Devinck et al., 2008; von der Heydt et al., 2003; and Zweig et al., 2015) suggest there may be neural mechanisms that discount the contributions of the fovea and the edges are given more neural weight in determining hue appearance.

One limitation of the present study was that observers did not closely investigate the uniformity of the stimuli themselves, and all of the data in the present experiment are built upon this assumption. Perhaps the annular and full field stimuli in this study were not actually uniform in appearance; however, the subtle differences were not enough to be salient and thus, observers' perception of the uniformity of the hue experience was assumed. Rensink, O'Regan, and Clark (1997) found that observers had difficulty noticing changes in stimuli, especially when they were presented for short durations and in relatively rapid succession. As the stimuli in the present study had to be consciously reported and briefly remembered, there could be some concerns about how iconic memory, which has very short temporal accuracy, played a role in reporting their details (Rensink et al., 1997). In a similar vein, Bompas et al. (2013) have suggested that lifelong learning of color experiences enables some color constancy among stimuli that are viewed across the retina. It is unclear how much this would apply to monochromatic stimuli that are not often seen in real-world settings. Based on wavelength-discrimination functions of the fovea and peripheral retina (Stabell et al., 1984) and between-session variability of unique hue loci (e.g. Nerger et al., 1998; Volbrecht, Nerger, Imhoff, and Ayde, 2000), humans are able to discriminate differences in stimuli which vary by as little as 3 nm; however, this is quite different from viewing a large monochromatic stimulus that may or may not have some variations in uniformity. Perhaps the large stimuli in the present study (both full-field and annular) look uniform because we have learned to adjust for the physiological differences, thus leading observers to recall slightly uneven hue experiences as uniform.

Another limitation of the present study was that while observers were reasonably consistent across trials with regard to their own hue responses within each condition, intra-observer agreement for hue percentages within most conditions was generally poor. This is not

outside the realm of expectations, as large individual differences have been noted across previous research (Kuehni, 2004; Malkoc, Kay, and Webster, 2005; Volbrecht, Nerger, and Harlow, 1997; Webster et al., 2000). Unique hues, which are defined as the wavelength-locus for a perceptual experience of a monochromatic hue (e.g., pure blue without a hint of green or red), provide a parsimonious way of measuring the boundaries of hue experience. Unique hue loci have been shown to vary across observers for unique green (Volbrecht et al., 1997) and unique blue and yellow (Webster, Miyahara, Malkoc, and Raker, 2000), with meta-analyses showing that unique hue perceptions cover 65% of the visible spectrum (Kuehni, 2004). In other words, the loci of unique green for one observer might be the loci of unique blue for another. Malkoc et al. (2005) have demonstrated that these differences are also present when observers engage in a hue-scaling task similar to what was used in the present study. The real-world implication of these findings is that color experience is not objectively and similarly experienced, even across color-normal observers. Beyond the clear psychophysical data that the same physical stimuli are given different hue percentages by each observer, the degree to which people use the same color label for different color experiences is unclear. As children (and even as adults), the color learning process involves being given color labels for presented objects or images, which serves to align individuals' agreement on what each perceptual experience should be called.

Overall, the trend of the annular stimuli appearing most similar to the full-field stimuli was unaffected, regardless of the individual differences in the hue percentages assigned to each wavelength; however, it should be noted that it would be very difficult to create a mathematical model that reflects the expected hue differences between annular, full-field, and foveal stimuli due to these individual differences. Any exploratory attempts to create a "Standard Observer" by averaging data from the four observers in the present study resulted in a large reduction of the

hue differences reported between stimulus conditions. Furthermore, hue data gleaned from one participant throughout different stimulus conditions could not readily be used to make predictions about what another observer would perceive. With data from the present study, it may be possible to create a model that indicates how much of the uniform hue perception is due to peripheral influence and how much is due to foveal influence. Future extensions of this research and attempts to model this data would benefit from a larger number of participants and more stimulus sizes, which would allow for a more detailed investigation of mechanisms of spatial integration.

Conclusion

The research and data surrounding the retinal mediator(s) of uniform hue perception is understandably complex and the present study adds more information to the psychophysical understanding of uniform hue experience. It is interesting to note that as foveally centered stimuli are made larger, they quickly (i.e., by 5˚) take on a similar hue as the large fields, suggesting that the fovea's influence on hue appearance of the stimulus field quickly wanes as the proportion of active peripheral retina to active foveal retina increases. Small (i.e., 3˚) peripherally placed stimuli yield a hue experience that is similar to the hue of large annular stimuli (23˚), with the specific retina region that appears most similar varying across observers; however, averaging the hue experience of 3˚ fields from multiple retinal regions yields a hue percentage that is close to that of the large fields for all observers. These findings suggest that the surface area of the retina consumed by stimuli plays a role in the hue experienced. As with previous studies conducted in this laboratory (Opper et al., 2014; Volbrecht et al., 2009), the largest differences between hue experience in the peripheral retina and fovea occur in the middle-wavelength portion of the visible spectrum, where stimuli appear green-yellow. When

investigating the impact of minimizing rod input (bleach conditions) relative to conditions with maximal rod input (dark-adaptation conditions), the present study found the bleaching field reduced the disparity between the full-field, annular, and foveal conditions for some hue terms. This finding suggests that a reduction of rod input may dilute the strength of the peripheral retina's influence on the hue experience of large fields, and/or, that cone influences are more pronounced in the conditions with minimal rod input, thus bringing hue experiences closer together across conditions.

In general, it seems unlikely that retinal signaling is exclusively responsible for the uniformity of hue experience, since the retinal mosaic varies wildly with eccentricity (Curcio et al., 1990) and the hue experience also varies considerably with eccentricity and stimulus size (Abramov et al., 1991; McKeefry et al., 2007; Stabell and Stabell, 1976). Additionally, it is clear that photoreceptor signals are controlled by gain mechanisms (Lee et al., 1997), but whether that occurs locally or is driven by higher level cortical processes has yet to be determined. Gain mechanisms would be crucial in helping to make the color appearance of large fields uniform with an underlying, uneven retinal mosaic.

The results of the present study show that the hue of stimuli presented to the peripheral retina appear more like the large fields than stimuli presented exclusively to the fovea; however, it is important to note that the responsible mechanisms are not necessarily contained locally within the peripheral retina. Whatever mechanisms are responsible for mediating uniform hue appearance (e.g., local retinal processes, neural convergence in the LGN and/or V1, top-down processing, etc) are likely large-scale perceptual constancy mechanisms that get applied to all stimuli that stimulate the peripheral retina. Given the complexity of each individual's visual system and life-long visual experiences, it is a wonder that our hue experiences are as consistent

and similar as they are. It seems reasonable that all of the perceptual mechanisms that serve to keep the human visual environment relatively stable and constant cannot compensate perfectly for all these factors; thus, this explains why stimulus size, eccentricity, luminance, temporal factors, and background fields all subtly impact the uniformity of hue experience.

REFERENCES

Abramov, I., Gordon, J. and Chan, H. (1991) Color appearance in the peripheral retina: effects of stimulus size. *Journal of the Optical Society of America A,* 8(2), 404-414.

Ahnelt, P.K., Kolb, H. and Pflug, R. (1987) Identification of a subtype of cone photoreceptor, likely to be blue sensitive, in the human retina. *Journal of Comparative Neurology,* 255, 18-34.

Albrecht, J., Jägle, H., Hood, D.C. and Sharpe, L.T. (2002) The multifocal electroretinogram (mfERG) and cone isolating stimuli: Variation in L- and M-cone driven signals across the retina. *Visual Neuroscience,* 2, 543-557.

Alpern, M. (1971). Rhodopsin kinetics in the human eye. *Journal of Physiology*, 217, 447 – 471.

Ambler, B. (1974). Hue discrimination in peripheral vision under conditions of dark and light adaptation. *Perception and Psychophysics,* 15(3), 586-590

Angel, C.L. (2003). The effect of rods on perceptive field size at 10° eccentricity in the four retinal quadrants. Doctoral Dissertation, Colorado State University.

Balas, B. and Sinha, P. (2007) Filling-in colour in natural scenes. *Visual Cognition,* 15, 765 – 778.

Beare, J. (1906). Greek Theories of Elementary Cognition from Alcmaeon to Aristotle. *Oxford University Press*. Vol. 16, No. 61, 118-126.

Bompas, A., Powell, G., Sumner, P. (2013). Systematic biases in adult color perception persist despite lifelong information sufficient to calibrate them. *Journal of Vision,* 13:19.

Bowmaker, J.K. and Dartnall, H.J.A. (1980). Visual pigments of rods and cones in a human retina. *Journal of Physiology*, 298, 501-511.

Boynton, R.M., Schafer, W. and Neun, M.E. (1964) Hue-wavelength relation measured by color-naming method for three retinal locations. *Science,* 146, 666-668.

Brainard, D. H., Roorda, A., Yamauchi, Y. Calderone, J. B., Metha, A., Neitz, M., Neitz, J., Williams, D. R., and Jacobs, G. H. (2000). Functional consequences of the relative numbers of L and M cones. *Journal of the Optical Society of America A*, 17, 607-614

Breitmeyer, B. and Jacob, J. (2012). Microgenesis of surface completion in visual objects: Evidence for filling-out. *Vision Research*, 55. 11-18

Broerse, J., Vladuusich, T., and O'Shea, R.P. (1999). Colour at edges and colour spreading in McCollough effects. *Vision Research,* 39, 1305 – 1320.

Brown, P.K. and Wald, G. (1964). Visual pigments in single rods and cones of the human retina. Direct measurements reveal mechanisms of human night and color vision. *Science*, 144 (3614), 45-52.

Buck, S. L., Thomas, L. P., Hillyer, N., and Samuelson, E. M. (2006). Do rods influence the hue of foveal stimuli? *Visual Neuroscience*, 23, 519-523.

Buck, S.L. and Knight, R. (2003) Stimulus duration affects rod influence on hue perception. In Normal & Defective Colour Vision. J.D Mollon, J. Pokorny, and K. Knoblauch (eds). *Oxford University Press*, 179-186.

Buck, S.L., Knight, R.F. and Bechtold, J. (2000) Opponent-color models and the influence of rod signals on the loci of unique hues. *Vision Research,* 40, 3333-3344

Buck, S.L., Thomas, L.P., Connor, C.R., Green, K.B. and Quintana, T. (2008) Time course of rod influences on hue perception. V*isual Neuroscience,* 25, 517-520.

Casagrande, V.A. (1994). A Third parallel visual pathway to primate area V1. *Trends Neuroscience,* 17, 305 – 310.

Cornsweet, T. (1970). *Visual Perception*. London: Academic Press.

Crook, J.D., Manookin, M.B., Packer, O.S., and Dacey, D.M. (2011). Horizontal cell feedback without cone type-selective inhibition mediates "red-green" color opponency in midget ganglion cells of the primate retina. *Journal of Neuroscience*, 31(5), 1762–1772.

Curcio, C.A. and Allen, K.A. (1990). Topography of ganglion cells in human retina. *The Journal of Comparative Neurology*, 300, 5-25.

Curcio, C.A., Allen, K.A., Sloan, K.R., Lerea, C.L., Hurley, J.B., Klock, I.G. and Milan. A.H. (1991) Distribution and morphology of human cone photoreceptors stained with anti-blue opsin. *Journal of Comparative Neurology*, 312, 610-624.

Curcio, C.A., Sloan, K.R., Kalina, R.E. and Henderson, A.E. (1990) Human photoreceptor topography. *Journal of Comparative Neurology*, 292, 497-523.

Dacey, D.M. and Lee, B.B. (1994) The 'blue-on' opponent pathway in primate retina originates from a distinct bistratified ganglion cell type. *Nature*, 367, 731-735.

Danilova, M.V., and Mollon, J.D. (2006). The comparison of spatially separated colours. *Vision Research*, 46 (6-7), 823 – 836.

Dartnall, H. J. A., Bowmaker, J. K., and Mollon, J. D. (1983). Human Visual Pigments: Microspectrophotometric Results from the Eyes of Seven Persons. *Proceedings of the Royal Society of London*, 220, 115-130.

Derrington, A.M., Krauskopf, J., and Lennie, P. (1984). Chromatic mechanisms in lateral geniculate nucleus of macaque. *J Physiol.* 357:241–265.

DeValois, R.L. (1965). Analysis and coding of color vision in the primate visual system. *Cold Spring Harb Symp Quant Bio*. 38:567–580.

DeValois, R.L, Abramov, I., and Jacobs, G.H. (1966). Analysis of response patterns of LGN cells. *Journal of the Optical Society of America,* 56. 966-977

DeValois, R.L. and DeValois, K.K. (1993) A multi-stage color model. *Vision Research,* 33, 1053-1065.

Devinck, F., Delahunt, P.B., Hardy, J.L., Spillmann, L., and Werner, J.S. (2005). The watercolor effect: Quantitative evidence for luminance-dependent mechanisms of long-range color assimilation. *Vision Research,* 45(11); 1413 – 1424.

Frumkes, T. E., and Eysteinsson, T. (1988). The cellular basis for suppressive rod-cone interaction. *Visual Neuroscience*, 1, 263-273.

Gordon, J., and Abramov, I. (1977). Color vision in the peripheral retina. II. Hue and saturation. *Journal of the Optical Society of America*, 67, 202-207.

Gouras, P. and Link, K. (1966). Rod and Cone Interaction in Dark-Adapted Monkey Ganglion Cells. *J. Physiol.*, 184, 499-510.

von Helmholtz, H. (1962). Compound Colors. Handbook of Psychological Optics. Translated by JPC Southall. Vol. 2. *New York: Dover*. 120 – 146. (Originally published 1867).

Hering, E. (1964). An outline of a theory of the light sense. *Harvard University Press*. Cambridge, Massachusetts. Translated by Hurvich, L.M. and Jameson, D. (Originally published 1878).

von der Heydt, R., Friedman, H.S., and Zhou, H. Searching for the neural mechanism of color filling-in. In: Pessoa L, DeWeerd P, editors. Filling-in: from perceptual completion to cortical reorganization. New York: *Oxford University Press*; 2003. pp. 106–127.

Huang, X. and Paradisio, M.A. (2008). V1 Response Timing and Surface Filling-In. *J Neurophysiol.* 100(1): 539 – 547.

Hurvich, L. M. and Jameson, D. (1957). An Opponent-Process Theory of Color Vision. *Psychological Review*, 64 (6), 384-404.

Jameson, D. and Hurvich, L. M. (1967). Fixation-light Bias: An Unwanted By-product of Fixation Control. *Vision Research*, 7, 805-809.

Johnson, E.N., Hawken M.J., and Shapley R. (2004). Cone inputs in macaque primary visual cortex. *J.Neurophysiol.* 91:2501–2514.

Kaplan, E. and Shapley, R. (1982). X and Y cells in the lateral geniculate nucleus of the macaque monkey. *J.Physiol*. 330:125–143.

Kaplan. E., Lee, B. B. and Shapley, R. M. (1990). New views of primate retinal function. *Progress in Retinal Research*, 9, 273-336.

Knight, R. and Buck, S.L. (2002). Time-Dependent Changes of Rod Influence on Hue Perception. *Vision Research,* 42, 1651-1662.

Kuehni, R.G. (2004). Variability in unique hue selection: A surprising phenomenon. *Color Research & Application.* 29, 158-162.

Land, M.F. and Nilsson, D.E. (2002) Animal Eyes. *Oxford: Oxford University Press.*

Lee, B.B., Smith, V.C., Pokorny, J., and Kremers, J. (1997). Rod Inputs to Macaque Ganglion Cells. *Vision Research*, 37 (20). 2813-2828

Lie, I. (1963). Dark adaptation and the photochromatic interval. *Documenta Ophthalmologica*, 17. 411-510

Livingstone, M.S. and Hubel, D.H. (1984). Anatomy and physiology of a color system in the primate visual cortex. *J. Neurosci*. 4: 309–356.

Malkoc, G., Kay, P., and Webster, M.A. (2005). Variations in normal color vision. IV. Binary hues and hue scaling. *Journal of the Optical Society of America.* 22 (10), 2154 – 2168.

Martin, P. R., Lee, B. B., White, A. J. R., Solomon, S. G., and Rüttiger, L. (2001). Chromatic sensitivity of ganglion cells in the peripheral primate retina. *Nature*, 410, 933-936.

Maxwell, James. (1860). On the theory of compound colours and the relations of the colours of the spectrum. *Philosophical Transactions of the Royal Society*. 150, 57- 84.

McKeefry, D.J., Murray, I.J. and Parry, N.R.A. (2007) Perceived shifts in saturation and hue of chromatic stimuli in the near peripheral retina. *Journal of the Optical Society of America A*, 24(10), 3168-3179.

Miyahara, E., Pokorny, J., Smith, V.C., Baron, R., and Baron, E. (1998). Color vision in two observers with highly biased LWS/MWS cone ratios. *Vision Research*, 38 (4): 601 – 612.

Moreland, J. D., and Cruz, A. (1959). Colour perception with the peripheral retina. *Optica Acta*, 6, 117-151.

Motoyoshi, I. (1999) Texture filling-in and texture segregation revealed by transient masking. *Vision Research*, 39, 1285 – 1291.

Mullen, K.T. and Kingdom, F.A. (2002). Differential distributions of red-green and blue-yellow cone opponency across the visual field. *Visual Neuroscience,* 19(1): 109 – 118.

Nagy, A.L. and Doyal, J.A. (1993). Red-green color discrimination as a function of stimulus field size in peripheral vision. *Journal of the Optical Society of America A*, 10(6), 1147-1156.

Nerger, J. L., and Cicerone, C. M. (1992). The ratio of L cones to M cones in the human parafoveal retina. *Vision Research*, 32, 879-888.

Nerger, J. L., Volbrecht, V. J., and Ayde, C. J. (1995). Unique hue judgments as a function of test size in the fovea and at 20-deg temporal eccentricity. *Journal of the Optical Society of America A*, 12, 1225-1232.

Nerger, J.L., Volbrecht, V.J., Ayde, C.J., and Imhoff, S.M. (1998) Effect of the S-cone mosaic and rods on red/green equilibria. *Journal of the Optical Society of America A*, 15(10), 2816-2826.

Newton, I. (1730). Opticks: Or, a treatise of the reflections, refractions, inflections and colours of light. The fourth edition, corrected. By Sir Isaac Newton, Knt. London: Printed for William Innys.

O'Neil, S.F., and Webster, M.A. (2014) Filling in, filling out, or filtering out: processes stabilizing processing color appearance near the center of gaze. *Journal of the Optical Society of America A,* 31 (4), 140 – 147.

Opper, J.K., Douda, N.D., Volbrecht, V.J., and Nerger, J.L. (2014) Supersaturation in the peripheral retina. *Journal of the Optical Society of America A*., 31 (4), 148 – 158.

Østerberg, G. (1935). Topography of the layer of rods and cones in the human retina. *Acta Ophthalmologica (Suppl.)*, 6, 1-102.

Paradisio, M.A., and Nakayama, K. (1991) Brightness perception and filling-in. *Vision Research,* 31, 1221 – 1236.

Parry, N. R. A., McKeefry, D. J., and Murray, I. J. (2006). Variant and invariant color perception in the near peripheral retina. *Journal of the Optical Society of America A*, 23, 1586-1597.

Pease, P.L., Adams, A.J., and Nuccio, E. (1987). Optical Density of Human Macular Pigment. *Vision Research,* 27 (5). 705 – 710.

Pinna, B., Brelstaff, G., and Spillman, L. (2001). Surface color from boundaries: A new ''watercolour'' illusion. *Vision Research*, 41, 2669-2676.

Rensink, R.A., O'Regan, J.K., and Clark, J.J. (1997). To see or not to see: The need for attention to perceive changes in visual scenes. *Psychological Science*, 8, 368–373.

Roorda, A., and Williams, D. R. (1999). The arrangement of the three cone classes in the living human eye. *Nature*, 397, 520-522.

Rushton, W. A. H., and Powell, D.S. (1972). The rhodopsin content and the visual threshold of human rods. *Vision Research*, 12, 1073 – 1081.

Shapley, R. and Hawken, M. (2011). Color in the Cortex – single- and double-opponent cells. *Vision Research, 51(7)*: 701 – 717.

Solomon S. G., Lee B. B., White A. J., Ruttiger L., and Martin P. R. (2005). Chromatic organization of ganglion cell receptive fields in the peripheral retina. *Journal of Neuroscience*, 25(18), 4527–4539.

Spillmann, L., Otte, T., Hamburger, K., and Magnussen, S. (2006). Perceptual Filling-in from the edge of the blind spot. *Vision Research*, 46, 4252-4257.

Spillmann, L. and Werner, J.S. (1996). Long-range interactions in visual perception. *Trends in Neurosciences*, 19, 428-434.

Stabell, B. and Stabell, U. (1976). Rod and cone contributions to peripheral colour vision. *Vision Research*, 16, 1099-1104.

Stabell, B. and Stabell, U. (1996). Peripheral color vision: Effects of rod intrusion at different eccentricities. *Vision Research*, 36(21), 3407-3414.

Stabell, U., and Stabell, B. (1999). Rod-cone color mixture: Effect of size and exposure time. *Journal of the Optical Society of America A*, 16, 2638-2642.

Stabell, U., and Stabell, B. (1984). Color-vision mechanisms of the extrafoveal retina. *Vision Research,* 24, 1969-1975.

Stabell, U., and Stabell, B. (1994). Mechanisms of chromatic rod vision in scotopic illumination. *Vision Research,* Vol. 34, Iss. 8: 1019-1027.

Stiles, W.S., and Burch, J.M. (1958). N.P.L. Colour-matching Investigation: Final Report. *Optica Acta: International Journal of Optics,* Vol. 6, Iss. 1.

Stiles, W.S. (1962). The directional sensitivity of the retina. *Ann. R. Coll. Surg. Engl.,* 30: 73 – 101.

Thomas, L. P., and Buck, S. L. (2006). Foveal and extra-foveal influences on rod hue biases. *Visual Neuroscience*, 23, 539-542.

Trezona, P.W. (1970). Rod participation in the 'blue' mechanism and its effect on color matching. *Vision Research*, 10(4), 317-332.

Troup, L.J., Pitts, M.A., Volbrecht, V.J. and Nerger, J.L. (2005). Effect of stimulus intensity on the sizes of chromatic perceptive field. *Journal of the Optical Society of America A,* 22(10), 2137-2142.

van Tuijl, H. F. J. M. (1975). A new visual illusion: neonlike color spreading and complementary color induction between subjective contours. *Acta Psychologica*, 390, 441–445.

Volbrecht, V. J., and Nerger, J. L. (2012). Color appearance at ±10° along the vertical and horizontal meridians. *Journal of the Optical Society of America A*, 29, A44-A51.

Volbrecht, V.J., Nerger, J.L., and Harlow, C.E. (1997). The bimodality of unique green revisited. *Vision Research.* 37(4). 407 – 416.

Volbrecht, V. J., Nerger, J. L., and Trujillo, A. R. (2011). Middle- and long-wavelength discrimination declines with rod photopigment regeneration. *Journal of the Optical Society of America A*, 28, 2600-2606.

Volbrecht, V.J., Clark, C.L., Nerger, J.L. and Randell, C.E. (2009). Chromatic perceptive field sizes measured at 10° along the horizontal and vertical meridians. *Journal of the Optical Society of America A,* 26(5), 1167-1177.

Volbrecht, V.J., Nerger, J.L., Imhoff, S.M., and Ayde, C.J. (2000). Effect of the short-wavelength sensitive-cone mosaic and rods on the locus of unique green. *Journal of the Optical Society of America A,* 17(3), 628-634.

Watson, A. B., and Yellott, J. I. (2012). A unified formula for light-adapted pupil size. *Journal of Vision*, 12, 1-16.

Webster, M.A., Miyahara, E., Malkoc, G., and Raker, V.E. (2000). Variations in normal color vision. II. Unique hues. *Journal of the Optical Society of America.* 17(9), 1545 – 1555.

Webster, M.A., and Leonard, D. (2008). Adaptation and perceptual norms in color vision. *J. Opt. Soc. Am. A Opt. Image Sci. Vis.* 25, 2817–2825.

Webster, M.A., Halen, K., Meyers, A.J., Winkler, P., and Werner, J.S. (2010). Colour appearance and compensation in the near periphery. *Proc. R. Soc. B*, 277; 1817-1825.

Westheimer, G. (1966) The Maxwellian view. *Vision Research,* 6, 669-682.

Williams, D.R., MacLeod, D.I.A., and Hayhoe, M.M. (1981a) Foveal tritanopia. *Vision Research,* 21, 1341-1356.

Wooten, B.R., and Hammond, B.R. Jr. (2005). Spectral absorbance and spatial distribution of macular pigment using heterochromatic flicker photometry. *Optom. Vis. Sci.,* 82, 378-386.

Wyszecki, G., and Stiles, W. S. (1982). Color Science: Concepts and Methods, Quantitative Data and Formulae. *John Wiley and Sons*, New York.

Young, T. (1802). On the Theory of Light and Colours. *Philos. Trans. R. Soc. London.,* 92, 20-71.

Zweig, S., Zurawel, G., Shapley, R., and Slovin, H. (2015). Representation of Color Surfaces in V1: Edge Enhancement and Unfilled Holes. *The Journal of Neuroscience*, 35(35). 12103-12115.

APPENDIX:

AIW 3-session Mean Data

1˚ Fovea			Mean			Standard Error of the Mean				
λ	*Blue*	*Green*	*Yellow*	*Red*	*Sat*	*Blue*	*Green*	*Yellow*	*Red*	*Sat*
420	79.64	0.00	0.00	12.03	91.67	3.62	0.00	0.00	0.75	2.91
440	93.98	0.42	0.00	2.04	96.44	1.09	0.42	0.00	1.21	0.44
460	95.04	0.85	0.00	0.00	95.89	1.42	0.37	0.00	0.00	1.06
480	71.51	7.83	0.00	0.00	79.33	0.22	2.00	0.00	0.00	2.12
500	14.89	47.66	0.00	0.00	62.56	2.23	5.46	0.00	0.00	5.11
520	3.87	70.47	5.99	0.00	80.33	2.37	11.92	1.48	0.00	11.01
540	1.67	55.90	15.76	0.00	73.33	1.67	15.50	3.22	0.00	17.00
560	0.00	12.75	46.03	0.00	58.78	0.00	4.24	14.92	0.00	13.69
580	0.00	1.01	50.50	2.27	53.78	0.00	1.01	1.67	0.46	0.22
600	0.00	0.00	32.68	40.43	73.11	0.00	0.00	13.85	14.46	5.86
620	0.00	0.00	6.45	79.22	85.67	0.00	0.00	2.03	3.86	3.53
640	0.40	0.00	4.78	88.48	93.67	0.20	0.00	1.75	2.72	2.14
660	0.53	0.00	2.94	90.98	94.44	0.53	0.00	0.82	1.10	0.99
23˚ w/ annulus			**Mean**			**Standard Error of the Mean**				
λ	*Blue*	*Green*	*Yellow*	*Red*	*Sat*	*Blue*	*Green*	*Yellow*	*Red*	*Sat*
420	78.38	0.00	0.00	14.29	92.67	5.17	0.00	0.00	3.84	1.33
440	93.90	0.96	0.00	1.59	96.44	1.69	0.48	0.00	0.79	1.47
460	91.78	1.77	0.00	0.00	93.56	0.30	0.70	0.00	0.00	0.40
480	61.38	17.73	0.00	0.00	79.11	10.48	9.00	0.00	0.00	1.56
500	3.25	87.75	2.89	0.00	93.89	1.63	2.17	2.17	0.00	2.15
520	0.00	84.61	8.72	0.00	93.33	0.00	1.32	1.55	0.00	2.27
540	0.00	68.62	13.38	0.00	82.00	0.00	4.23	1.34	0.00	4.73
560	0.00	14.73	44.05	0.00	58.78	0.00	6.11	8.70	0.00	7.57
580	0.00	0.39	38.85	2.31	41.56	0.00	0.39	3.72	0.64	3.58
600	0.00	0.00	40.10	13.23	53.33	0.00	0.00	6.58	1.69	5.29
620	0.00	0.00	17.73	58.16	75.89	0.00	0.00	4.25	6.97	3.56
640	0.00	0.00	3.25	86.64	89.89	0.00	0.00	0.23	1.49	1.68
660	1.49	0.00	1.03	88.15	90.67	0.42	0.00	0.52	2.48	2.52

AIW 3-session Mean Data

23˚ full-field			Mean			Standard Error of the Mean				
λ	*Blue*	*Green*	*Yellow*	*Red*	*Sat*	*Blue*	*Green*	*Yellow*	*Red*	*Sat*
420	78.09	0.00	0.00	11.69	89.78	1.71	0.00	0.00	2.87	1.49
440	91.01	0.36	0.00	1.18	92.56	3.94	0.36	0.00	0.60	4.15
460	92.30	0.70	0.00	0.11	93.11	2.89	0.10	0.00	0.11	3.01
480	58.25	15.97	0.00	0.00	74.22	7.36	5.16	0.00	0.00	3.18
500	3.63	82.35	2.68	0.00	88.67	3.63	4.79	1.39	0.00	2.52
520	0.00	89.50	7.50	0.00	97.00	0.00	1.61	0.64	0.00	1.17
540	0.00	74.10	14.23	0.00	88.33	0.00	7.49	4.82	0.00	2.80
560	0.00	17.00	53.00	0.00	70.00	0.00	6.98	8.68	0.00	5.87
580	0.00	0.40	51.68	3.48	55.56	0.00	0.40	10.16	0.66	10.46
600	0.00	0.00	44.13	15.20	59.33	0.00	0.00	8.56	4.07	7.04
620	0.00	0.00	13.35	71.09	84.44	0.00	0.00	5.72	7.68	2.12
640	0.52	0.00	3.11	89.93	93.56	0.28	0.00	1.01	2.97	2.26
660	2.74	0.00	0.44	92.16	95.33	0.17	0.00	0.44	1.59	1.53
35˚ w/ annulus			**Mean**			**Standard Error of the Mean**				
λ	*Blue*	*Green*	*Yellow*	*Red*	*Sat*	*Blue*	*Green*	*Yellow*	*Red*	*Sat*
420	78.55	0.00	0.00	11.12	89.67	0.33	0.00	0.00	1.02	1.35
440	91.87	0.42	0.00	2.59	94.89	1.82	0.28	0.00	1.47	1.28
460	95.05	1.40	0.00	0.00	96.44	1.24	0.58	0.00	0.00	1.28
480	56.43	21.90	0.00	0.00	78.33	6.05	2.54	0.00	0.00	7.22
500	13.67	63.68	2.09	0.00	79.44	10.13	12.33	2.09	0.00	7.44
520	0.76	88.53	5.93	0.00	95.22	0.76	3.44	2.65	0.00	1.37
540	0.00	52.06	12.49	0.00	64.56	0.00	5.99	1.77	0.00	6.51
560	0.00	9.46	46.43	0.00	55.89	0.00	2.15	9.10	0.00	11.06
580	0.00	0.58	44.38	2.15	47.11	0.00	0.58	7.41	0.58	6.63
600	0.00	0.00	37.22	22.56	59.78	0.00	0.00	8.38	7.61	9.63
620	0.00	0.00	10.06	57.72	67.78	0.00	0.00	3.80	4.93	7.98
640	0.18	0.00	3.31	86.95	90.44	0.18	0.00	1.35	1.35	0.29
660	1.97	0.00	0.82	90.32	93.11	0.34	0.00	0.23	2.26	1.94
35˚ full-field			**Mean**			**Standard Error of the Mean**				
λ	*Blue*	*Green*	*Yellow*	*Red*	*Sat*	*Blue*	*Green*	*Yellow*	*Red*	*Sat*
420	77.93	0.00	0.00	13.51	91.44	2.93	0.00	0.00	1.56	1.44
440	93.80	0.22	0.00	2.65	96.67	2.06	0.11	0.00	1.04	1.39
460	96.58	0.98	0.00	0.00	97.56	0.11	0.38	0.00	0.00	0.40
480	70.52	13.59	0.00	0.00	84.11	3.21	1.39	0.00	0.00	1.95
500	4.14	86.05	3.14	0.00	93.33	2.91	4.31	1.57	0.00	3.02
520	0.00	85.35	8.32	0.00	93.67	0.00	2.31	1.47	0.00	2.52
540	0.00	70.95	9.94	0.00	80.89	0.00	5.88	0.38	0.00	5.78
560	0.00	14.05	37.40	0.00	51.44	0.00	4.83	12.86	0.00	14.45
580	0.00	0.48	44.59	2.60	47.67	0.00	0.37	9.61	0.40	9.23
600	0.00	0.00	54.08	15.14	69.22	0.00	0.00	3.02	1.01	2.44
620	0.00	0.00	12.20	70.13	82.33	0.00	0.00	3.79	7.11	4.34
640	0.41	0.00	3.00	89.93	93.33	0.41	0.00	1.13	1.01	1.53
660	2.48	0.00	1.03	86.82	90.33	0.40	0.00	0.56	1.69	1.76

JO 3-session Mean Data

1˚ Fovea	Mean					Standard Error of the Mean				
λ	*Blue*	*Green*	*Yellow*	*Red*	*Sat*	*Blue*	*Green*	*Yellow*	*Red*	*Sat*
420	16.39	0.00	0.00	69.95	86.33	5.29	0.00	0.00	5.90	0.77
440	81.45	0.00	0.00	5.55	87.00	4.09	0.00	0.00	1.29	3.01
460	81.05	0.91	0.00	3.93	85.89	1.87	0.51	0.00	1.12	1.44
480	66.46	12.54	0.00	0.00	79.00	1.89	1.88	0.00	0.00	2.41
500	9.58	74.55	0.31	0.00	84.44	2.82	2.96	0.31	0.00	0.78
520	0.00	70.66	11.56	0.00	82.22	0.00	0.84	0.37	0.00	0.48
540	0.00	44.55	24.67	0.00	69.22	0.00	6.08	5.41	0.00	6.49
560	0.00	14.98	58.80	0.00	73.78	0.00	5.62	10.32	0.00	4.70
580	0.00	0.00	51.31	20.36	71.67	0.00	0.00	7.09	6.73	2.36
600	0.00	0.00	23.20	51.14	74.33	0.00	0.00	0.38	2.24	2.59
620	0.00	0.00	8.69	77.42	86.11	0.00	0.00	1.58	4.31	2.72
640	0.43	0.00	2.92	91.98	95.33	0.22	0.00	0.71	1.88	1.15
660	1.63	0.00	0.43	95.83	97.89	0.19	0.00	0.43	0.47	0.22
23˚ w/ annulus	**Mean**					**Standard Error of the Mean**				
λ	*Blue*	*Green*	*Yellow*	*Red*	*Sat*	*Blue*	*Green*	*Yellow*	*Red*	*Sat*
420	53.35	0.00	0.00	32.21	85.56	19.55	0.00	0.00	19.15	1.06
440	70.65	0.00	0.00	13.69	84.33	8.73	0.00	0.00	7.59	1.26
460	82.02	5.31	0.00	2.33	89.67	1.80	1.26	0.00	1.75	1.35
480	28.03	54.30	0.00	0.00	82.33	3.18	3.58	0.00	0.00	0.69
500	0.00	72.88	11.62	0.00	89.78	0.00	9.48	3.57	0.00	1.82
520	0.00	69.64	15.58	0.00	85.22	0.00	4.48	4.12	0.00	0.40
540	0.00	53.15	24.96	0.00	78.11	0.00	1.31	1.45	0.00	0.68
560	0.00	21.20	46.91	0.00	68.11	0.00	2.56	5.68	0.00	3.20
580	0.00	0.00	52.89	20.64	74.33	0.00	0.00	4.24	2.26	2.08
600	0.00	0.00	32.06	45.49	77.56	0.00	0.00	5.35	4.64	1.16
620	0.00	0.00	9.50	80.28	89.78	0.00	0.00	1.96	3.34	1.44
640	1.90	0.00	2.14	90.96	95.00	1.07	0.00	2.14	3.44	2.22
660	2.35	0.00	0.63	93.57	96.56	0.55	0.00	0.63	2.24	1.39
23˚ full-field	**Mean**					**Standard Error of the Mean**				
λ	*Blue*	*Green*	*Yellow*	*Red*	*Sat*	*Blue*	*Green*	*Yellow*	*Red*	*Sat*
420	46.06	0.00	0.00	42.27	88.33	12.07	0.00	0.00	11.08	2.22
440	85.07	0.32	0.00	4.61	90.00	2.96	0.32	0.00	1.06	2.91
460	86.52	4.21	0.00	0.61	91.33	1.15	2.43	0.00	0.35	1.53
480	39.84	42.71	0.00	0.00	82.56	7.02	5.70	0.00	0.00	2.32
500	8.34	83.71	0.61	0.00	92.67	3.37	3.90	0.61	0.00	1.07
520	0.00	74.89	13.78	0.00	88.67	0.00	3.79	1.57	0.00	2.36
540	0.00	44.07	35.37	0.00	79.44	0.00	14.91	12.61	0.00	3.02
560	0.00	16.25	57.86	0.00	74.11	0.00	4.03	4.37	0.00	0.40
580	0.00	0.00	48.69	23.76	72.44	0.00	0.00	11.52	9.22	3.07
600	0.00	0.00	33.31	45.13	78.44	0.00	0.00	6.65	5.69	1.75
620	0.00	0.00	9.68	79.21	88.89	0.00	0.00	0.71	0.06	0.68
640	1.08	0.00	2.66	92.82	96.56	0.54	0.00	0.48	0.19	0.11
660	1.76	0.00	0.22	96.80	98.78	0.22	0.00	0.22	0.29	0.29

JO 3-session Mean Data

35˚ w/ annulus	Mean				
λ	*Blue*	*Green*	*Yellow*	*Red*	*Sat*
420	27.04	0.00	0.00	55.74	82.78
440	82.75	0.77	0.00	5.03	88.56
460	84.81	2.80	0.00	2.17	89.78
480	35.53	38.92	0.00	0.00	74.44
500	5.40	73.65	5.95	0.00	85.00
520	0.00	61.81	16.96	0.00	78.78
540	0.00	46.01	23.33	0.00	69.33
560	0.00	24.29	36.49	0.00	60.78
580	0.00	0.00	38.23	25.44	63.67
600	0.00	0.00	24.16	45.84	70.00
620	0.00	0.00	7.72	81.05	88.78
640	0.76	0.00	2.85	92.06	95.67
660	1.63	0.00	0.64	94.96	97.22
35˚ full-field	**Mean**				
λ	*Blue*	*Green*	*Yellow*	*Red*	*Sat*
420	27.70	0.00	0.00	57.25	87.89
440	79.88	0.00	0.00	6.79	86.67
460	83.30	6.22	0.00	0.60	90.11
480	39.83	41.51	0.00	0.00	81.33
500	4.64	86.73	0.62	0.00	92.00
520	0.00	76.90	11.88	0.00	88.78
540	0.00	54.69	21.87	0.00	76.56
560	0.00	18.83	46.73	0.00	65.56
580	0.00	2.03	52.36	8.83	63.22
600	0.00	0.00	32.96	42.71	75.67
620	0.00	0.00	8.32	79.56	87.89
640	0.44	0.00	2.84	92.50	95.78
660	1.31	0.00	0.76	96.04	98.11

Standard Error of the Mean				
Blue	*Green*	*Yellow*	*Red*	*Sat*
11.08	0.00	0.00	12.11	1.82
3.31	0.77	0.00	0.91	4.14
1.01	1.06	0.00	0.84	0.59
6.32	6.45	0.00	0.00	0.99
4.35	0.31	2.81	0.00	1.64
0.00	5.15	3.09	0.00	2.25
0.00	3.36	0.57	0.00	3.20
0.00	4.32	1.94	0.00	3.37
0.00	0.00	8.63	5.94	6.87
0.00	0.00	3.81	4.83	4.81
0.00	0.00	2.09	4.94	2.86
0.47	0.00	0.47	0.57	0.58
0.33	0.00	0.32	0.92	0.95
Standard Error of the Mean				
Blue	*Green*	*Yellow*	*Red*	*Sat*
9.90	0.00	0.00	11.23	1.13
4.29	0.00	0.00	1.59	2.69
3.23	1.87	0.00	0.60	2.44
6.83	6.83	0.00	0.00	0.00
1.86	2.88	0.36	0.00	1.58
0.00	2.25	1.96	0.00	0.80
0.00	5.18	3.44	0.00	1.79
0.00	10.25	8.26	0.00	3.16
0.00	2.03	4.02	2.04	3.89
0.00	0.00	2.37	2.57	0.51
0.00	0.00	2.39	5.18	2.80
0.22	0.00	0.33	0.19	0.11
0.66	0.00	0.76	0.50	0.40

KY 3-session Mean Data

1˚ Fovea	Mean					Standard Error of the Mean				
λ	*Blue*	*Green*	*Yellow*	*Red*	*Sat*	*Blue*	*Green*	*Yellow*	*Red*	*Sat*
420	52.64	0.00	0.00	40.36	93.00	9.22	0.00	0.00	7.70	1.53
440	75.18	0.00	0.00	16.60	91.78	3.81	0.00	0.00	4.25	1.31
460	83.89	1.50	0.00	4.27	89.67	1.34	0.86	0.00	1.43	0.51
480	72.32	18.24	0.00	0.00	90.56	5.82	5.03	0.00	0.00	0.87
500	19.39	64.83	0.00	0.00	84.22	5.61	7.21	0.00	0.00	2.31
520	2.28	69.29	6.54	0.00	78.11	1.22	3.49	1.75	0.00	2.63
540	0.34	58.91	13.30	0.00	72.56	0.34	6.63	4.69	0.00	2.70
560	0.00	15.68	40.65	0.00	56.33	0.00	1.68	5.26	0.00	5.67
580	0.00	0.00	42.90	20.54	63.44	0.00	0.00	0.50	1.80	1.79
600	0.00	0.00	19.40	53.49	72.89	0.00	0.00	1.54	2.93	1.42
620	0.00	0.00	10.19	73.14	83.33	0.00	0.00	1.20	1.27	1.17
640	1.20	0.00	1.76	85.60	88.56	0.62	0.00	0.65	1.41	1.46
660	1.74	0.00	1.35	84.57	87.67	0.15	0.00	0.76	2.15	1.45
23˚ w/ annulus	**Mean**					**Standard Error of the Mean**				
λ	*Blue*	*Green*	*Yellow*	*Red*	*Sat*	*Blue*	*Green*	*Yellow*	*Red*	*Sat*
420	56.28	0.00	0.00	41.17	97.44	3.73	0.00	0.00	3.83	0.59
440	88.95	0.00	0.00	7.16	96.11	1.41	0.00	0.00	1.71	0.48
460	90.14	0.51	0.00	2.91	93.56	1.85	0.51	0.00	0.74	0.97
480	60.04	32.05	0.00	0.00	93.11	6.00	7.04	0.00	0.00	0.78
500	3.87	86.30	1.49	0.00	91.67	0.43	2.09	1.49	0.00	1.07
520	1.48	85.12	5.18	0.00	91.78	1.48	1.99	1.68	0.00	2.11
540	0.00	77.05	10.29	0.00	87.33	0.00	2.01	1.40	0.00	0.96
560	0.00	19.25	52.64	0.00	71.89	0.00	5.11	9.89	0.00	4.95
580	0.00	0.00	44.43	22.68	67.11	0.00	0.00	8.43	1.10	7.42
600	0.00	0.00	18.49	54.51	73.00	0.00	0.00	1.30	5.84	5.68
620	0.00	0.00	10.14	76.64	86.78	0.00	0.00	1.13	3.38	2.26
640	0.20	0.00	3.09	84.27	87.56	0.20	0.00	0.32	1.55	1.35
660	0.98	0.00	1.69	85.43	88.11	0.70	0.00	1.54	3.61	2.51
23˚ full-field	**Mean**					**Standard Error of the Mean**				
λ	*Blue*	*Green*	*Yellow*	*Red*	*Sat*	*Blue*	*Green*	*Yellow*	*Red*	*Sat*
420	51.03	0.00	0.00	45.52	96.56	4.01	0.00	0.00	2.97	1.11
440	84.19	0.00	0.00	9.37	93.56	3.79	0.00	0.00	4.66	1.79
460	89.34	0.10	0.00	3.12	92.56	1.64	0.10	0.00	0.93	2.06
480	68.96	23.04	0.00	0.00	92.00	3.57	3.15	0.00	0.00	0.69
500	6.51	83.10	1.50	0.00	91.11	1.19	1.11	0.85	0.00	1.24
520	0.00	80.83	9.06	0.00	89.89	0.00	2.02	1.36	0.00	0.95
540	0.00	64.50	16.39	0.00	80.89	0.00	2.64	0.99	0.00	1.68
560	0.00	14.36	50.87	0.00	65.22	0.00	3.14	8.12	0.00	5.00
580	0.00	0.00	35.95	17.83	53.78	0.00	0.00	4.89	6.91	4.56
600	0.00	0.00	16.20	55.14	71.33	0.00	0.00	2.57	1.80	1.90
620	0.00	0.00	7.00	78.89	85.89	0.00	0.00	0.39	3.10	2.88
640	0.10	0.00	2.65	88.81	91.56	0.10	0.00	0.74	0.35	0.40
660	1.80	0.00	0.81	87.84	90.44	0.64	0.00	0.27	0.39	0.29

KY 3-session Mean Data

35˚ w/ annulus			Mean		
λ	*Blue*	*Green*	*Yellow*	*Red*	*Sat*
420	54.02	0.00	0.00	42.98	97.00
440	84.18	0.00	0.00	9.71	93.89
460	89.77	0.70	0.00	2.09	92.56
480	67.51	24.27	0.00	0.00	91.78
500	6.52	83.10	0.61	0.00	90.22
520	2.02	81.29	6.35	0.00	89.67
540	0.00	68.31	12.91	0.00	81.22
560	0.00	12.19	50.81	0.00	63.00
580	0.00	0.00	46.78	16.22	63.00
600	0.00	0.00	17.72	60.05	77.78
620	0.00	0.00	7.80	79.76	87.56
640	0.20	0.00	2.70	87.21	90.11
660	2.21	0.00	0.20	88.04	90.44
35˚ full-field			**Mean**		
λ	*Blue*	*Green*	*Yellow*	*Red*	*Sat*
420	51.65	0.00	0.00	44.57	96.22
440	86.94	0.00	0.00	7.73	94.67
460	89.05	0.43	0.00	2.86	92.33
480	61.31	29.36	0.00	0.00	90.67
500	8.42	77.21	2.59	0.00	88.22
520	0.00	80.90	8.66	0.00	89.56
540	0.00	59.78	16.22	0.00	76.00
560	0.00	13.53	52.80	0.00	66.33
580	0.00	0.00	40.19	26.48	66.67
600	0.00	0.00	20.35	52.76	73.11
620	0.00	0.00	9.88	75.01	84.89
640	0.20	0.00	3.59	86.09	89.89
660	0.70	0.00	1.50	87.69	89.89

Standard Error of the Mean				
Blue	*Green*	*Yellow*	*Red*	*Sat*
1.93	0.00	0.00	1.16	0.84
0.26	0.00	0.00	0.42	0.68
1.19	0.44	0.00	0.60	1.25
0.83	0.94	0.00	0.00	0.11
2.04	1.42	0.61	0.00	0.29
2.02	0.95	2.08	0.00	0.58
0.00	4.18	0.91	0.00	3.76
0.00	4.07	2.28	0.00	2.36
0.00	0.00	5.00	2.15	2.89
0.00	0.00	2.02	2.05	2.12
0.00	0.00	1.81	2.75	0.99
0.20	0.00	0.86	1.05	0.62
0.50	0.00	0.20	1.04	0.48
Standard Error of the Mean				
Blue	*Green*	*Yellow*	*Red*	*Sat*
3.95	0.00	0.00	1.95	2.28
1.10	0.00	0.00	1.21	2.01
1.16	0.29	0.00	0.39	1.64
3.30	3.15	0.00	0.00	2.19
3.91	3.07	1.56	0.00	1.28
0.00	0.54	0.58	0.00	0.95
0.00	2.93	1.08	0.00	2.91
0.00	3.95	3.70	0.00	2.12
0.00	0.00	3.33	4.08	1.50
0.00	0.00	2.71	4.85	2.16
0.00	0.00	1.62	3.97	2.98
0.20	0.00	1.42	0.94	0.29
0.10	0.00	0.18	0.76	0.73

VV 3-session Mean Data

1˚ Fovea			Mean		
λ	*Blue*	*Green*	*Yellow*	*Red*	*Sat*
420	68.53	0.00	0.00	22.80	91.33
440	84.73	0.70	0.00	6.01	91.44
460	90.24	1.37	0.00	2.50	94.11
480	77.71	11.51	0.00	0.00	89.22
500	38.27	52.18	0.00	0.00	90.44
520	3.18	76.56	5.81	0.00	85.56
540	1.43	69.79	9.79	0.00	81.00
560	0.00	22.96	49.93	0.00	72.89
580	0.00	0.00	72.78	2.56	76.11
600	0.00	0.00	28.15	48.96	77.11
620	0.00	0.00	13.92	74.75	88.67
640	0.00	0.00	9.03	82.85	91.89
660	0.00	0.00	7.18	86.71	93.89
23˚ w/ annulus			**Mean**		
λ	*Blue*	*Green*	*Yellow*	*Red*	*Sat*
420	71.34	0.00	0.00	15.11	86.44
440	80.81	0.49	0.00	4.92	86.22
460	87.83	2.03	0.00	2.25	92.11
480	79.97	12.03	0.00	0.00	92.00
500	0.00	88.42	6.36	0.00	94.78
520	0.00	80.57	12.99	0.00	93.56
540	0.00	69.17	17.58	0.00	87.33
560	0.00	9.11	70.56	0.00	79.67
580	0.00	0.00	71.86	5.81	77.67
600	0.00	0.00	26.94	45.84	72.78
620	0.00	0.00	12.27	73.50	85.78
640	0.00	0.00	8.58	84.54	93.11
660	0.00	0.00	4.62	90.05	94.67
23˚ full-field			**Mean**		
λ	*Blue*	*Green*	*Yellow*	*Red*	*Sat*
420	62.45	0.00	0.00	25.33	87.78
440	83.20	1.58	0.00	2.89	87.67
460	84.80	5.67	0.00	0.53	91.00
480	74.38	15.40	0.00	0.00	89.78
500	1.25	87.53	5.66	0.00	94.44
520	0.00	75.70	17.75	0.00	93.44
540	0.00	65.48	24.19	0.00	88.67
560	0.00	17.46	61.52	0.00	78.11
580	0.00	0.00	67.36	6.75	74.11
600	0.00	0.00	27.95	44.27	72.22
620	0.00	0.00	17.34	67.22	84.56
640	0.00	0.00	7.45	85.88	93.33
660	0.00	0.00	3.77	90.89	94.67

Standard Error of the Mean				
Blue	*Green*	*Yellow*	*Red*	*Sat*
0.42	0.00	0.00	1.25	1.20
0.55	0.70	0.00	2.30	1.06
1.22	1.37	0.00	0.81	0.95
1.07	1.15	0.00	0.00	0.78
6.50	7.61	0.00	0.00	1.31
3.18	0.77	3.09	0.00	1.06
1.43	5.26	5.94	0.00	0.51
0.00	10.54	10.85	0.00	4.05
0.00	0.00	6.71	0.49	5.57
0.00	0.00	2.36	2.87	3.91
0.00	0.00	1.47	2.43	1.15
0.00	0.00	1.84	2.57	0.80
0.00	0.00	0.33	0.44	0.62
Standard Error of the Mean				
Blue	*Green*	*Yellow*	*Red*	*Sat*
3.91	0.00	0.00	1.86	2.06
2.27	0.49	0.00	1.74	1.06
2.27	1.31	0.00	0.39	1.49
1.89	0.71	0.00	0.00	1.39
0.00	0.77	1.94	0.00	1.18
0.00	0.69	0.71	0.00	1.16
0.00	1.33	3.06	0.00	1.26
0.00	1.95	5.11	0.00	3.17
0.00	0.00	3.60	2.49	3.37
0.00	0.00	0.97	1.84	2.78
0.00	0.00	0.21	2.22	2.32
0.00	0.00	0.74	1.35	1.24
0.00	0.00	0.47	0.73	0.69
Standard Error of the Mean				
Blue	*Green*	*Yellow*	*Red*	*Sat*
3.83	0.00	0.00	5.24	2.30
1.65	0.82	0.00	1.03	1.17
2.48	2.86	0.00	0.53	0.19
1.62	1.71	0.00	0.00	1.37
1.25	0.40	0.94	0.00	0.29
0.00	2.43	2.66	0.00	0.29
0.00	1.71	1.41	0.00	1.86
0.00	8.83	10.94	0.00	5.24
0.00	0.00	4.08	3.33	6.78
0.00	0.00	1.11	3.87	4.84
0.00	0.00	1.36	4.09	2.91
0.00	0.00	0.85	0.64	0.51
0.00	0.00	0.15	1.11	1.02

VV 3-session Mean Data

35˚ w/ annulus			Mean		
λ	*Blue*	*Green*	*Yellow*	*Red*	*Sat*
420	55.80	0.00	0.00	30.64	86.44
440	79.98	0.00	0.00	6.80	86.78
460	83.42	3.68	0.00	1.24	88.33
480	71.94	15.06	0.00	0.00	87.00
500	9.71	70.75	10.45	0.00	91.11
520	0.00	72.49	15.84	0.00	88.33
540	0.00	50.02	23.42	0.00	73.44
560	0.00	5.82	45.63	0.00	51.44
580	0.00	0.00	44.61	2.94	47.56
600	0.00	0.00	27.39	42.39	69.78
620	0.00	0.00	17.42	72.03	89.44
640	0.00	0.00	11.08	82.25	93.33
660	0.00	0.00	4.94	89.95	94.89
35˚ full-field			**Mean**		
λ	*Blue*	*Green*	*Yellow*	*Red*	*Sat*
420	59.65	0.00	0.00	28.91	88.56
440	84.74	0.29	0.00	4.74	89.78
460	82.11	6.89	0.00	1.00	90.00
480	73.46	13.31	0.00	0.00	86.78
500	1.11	81.84	9.93	0.00	92.89
520	0.00	69.22	19.67	0.00	88.89
540	0.00	61.16	15.40	0.00	76.56
560	0.00	10.17	51.64	0.00	62.56
580	0.00	0.00	51.39	2.28	53.67
600	0.00	0.00	24.94	42.61	67.56
620	0.00	0.00	13.89	75.89	89.78
640	0.00	0.00	7.66	84.56	92.22
660	0.00	0.00	6.02	88.31	94.33

Standard Error of the Mean				
Blue	*Green*	*Yellow*	*Red*	*Sat*
3.49	0.00	0.00	4.03	1.16
2.47	0.00	0.00	1.15	1.39
1.56	2.13	0.00	0.84	0.51
1.53	0.97	0.00	0.00	2.36
9.71	5.75	3.11	0.00	1.11
0.00	4.27	3.70	0.00	0.84
0.00	5.81	0.44	0.00	5.50
0.00	2.48	4.00	0.00	6.44
0.00	0.00	3.34	0.25	3.58
0.00	0.00	3.32	4.82	1.56
0.00	0.00	3.39	3.05	1.75
0.00	0.00	1.26	1.80	0.88
0.00	0.00	0.71	1.45	0.91
Standard Error of the Mean				
Blue	*Green*	*Yellow*	*Red*	*Sat*
0.99	0.00	0.00	0.82	0.87
0.70	0.29	0.00	1.34	0.99
1.27	1.51	0.00	0.50	0.00
1.00	0.40	0.00	0.00	0.89
0.56	3.44	3.49	0.00	0.59
0.00	4.08	3.36	0.00	0.80
0.00	1.16	2.88	0.00	3.31
0.00	1.68	5.73	0.00	3.35
0.00	0.00	9.59	0.32	9.57
0.00	0.00	5.41	2.47	6.77
0.00	0.00	1.93	2.33	0.73
0.00	0.00	0.60	1.16	0.59
0.00	0.00	1.15	1.54	0.88

AIW 3-session Mean Spatial Integration Data

Inferior			Mean			Standard Error of the Mean				
λ	*Blue*	*Green*	*Yellow*	*Red*	*Sat*	*Blue*	*Green*	*Yellow*	*Red*	*Sat*
420	84.88	0.00	0.00	8.01	92.89	1.52	0.00	0.00	1.43	2.23
440	90.21	0.40	0.00	2.06	92.67	0.97	0.40	0.00	0.79	0.88
460	89.18	1.71	0.00	0.00	90.89	1.42	0.41	0.00	0.00	1.57
480	74.30	3.59	0.00	0.00	77.89	3.37	0.48	0.00	0.00	3.26
500	11.80	85.31	0.00	0.00	97.11	8.56	8.61	0.00	0.00	0.11
520	0.64	91.53	3.94	0.00	96.11	0.32	1.34	1.06	0.00	0.99
540	0.00	75.93	17.07	0.00	93.00	0.00	8.06	8.16	0.00	0.88
560	0.00	5.71	82.84	0.00	88.56	0.00	0.88	1.20	0.00	0.48
580	0.00	0.36	78.77	1.76	80.89	0.00	0.36	1.58	0.64	1.25
600	0.00	0.00	72.37	10.63	83.00	0.00	0.00	1.24	1.43	0.69
620	0.00	0.00	12.81	75.47	87.33	0.00	0.00	1.38	0.59	0.88
640	0.00	0.00	7.72	78.57	93.89	0.00	0.00	0.52	7.29	0.78
660	0.28	0.00	4.11	86.61	91.00	0.28	0.00	0.74	2.15	2.60
Superior			**Mean**			**Standard Error of the Mean**				
λ	*Blue*	*Green*	*Yellow*	*Red*	*Sat*	*Blue*	*Green*	*Yellow*	*Red*	*Sat*
420	86.35	0.00	0.00	6.10	92.44	0.62	0.00	0.00	1.27	1.28
440	90.37	0.19	0.00	1.66	92.22	1.75	0.19	0.00	0.27	1.66
460	86.38	1.96	0.00	0.00	88.33	2.49	0.16	0.00	0.00	2.40
480	79.74	3.48	0.00	0.00	83.22	1.83	0.91	0.00	0.00	0.95
500	2.64	95.48	0.88	0.00	99.00	0.33	0.11	0.44	0.00	0.00
520	0.33	93.31	4.70	0.00	98.33	0.33	0.30	0.78	0.00	0.19
540	0.00	83.77	8.78	0.00	92.56	0.00	1.53	0.91	0.00	2.19
560	0.00	15.39	73.61	0.00	89.00	0.00	10.53	8.59	0.00	2.04
580	0.00	0.17	77.46	2.14	79.78	0.00	0.17	2.82	0.41	3.04
600	0.00	0.00	60.43	25.12	85.56	0.00	0.00	13.24	16.47	3.27
620	0.00	0.00	7.62	80.60	88.22	0.00	0.00	0.10	2.27	2.19
640	0.00	0.00	5.25	87.75	93.00	0.00	0.00	0.66	1.75	1.17
660	0.00	0.00	4.05	91.62	95.67	0.00	0.00	0.63	0.77	1.26
Nasal			**Mean**			**Standard Error of the Mean**				
λ	*Blue*	*Green*	*Yellow*	*Red*	*Sat*	*Blue*	*Green*	*Yellow*	*Red*	*Sat*
420	85.94	0.00	0.00	7.50	93.44	1.94	0.00	0.00	0.87	2.79
440	89.36	0.20	0.00	1.22	90.78	2.49	0.20	0.00	0.37	2.58
460	86.23	1.43	0.00	0.00	87.67	1.33	0.17	0.00	0.00	1.33
480	77.01	6.10	0.00	0.00	83.11	2.22	1.06	0.00	0.00	2.44
500	2.49	91.43	1.30	0.00	95.22	0.96	1.69	0.85	0.00	1.46
520	1.18	91.94	3.66	0.00	96.78	0.66	1.34	1.20	0.00	0.87
540	0.00	87.35	7.21	0.00	94.56	0.00	2.63	0.84	0.00	1.79
560	0.00	29.50	56.95	0.00	86.44	0.00	2.36	4.22	0.00	5.29
580	0.00	0.00	79.52	2.48	82.00	0.00	0.00	5.33	0.16	5.40
600	0.00	0.00	72.52	10.59	83.11	0.00	0.00	5.08	1.49	4.33
620	0.00	0.00	22.24	61.75	83.22	0.00	0.00	4.66	9.42	6.82
640	0.00	0.00	6.71	83.62	90.33	0.00	0.00	0.92	2.08	2.46
660	0.27	0.00	4.06	85.45	89.78	0.27	0.00	0.74	2.05	1.75

AIW 3-session Mean Spatial Integration Data

Temporal			Mean		
λ	*Blue*	*Green*	*Yellow*	*Red*	*Sat*
420	82.27	0.00	0.00	7.07	89.33
440	86.58	0.47	0.00	2.06	89.11
460	86.87	1.69	0.00	0.00	88.56
480	75.64	5.91	0.00	0.00	81.56
500	2.10	91.52	1.71	0.00	95.33
520	0.86	92.97	4.61	0.00	98.44
540	0.00	79.35	15.65	0.00	95.00
560	0.00	23.11	66.78	0.00	89.89
580	0.00	0.20	77.84	2.41	80.44
600	0.00	0.00	73.14	9.75	82.89
620	0.00	0.00	7.54	79.68	87.22
640	0.00	0.00	6.04	81.96	88.00
660	1.08	0.00	1.36	81.78	84.22
23˚ w/ annulus			**Mean**		
λ	*Blue*	*Green*	*Yellow*	*Red*	*Sat*
420	87.81	0.00	0.00	5.97	93.78
440	90.59	0.53	0.00	1.22	92.33
460	89.44	1.00	0.00	0.00	90.44
480	77.15	5.40	0.00	0.00	82.56
500	2.95	94.30	0.64	0.00	97.89
520	0.66	93.56	3.45	0.00	97.67
540	0.00	86.60	8.63	0.00	95.22
560	0.00	14.27	73.73	0.00	88.00
580	0.00	0.00	79.36	2.20	81.56
600	0.00	0.00	75.04	7.63	82.67
620	0.00	0.00	8.58	83.42	92.00
640	0.00	0.00	5.32	90.35	95.67
660	0.61	0.00	3.55	89.40	93.56

Standard Error of the Mean				
Blue	*Green*	*Yellow*	*Red*	*Sat*
3.01	0.00	0.00	2.50	0.51
2.67	0.35	0.00	0.95	3.26
1.30	0.36	0.00	0.00	0.99
1.88	1.73	0.00	0.00	0.68
0.98	1.40	0.87	0.00	1.26
0.43	1.15	0.51	0.00	0.40
0.00	8.61	9.26	0.00	1.35
0.00	8.88	10.56	0.00	1.72
0.00	0.20	2.83	0.91	2.63
0.00	0.00	1.85	1.84	0.59
0.00	0.00	0.60	4.73	4.19
0.00	0.00	0.70	2.12	1.95
0.32	0.00	0.33	0.48	0.44
Standard Error of the Mean				
Blue	*Green*	*Yellow*	*Red*	*Sat*
1.97	0.00	0.00	0.64	1.74
2.41	0.39	0.00	0.52	2.33
2.97	0.25	0.00	0.00	2.98
0.98	0.54	0.00	0.00	1.31
0.40	0.91	0.32	0.00	1.11
0.33	1.23	1.01	0.00	0.58
0.00	0.92	1.83	0.00	1.11
0.00	9.75	9.09	0.00	2.55
0.00	0.00	2.49	0.24	2.72
0.00	0.00	2.64	1.56	1.58
0.00	0.00	0.80	1.24	0.77
0.00	0.00	0.51	0.27	0.69
0.31	0.00	0.82	1.46	1.44

KY 3-session Mean Spatial Integration Data

Inferior			Mean		
λ	*Blue*	*Green*	*Yellow*	*Red*	*Sat*
420	41.05	0.00	0.00	51.95	93.00
440	83.95	0.00	0.00	8.82	92.78
460	90.05	0.00	0.00	1.95	92.00
480	55.37	34.96	0.00	0.00	90.33
500	8.41	81.37	0.00	0.00	89.78
520	2.50	83.57	3.16	0.00	89.22
540	0.00	69.69	9.53	0.00	79.22
560	0.00	11.16	46.93	0.47	58.56
580	0.00	0.00	36.09	23.13	59.22
600	0.00	0.00	18.65	54.57	73.22
620	0.00	0.00	9.62	70.71	80.33
640	0.28	0.00	3.86	80.85	85.00
660	1.02	0.00	2.58	81.40	85.00
Superior			**Mean**		
λ	*Blue*	*Green*	*Yellow*	*Red*	*Sat*
420	44.98	0.00	0.00	49.35	94.33
440	84.23	0.00	0.00	8.77	93.00
460	88.28	0.40	0.00	2.10	90.78
480	49.21	42.79	0.00	0.00	92.00
500	6.61	82.66	0.40	0.00	89.67
520	2.35	80.06	3.82	0.00	86.22
540	0.00	56.80	18.87	0.00	75.67
560	0.00	11.42	56.58	0.00	68.00
580	0.00	0.00	32.58	31.87	64.44
600	0.00	0.00	18.54	57.13	75.67
620	0.00	0.00	5.02	80.54	85.56
640	1.06	0.00	1.37	84.68	87.11
660	1.88	0.00	0.77	82.46	85.11
Nasal			**Mean**		
λ	*Blue*	*Green*	*Yellow*	*Red*	*Sat*
420	40.18	0.00	0.00	51.82	92.00
440	84.83	0.00	0.00	4.39	89.22
460	86.73	0.20	0.00	2.52	89.44
480	50.55	40.56	0.00	0.00	91.11
500	12.82	76.84	0.00	0.00	89.67
520	0.75	75.23	5.47	0.00	81.44
540	0.35	62.84	14.26	0.00	77.44
560	0.00	18.18	36.71	0.00	54.89
580	0.00	0.00	41.79	17.33	59.11
600	0.00	0.00	19.87	51.02	70.89
620	0.00	0.00	10.31	68.36	78.67
640	1.00	0.00	1.97	80.37	83.33
660	1.84	0.00	1.01	78.70	81.56

Standard Error of the Mean				
Blue	*Green*	*Yellow*	*Red*	*Sat*
1.39	0.00	0.00	1.21	0.33
1.10	0.00	0.00	0.96	1.68
1.56	0.00	0.00	0.11	1.58
1.24	1.38	0.00	0.00	0.33
1.33	1.34	0.00	0.00	0.11
0.36	1.05	1.58	0.00	0.62
0.00	3.49	1.45	0.00	2.06
0.00	2.87	1.77	0.47	2.56
0.00	0.00	8.08	4.27	4.24
0.00	0.00	0.27	1.47	1.61
0.00	0.00	2.38	2.21	0.88
0.17	0.00	1.37	0.73	0.84
0.56	0.00	1.20	0.33	0.38
Standard Error of the Mean				
Blue	*Green*	*Yellow*	*Red*	*Sat*
2.24	0.00	0.00	0.89	1.39
2.83	0.00	0.00	1.73	1.68
1.86	0.20	0.00	0.77	1.87
7.42	7.80	0.00	0.00	0.58
2.01	0.96	0.40	0.00	1.20
1.27	4.41	1.52	0.00	3.45
0.00	5.36	1.17	0.00	4.48
0.00	5.73	8.15	0.00	4.07
0.00	0.00	1.25	2.10	2.50
0.00	0.00	0.56	3.14	2.85
0.00	0.00	1.21	1.29	0.22
0.26	0.00	0.80	0.49	0.73
0.32	0.00	0.51	0.77	0.99
Standard Error of the Mean				
Blue	*Green*	*Yellow*	*Red*	*Sat*
1.13	0.00	0.00	0.86	1.07
1.38	0.00	0.00	1.21	1.47
1.09	0.10	0.00	0.58	1.46
2.87	2.16	0.00	0.00	0.87
2.45	3.07	0.00	0.00	0.84
0.75	4.40	1.85	0.00	3.40
0.35	5.73	3.99	0.00	3.02
0.00	5.15	5.08	0.00	1.06
0.00	0.00	5.52	4.11	1.47
0.00	0.00	2.35	2.47	2.58
0.00	0.00	3.48	5.59	3.08
0.64	0.00	1.03	0.83	1.35
0.79	0.00	1.01	1.88	1.74

KY 3-session Mean Spatial Integration Data

Temporal			Mean		
λ	*Blue*	*Green*	*Yellow*	*Red*	*Sat*
420	43.53	0.00	0.00	48.47	92.00
440	82.52	0.00	0.00	7.59	90.11
460	84.40	0.00	0.00	4.44	88.44
480	52.84	36.39	0.00	0.00	89.22
500	6.41	82.25	0.00	0.00	88.67
520	1.08	79.41	6.07	0.00	86.56
540	0.36	52.22	21.50	0.00	73.22
560	0.00	2.90	47.54	0.89	51.33
580	0.00	0.00	41.54	15.46	57.00
600	0.00	0.00	13.04	62.40	75.44
620	0.18	0.00	5.49	75.34	81.00
640	0.73	0.00	1.91	80.24	82.89
660	1.60	0.00	0.77	83.29	85.67
23˚ w/ annulus			**Mean**		
λ	*Blue*	*Green*	*Yellow*	*Red*	*Sat*
420	42.41	0.00	0.00	53.25	95.67
440	87.54	0.00	0.00	5.68	93.22
460	89.62	0.00	0.00	1.82	91.44
480	49.89	43.11	0.00	0.00	93.00
500	6.48	84.52	0.00	0.00	91.00
520	0.40	84.73	5.43	0.00	90.56
540	1.17	74.74	9.75	0.00	85.67
560	0.00	12.90	59.18	0.25	72.33
580	0.00	0.00	38.40	26.71	65.11
600	0.00	0.00	19.53	53.81	73.33
620	0.19	0.00	5.82	79.54	85.56
640	0.78	0.00	1.38	86.07	88.22
660	1.38	0.00	0.60	86.91	88.89

Standard Error of the Mean				
Blue	*Green*	*Yellow*	*Red*	*Sat*
2.22	0.00	0.00	2.49	0.67
0.68	0.00	0.00	1.93	1.25
0.67	0.00	0.00	0.50	0.59
5.95	6.09	0.00	0.00	0.40
1.21	1.09	0.00	0.00	0.38
0.55	1.85	1.71	0.00	0.62
0.36	7.99	5.39	0.00	2.90
0.00	0.54	5.21	0.51	5.06
0.00	0.00	6.42	5.46	1.26
0.00	0.00	1.34	2.19	1.75
0.18	0.00	2.06	2.68	1.33
0.15	0.00	0.18	1.84	1.82
0.22	0.00	0.37	2.05	2.01
Standard Error of the Mean				
Blue	*Green*	*Yellow*	*Red*	*Sat*
0.80	0.00	0.00	1.02	1.26
3.53	0.00	0.00	1.67	1.90
2.05	0.00	0.00	0.60	1.46
1.30	1.68	0.00	0.00	0.38
0.65	0.19	0.00	0.00	0.51
0.40	1.51	0.41	0.00	0.91
1.17	2.98	3.19	0.00	1.58
0.00	2.47	4.04	0.25	2.00
0.00	0.00	5.04	5.29	1.31
0.00	0.00	2.73	5.39	2.69
0.19	0.00	0.87	0.88	1.46
0.09	0.00	0.09	1.24	1.13
0.70	0.00	0.46	0.22	0.59

VV 3-session Mean Spatial Integration Data

Inferior			Mean			Standard Error of the Mean				
λ	*Blue*	*Green*	*Yellow*	*Red*	*Sat*	*Blue*	*Green*	*Yellow*	*Red*	*Sat*
420	60.92	0.00	0.00	22.97	83.89	3.23	0.00	0.00	3.49	1.47
440	73.71	0.00	0.00	13.62	87.33	5.68	0.00	0.00	7.00	1.35
460	78.90	1.81	0.00	0.74	81.44	0.68	0.33	0.00	0.39	0.78
480	73.28	10.39	0.00	0.00	83.67	1.21	0.57	0.00	0.00	0.69
500	0.00	70.49	8.10	9.30	87.89	0.00	9.09	1.33	9.30	1.11
520	0.00	67.86	17.25	0.00	85.11	0.00	5.08	4.29	0.00	2.56
540	0.00	44.55	33.34	0.00	77.89	0.00	4.27	4.55	0.00	2.00
560	0.00	8.91	59.09	0.00	68.00	0.00	0.36	1.81	0.00	1.53
580	0.00	0.00	70.64	1.36	72.00	0.00	0.00	1.15	0.23	1.26
600	0.00	0.00	38.34	40.88	79.22	0.00	0.00	6.47	4.63	3.78
620	0.00	0.00	14.63	71.93	86.56	0.00	0.00	1.83	3.40	1.61
640	0.00	0.00	9.63	83.03	92.67	0.00	0.00	1.40	2.52	1.15
660	0.00	0.00	6.26	86.52	92.78	0.00	0.00	1.25	2.38	1.13
Superior			**Mean**			**Standard Error of the Mean**				
λ	*Blue*	*Green*	*Yellow*	*Red*	*Sat*	*Blue*	*Green*	*Yellow*	*Red*	*Sat*
420	53.16	0.00	0.00	27.06	80.22	3.01	0.00	0.00	2.10	1.31
440	68.34	2.43	0.00	7.79	78.56	2.46	2.43	0.00	2.47	1.57
460	78.88	1.38	0.00	0.74	81.00	0.55	0.81	0.00	0.40	0.19
480	69.52	11.70	0.00	0.00	81.22	1.92	1.02	0.00	0.00	0.91
500	0.00	76.43	13.79	0.00	90.22	0.00	0.89	1.17	0.00	0.62
520	0.00	60.97	30.03	0.00	91.00	0.00	4.42	4.29	0.00	0.19
540	0.00	23.64	63.36	0.00	87.00	0.00	4.41	5.31	0.00	1.73
560	0.00	2.06	82.38	0.00	84.44	0.00	0.31	4.38	0.00	4.16
580	0.00	0.00	78.57	6.32	84.89	0.00	0.00	3.53	1.86	1.68
600	0.00	0.00	31.43	46.12	77.56	0.00	0.00	1.29	3.91	2.63
620	0.00	0.00	15.01	73.10	88.11	0.00	0.00	0.70	2.09	1.44
640	0.00	0.00	10.59	77.85	88.44	0.00	0.00	1.67	2.80	1.78
660	0.00	0.00	8.56	83.33	91.89	0.00	0.00	0.38	1.52	1.16
Nasal			**Mean**			**Standard Error of the Mean**				
λ	*Blue*	*Green*	*Yellow*	*Red*	*Sat*	*Blue*	*Green*	*Yellow*	*Red*	*Sat*
420	55.66	0.00	0.00	24.01	79.67	0.86	0.00	0.00	2.63	2.78
440	75.60	0.00	0.00	6.18	81.78	0.67	0.00	0.00	1.78	1.11
460	81.96	0.92	0.00	1.34	84.22	0.18	0.46	0.00	0.25	0.48
480	72.25	10.41	0.00	0.00	82.67	1.45	0.78	0.00	0.00	0.84
500	0.42	82.68	6.01	0.00	89.11	0.42	0.57	1.79	0.00	1.16
520	0.00	76.95	10.94	0.00	87.89	0.00	3.93	2.36	0.00	3.53
540	0.00	62.14	18.19	0.00	80.33	0.00	4.48	2.20	0.00	2.36
560	0.00	3.63	66.70	0.00	70.33	0.00	1.90	7.39	0.00	6.11
580	0.00	0.00	64.70	6.10	71.11	0.00	0.00	1.33	2.55	3.04
600	0.00	0.00	29.48	49.63	79.11	0.00	0.00	1.33	1.92	3.25
620	0.00	0.00	12.60	75.40	88.00	0.00	0.00	0.37	0.98	1.20
640	0.00	0.00	9.75	81.81	91.56	0.00	0.00	2.08	2.55	0.48
660	0.00	0.00	5.07	88.70	93.78	0.00	0.00	0.70	1.26	0.59

VV 3-session Mean Spatial Integration Data

Temporal			Mean		
λ	*Blue*	*Green*	*Yellow*	*Red*	*Sat*
420	62.01	0.00	0.00	22.32	84.33
440	75.75	0.18	0.00	6.18	82.11
460	83.62	3.03	0.00	1.47	88.11
480	76.61	9.51	0.00	0.00	86.11
500	0.72	83.81	5.69	0.00	90.22
520	0.00	73.29	16.71	0.00	90.00
540	0.00	45.35	37.76	0.00	83.11
560	0.00	3.65	65.69	0.00	69.33
580	0.00	0.00	64.17	4.94	69.11
600	0.00	0.00	24.30	50.37	74.67
620	0.00	0.00	13.81	72.53	86.33
640	0.00	0.00	8.85	82.93	91.78
660	0.00	0.00	4.68	89.43	94.11
23˚ w/ annulus			**Mean**		
λ	*Blue*	*Green*	*Yellow*	*Red*	*Sat*
420	64.49	0.00	0.00	18.51	83.00
440	80.32	0.94	0.00	1.63	82.89
460	86.89	0.00	0.00	1.89	88.78
480	75.29	12.37	0.00	0.00	87.67
500	1.02	73.72	8.23	8.03	91.00
520	0.00	76.86	13.45	0.00	91.33
540	0.00	52.20	34.36	0.00	86.56
560	0.00	9.36	75.31	0.00	84.67
580	0.00	0.00	65.32	8.46	73.78
600	0.00	0.00	26.38	50.06	76.44
620	0.00	0.00	14.72	68.06	82.78
640	0.00	0.00	8.57	81.54	90.11
660	0.00	0.00	6.55	84.45	91.00

Standard Error of the Mean				
Blue	*Green*	*Yellow*	*Red*	*Sat*
0.52	0.00	0.00	1.13	0.84
1.48	0.18	0.00	1.30	0.22
0.96	0.95	0.00	0.77	0.40
0.64	0.69	0.00	0.00	0.87
0.72	1.47	0.54	0.00	1.37
0.00	3.69	3.28	0.00	1.20
0.00	6.95	8.08	0.00	1.16
0.00	0.91	3.18	0.00	2.33
0.00	0.00	2.50	0.29	2.70
0.00	0.00	0.90	1.39	0.69
0.00	0.00	0.80	1.68	2.33
0.00	0.00	0.96	1.25	0.29
0.00	0.00	0.32	0.21	0.29
Standard Error of the Mean				
Blue	*Green*	*Yellow*	*Red*	*Sat*
1.96	0.00	0.00	2.80	2.22
2.99	0.47	0.00	1.21	2.56
1.24	0.00	0.00	0.87	0.99
3.43	1.61	0.00	0.00	2.36
1.02	10.80	2.85	8.03	0.67
0.00	3.91	3.09	0.00	0.67
0.00	6.44	5.89	0.00	0.73
0.00	0.65	1.35	0.00	0.69
0.00	0.00	1.09	1.78	1.64
0.00	0.00	0.68	1.78	2.12
0.00	0.00	2.58	4.70	2.13
0.00	0.00	0.56	1.05	0.56
0.00	0.00	0.48	1.27	0.88

AIW 2-session Mean Bleach Condition Data

1˚ Fovea			Mean			Standard Error of the Mean				
λ	*Blue*	*Green*	*Yellow*	*Red*	*Sat*	*Blue*	*Green*	*Yellow*	*Red*	*Sat*
420	75.97	0.00	0.00	16.36	92.33	2.84	0.00	0.00	3.84	1.00
440	93.11	0.60	0.00	1.62	95.33	0.31	0.60	0.00	1.29	1.00
460	93.96	1.05	0.00	0.00	95.00	4.72	0.72	0.00	0.00	4.00
480	75.28	5.55	0.00	0.00	80.83	0.76	1.26	0.00	0.00	0.50
500	17.69	66.48	0.00	0.00	84.17	6.04	8.54	0.00	0.00	2.50
520	0.60	80.72	9.51	0.00	90.83	0.60	1.45	0.89	0.00	1.17
540	0.00	77.27	12.90	0.00	90.17	0.00	2.40	1.10	0.00	3.50
560	0.00	3.89	73.45	0.00	77.33	0.00	0.07	10.73	0.00	10.67
580	0.00	0.24	73.76	2.51	76.50	0.00	0.24	5.61	1.35	4.50
600	0.00	0.00	56.74	23.26	80.00	0.00	0.00	16.78	8.44	8.33
620	0.00	0.00	7.76	85.24	93.00	0.00	0.00	0.14	2.47	2.33
640	0.00	0.00	4.26	88.74	93.00	0.00	0.00	1.68	4.32	6.00
660	1.29	0.00	2.81	94.24	98.33	1.29	0.00	1.82	0.15	0.67
23˚ w/ annulus			**Mean**			**Standard Error of the Mean**				
λ	*Blue*	*Green*	*Yellow*	*Red*	*Sat*	*Blue*	*Green*	*Yellow*	*Red*	*Sat*
420	79.97	0.00	0.00	11.03	91.00	1.66	0.00	0.00	0.00	1.67
440	93.42	0.16	0.00	2.26	95.83	0.68	0.16	0.00	0.98	1.50
460	94.87	0.47	0.00	0.00	95.33	0.17	0.16	0.00	0.00	0.33
480	63.56	10.11	0.00	0.00	73.67	4.11	1.90	0.00	0.00	6.00
500	1.12	89.66	5.39	0.00	96.17	1.12	1.55	3.17	0.00	0.50
520	0.00	86.09	9.58	0.00	95.67	0.00	0.94	0.94	0.00	0.00
540	0.00	79.73	9.78	0.00	89.50	0.00	0.69	0.86	0.00	0.17
560	0.00	8.10	62.57	0.00	70.67	0.00	3.51	1.49	0.00	5.00
580	0.00	0.00	60.69	10.14	70.83	0.00	0.00	13.63	7.13	6.50
600	0.00	0.00	14.80	58.87	73.67	0.00	0.00	1.17	3.51	2.33
620	0.29	0.00	3.01	85.37	88.67	0.29	0.00	0.38	1.58	1.67
640	0.85	0.00	3.06	85.43	89.33	0.85	0.00	2.16	1.68	3.00
660	2.48	0.00	1.44	80.07	84.00	1.88	0.00	1.44	2.44	2.00
23˚ full-field			**Mean**			**Standard Error of the Mean**				
λ	*Blue*	*Green*	*Yellow*	*Red*	*Sat*	*Blue*	*Green*	*Yellow*	*Red*	*Sat*
420	87.51	0.00	0.00	8.83	96.33	0.74	0.00	0.00	0.59	1.33
440	91.63	0.59	0.00	1.61	93.83	4.41	0.59	0.00	1.02	4.83
460	98.51	0.32	0.00	0.00	98.83	0.49	0.32	0.00	0.00	0.17
480	78.05	7.12	0.00	0.00	85.17	3.86	2.64	0.00	0.00	6.50
500	3.35	89.66	0.49	0.00	93.50	1.42	4.77	0.49	0.00	3.83
520	0.00	90.72	6.62	0.00	97.33	0.00	3.35	2.35	0.00	1.00
540	0.00	82.66	9.84	0.00	92.50	0.00	0.66	3.50	0.00	2.83
560	0.00	11.23	73.94	0.00	85.17	0.00	2.98	6.48	0.00	3.50
580	0.00	0.00	78.29	2.71	81.00	0.00	0.00	1.28	0.05	1.33
600	0.00	0.00	49.19	30.65	79.83	0.00	0.00	15.96	13.13	2.83
620	0.00	0.00	5.64	86.69	92.33	0.00	0.00	1.52	4.52	3.00
640	1.13	0.00	1.32	90.05	92.50	0.53	0.00	0.12	3.43	3.83
660	2.39	0.00	0.59	86.52	89.50	0.35	0.00	0.59	1.73	1.50

KY 2-session Mean Bleach Condition Data

1˚ Fovea			Mean			Standard Error of the Mean				
λ	*Blue*	*Green*	*Yellow*	*Red*	*Sat*	*Blue*	*Green*	*Yellow*	*Red*	*Sat*
420	44.25	0.00	0.00	46.41	90.67	2.70	0.00	0.00	2.36	0.33
440	79.13	0.00	0.00	8.37	87.50	4.27	0.00	0.00	0.77	3.50
460	81.97	0.00	0.00	5.53	87.50	1.34	0.00	0.00	0.17	1.17
480	68.57	17.26	0.00	0.00	85.83	0.94	1.78	0.00	0.00	0.83
500	19.34	62.91	0.00	0.00	83.67	4.44	5.19	0.00	0.00	0.67
520	3.03	71.69	6.61	0.00	81.33	3.03	3.35	3.71	0.00	2.67
540	0.00	60.73	16.93	0.00	77.67	0.00	9.37	0.97	0.00	10.33
560	0.00	11.37	57.96	0.00	69.33	0.00	3.68	1.99	0.00	5.67
580	0.00	0.00	26.73	36.61	63.33	0.00	0.00	0.66	5.33	4.67
600	0.00	0.00	17.65	63.85	81.50	0.00	0.00	3.14	2.03	5.17
620	0.00	0.00	9.60	76.07	85.67	0.00	0.00	0.82	2.82	2.00
640	0.90	0.00	2.69	85.24	88.83	0.90	0.00	1.23	0.63	1.50
660	1.97	0.00	0.74	86.79	89.50	1.40	0.00	0.15	0.04	1.50
23˚ w/ annulus			**Mean**			**Standard Error of the Mean**				
λ	*Blue*	*Green*	*Yellow*	*Red*	*Sat*	*Blue*	*Green*	*Yellow*	*Red*	*Sat*
420	43.38	0.00	0.00	51.96	95.33	0.05	0.00	0.00	1.72	1.67
440	74.91	0.00	0.00	17.26	92.17	1.20	0.00	0.00	0.37	0.83
460	83.05	0.00	0.00	5.29	88.33	1.23	0.00	0.00	0.10	1.33
480	46.51	43.15	0.00	0.00	89.67	2.91	3.25	0.00	0.00	0.33
500	1.35	84.88	3.43	0.00	89.67	1.35	1.22	0.47	0.00	0.33
520	2.12	79.08	7.63	0.00	88.83	2.12	0.50	0.13	0.00	1.50
540	0.00	58.40	19.77	0.00	78.17	0.00	2.20	2.37	0.00	0.17
560	0.00	10.04	60.60	0.70	71.33	0.00	7.30	8.94	0.70	2.33
580	0.00	0.00	33.12	36.72	69.83	0.00	0.00	0.61	0.56	1.17
600	0.00	0.00	13.74	66.76	80.50	0.00	0.00	1.76	3.26	1.50
620	0.30	0.00	5.40	84.30	90.00	0.30	0.00	2.06	2.43	0.67
640	2.03	0.00	1.07	85.57	88.67	0.30	0.00	0.14	0.51	0.67
660	3.80	0.00	0.00	84.20	88.00	0.28	0.00	0.00	0.62	0.33
23˚ full-field			**Mean**			**Standard Error of the Mean**				
λ	*Blue*	*Green*	*Yellow*	*Red*	*Sat*	*Blue*	*Green*	*Yellow*	*Red*	*Sat*
420	44.50	0.00	0.00	50.17	94.67	1.75	0.00	0.00	0.08	1.67
440	81.43	0.00	0.00	9.58	91.00	0.49	0.00	0.00	1.16	0.67
460	87.47	0.00	0.00	3.19	90.67	0.53	0.00	0.00	0.81	1.33
480	58.19	32.65	0.00	0.00	90.83	17.69	18.19	0.00	0.00	0.50
500	11.81	76.44	0.58	0.00	88.83	4.24	4.50	0.58	0.00	0.83
520	0.00	78.93	9.08	0.00	88.00	0.00	0.33	1.34	0.00	1.67
540	0.00	71.77	12.40	0.00	84.17	0.00	7.74	3.24	0.00	4.50
560	0.00	6.32	68.74	0.62	75.67	0.00	0.25	1.03	0.62	0.67
580	0.00	0.00	42.91	34.92	77.83	0.00	0.00	1.14	0.64	0.50
600	0.00	0.00	18.27	66.06	84.33	0.00	0.00	0.81	2.19	3.00
620	0.29	0.00	4.13	84.75	89.17	0.29	0.00	1.42	2.88	1.17
640	0.00	0.00	2.71	87.96	90.67	0.00	0.00	0.55	2.22	1.67
660	1.18	0.00	0.90	87.08	89.17	0.02	0.00	0.90	1.72	0.83

VV 2-session Mean Bleach Condition Data

1˚ Fovea			Mean			Standard Error of the Mean				
λ	*Blue*	*Green*	*Yellow*	*Red*	*Sat*	*Blue*	*Green*	*Yellow*	*Red*	*Sat*
420	76.59	0.00	0.00	14.08	90.67	4.67	0.00	0.00	3.00	1.67
440	84.18	0.00	0.00	6.48	90.67	4.05	0.00	0.00	4.05	0.00
460	87.27	0.00	0.00	2.40	89.67	0.38	0.00	0.00	0.62	1.00
480	86.08	3.58	0.00	0.00	89.67	0.62	0.28	0.00	0.00	0.33
500	21.77	66.69	0.71	0.00	89.17	8.83	10.37	0.71	0.00	0.83
520	0.00	77.83	9.00	0.00	86.83	0.00	6.10	4.27	0.00	1.83
540	0.00	70.39	15.61	0.00	86.00	0.00	2.44	3.11	0.00	0.67
560	0.00	16.33	64.17	0.00	80.50	0.00	3.65	5.15	0.00	1.50
580	0.00	0.00	84.16	2.01	86.17	0.00	0.00	0.20	0.30	0.50
600	0.00	0.00	26.40	58.10	84.50	0.00	0.00	2.02	3.52	1.50
620	0.00	0.00	11.37	77.30	88.67	0.00	0.00	0.66	1.33	0.67
640	0.00	0.00	7.02	84.98	92.00	0.00	0.00	0.03	0.64	0.67
660	0.00	0.00	6.68	86.99	93.67	0.00	0.00	0.98	2.65	1.67
23˚ w/ annulus			**Mean**			**Standard Error of the Mean**				
λ	*Blue*	*Green*	*Yellow*	*Red*	*Sat*	*Blue*	*Green*	*Yellow*	*Red*	*Sat*
420	72.16	0.00	0.00	15.84	88.00	2.24	0.00	0.00	0.91	1.33
440	81.58	0.00	0.00	3.09	84.67	0.42	0.00	0.00	0.58	1.00
460	87.58	0.30	0.00	0.45	88.33	0.25	0.30	0.00	0.45	1.00
480	75.81	9.36	0.00	0.00	85.17	0.46	0.37	0.00	0.00	0.83
500	0.00	84.19	6.48	0.00	90.67	0.00	1.39	0.72	0.00	0.67
520	0.00	66.82	23.35	0.00	90.17	0.00	3.25	2.75	0.00	0.50
540	0.00	43.27	42.56	0.00	85.83	0.00	5.67	4.50	0.00	1.17
560	0.00	1.82	82.35	0.00	84.17	0.00	0.45	0.71	0.00	1.17
580	0.00	0.00	66.38	16.96	83.33	0.00	0.00	0.02	0.02	0.00
600	0.00	0.00	19.61	67.06	86.67	0.00	0.00	3.51	6.17	2.67
620	0.00	0.00	8.89	82.11	91.00	0.00	0.00	0.15	0.18	0.33
640	0.00	0.00	7.35	84.82	92.17	0.00	0.00	2.40	3.23	0.83
660	0.00	0.00	4.53	89.47	94.00	0.00	0.00	0.42	1.41	1.00
23˚ full-field			**Mean**			**Standard Error of the Mean**				
λ	*Blue*	*Green*	*Yellow*	*Red*	*Sat*	*Blue*	*Green*	*Yellow*	*Red*	*Sat*
420	73.14	0.00	0.00	18.69	91.83	2.46	0.00	0.00	3.63	1.17
440	85.87	0.00	0.00	2.97	88.83	0.41	0.00	0.00	0.91	0.50
460	87.64	1.02	0.00	1.51	90.17	0.02	0.15	0.00	0.33	0.17
480	79.05	8.95	0.00	0.00	88.00	0.14	0.47	0.00	0.00	0.33
500	0.00	85.89	5.62	0.00	91.50	0.00	0.36	0.48	0.00	0.83
520	0.00	80.85	9.98	0.00	90.83	0.00	3.22	2.05	0.00	1.17
540	0.00	63.61	23.06	0.00	86.67	0.00	4.21	2.54	0.00	1.67
560	0.00	13.15	69.52	0.00	82.67	0.00	6.45	3.78	0.00	2.67
580	0.00	0.00	61.48	16.68	78.17	0.00	0.00	10.05	7.55	2.50
600	0.00	0.00	22.04	61.79	83.83	0.00	0.00	0.93	1.76	0.83
620	0.00	0.00	10.36	79.64	90.00	0.00	0.00	0.68	1.34	0.67
640	0.00	0.00	5.82	88.69	94.50	0.00	0.00	0.83	0.34	0.50
660	0.00	0.00	6.01	89.00	95.00	0.00	0.00	1.22	1.89	0.67